Analytical Heat Transfer Analysis under Boundary Conditions of the Fourth Kind (Conjugate)

Abram Dorfman

University of Michigan

Abram_dorfman@hotmail.com

Abstract

The conjugate heat transfer approach is a contemporary powerful tool for solution of heat transfer problems, and numerous results obtained numerically for different particular industrial and natural topics are now available. In contrast, this article presents analytical solutions of laminar (exact) and turbulent thermal boundary layer equations and formulate general features of conjugate convective heat transfer. These analytical results differ in principle from those gained by common methods based on heat transfer coefficients which in fact are empirical means. Two forms, in series and in integral, of analytical expressions for heat flux at arbitrary body surface temperature provide the high accurate calculations using the first form when the series converges fast applying the second one otherwise. On the base of these fundamental relations, the simple methods of solution of the conjugate heat transfer problems for thin and thermally thin plate are developed. Analysis of presented solutions shows that: (i) the surface temperature head variation and Biot number for isothermal surface are the basic characteristics defining the conjugate heat transfer intensity, (ii) the effect of temperature head gradient on the heat transfer coefficient is similar to influence of velocity gradient on friction coefficient: the positive gradients in both cases lead to growing coefficients, and decreasing velocity or temperature head results in lessening of appropriate coefficients and separation flow or heat flux inversion which is analogous to separation phenomenon, (iii) the basic relation in the form of series is a general boundary condition containing known particular cases.

Keywords

Analytical Solutions, Laminar Flows, Turbulent Flows, Conjugate Heat Transfer, Gradient Analogy

Introduction

It has been long known that exact solutions of convective heat transfer problems require satisfaction of the boundary conditions of the forth kind which are in essence the same as conjugate conditions. Such boundary conditions consist of the conjugation of the body and fluid temperature fields at their interface. However, in practice before computer advent, availability of problem solutions with such boundary conditions was restricted only to very simple cases. Due to that instead of exact formulation, a boundary condition of the third kind has been used since the time of Newton. In fact, this means that exact relations of the fourth kind are substituted by assumption that a heat flux q_w through a solid-fluid interface is proportional to difference between the body temperature T_w and the fluid temperature T_∞ far away from a solid

$$q_w = h\left(T_w - T_\infty\right) \tag{1}$$

In such approach, the accuracy rests on a successful determining a proportionality factor-the heat transfer coefficient h. Since there was no well-grounded theoretical heat transfer coefficient estimation, until the last few decades only, experimental results might be used as a reliable data. Therefore, in practical calculations, the heat transfer coefficient was usually estimated from available experimental data or otherwise the values for the simplest cases of constant interface heat flux or temperature were employed. Such simplified approach, when the effect of actual wall temperature distribution on the interface is neglected, was acceptable before the computers came to use resulting in significant increasing of the computing accuracy.

2325-6796/16/02 065-20, © 2016 DEStech Publications, Inc.
doi: 10.12783/fae.2016.0502.01

Practically at the same time, at the middle of 1960s, the interest in the conjugate convective heat transfer was developed, and since that time, many convective heat transfer problems have been considered using a conjugate, coupled, or adjoint statement. These three equivalent terms correspond to situation when the solution domain consists of two or more subdomains in which parts of studied phenomena are described by different differential equations. After solving the problem in each of subdomains, these solutions should be conjugated. The heat transfer between a body and a fluid flowing past it is a typical conjugate problem, because the heat transfer inside the body is governed by the elliptic Laplace equation or by the parabolic differential equation, while the heat transfer inside the flowing fluid is governed by the elliptic Navier-Stokes equation or by the parabolic boundary layer equation. The solution of such conjugate problem gives the temperature and heat flux distributions along the body-fluid interface, and there is no need for a heat transfer coefficient. Moreover, heat transfer coefficient can be computed using these data.

The conjugate procedure is needed also if the problem is governed by only one differential equation, but the subdomains problems contain different materials or other not identical properties. For example, the transient heat transfer between a hot plate and a cooling thin fluid film flowing along it is a conjugate problem. In such a case, the plate at each moment is divided into a wet part covered with moving film and a dry one which is still uncovered. Although heat transfer in both portions of the plate is governed by the conduction equation, the solutions for each of these parts differ from each other and should be conjugated, because thermal properties of wet and dry portions are different.

Numerous publications show that conjugate methods in heat transfer starting in the sixties of the last century with simple problems, like [1-3], now became a powerful tool for modeling and investigating problems of wide scope from rockets, nuclear reactors, turbomachines and other engineering and industrial systems [4-13] to different technology processes such as drying, thermal material treatment, food production [13-21], and biology and medical processes [22, 23]. More than 200 solutions of conjugate heat transfer problems from early publications to modern results are reviewed in the author's book [24] showing applicability of this modern approach.

There are many conjugate problems not only in heat transfer, but also in other areas of science and technology. For instance, studying subsonic-supersonic flows requires conjugation, because the subsonic flow is governed by elliptic or parabolic differential equations, while the supersonic flow is described by hyperbolic differential equation. Combustion theory and biological processes are the other two examples. Every combustion process has two areas containing fresh and burnt gases with different properties. An example of treating combustion as conjugate problem is given in [25]. In biology, the diffusion processes usually proceed simultaneously in qualitatively different areas (through membranes), and, therefore, require a conjugation procedure. The flow of blood or urine in human organs is another example of typical conjugate problem in biology, because such flow exists due to peristaltic motion which occurs as a result of interaction between the elastic vessel walls and fluid inside it. Similar studies in mathematics, called mixed problems, began to be considered much earlier than conjugate physical systems. The one of the first parabolic/ hyperbolic mixed equation was studied by Tricomi in 1923.

It follows from available literature that practically any heat transfer problem may be solved by contemporary numerical conjugate methods if a relevant mathematical model could be formulated. Each of such solution gives a particular reliable fundamental or applicable result for some specific problem or a case. In contrast to that, this article presents analytical solutions of laminar (exact) and turbulent thermal boundary layer equations and formulate general features of conjugate convective heat transfer. These analytical results differ in principle from those gained by common methods based on heat transfer coefficient which in fact are empirical means.

The article is organized in five sections following the introduction which consists of explanation of conjugation idea and short literature review. The first section presents general expression for heat flux on streamlined body surface with arbitrary temperature distribution obtained by solutions of laminar (exact) and turbulent thermal boundary layer equations. In section 2, on the basis of this universal expression, the charts for conjugate solution of simple heat transfer problems in laminar and turbulent flows are developed. Eight examples of solution of the

conjugate heat transfer problems under different boundary conditions demonstrate how much the modern strong conjugate solutions differ from data gained by common approach based on heat transfer coefficient. Analysis of conjugate results reveals the basic features of heat transfer process and the role of various parameters in determining the intensity of the conjugate heat transfer. In the next three sections, the properties observed in particular problems are generalized using presented in the first section universal expression for heat flux on a streamlined body surface with arbitrary temperature distribution. The effect of temperature head variation is analyzed in section 3, indicating that this issue is the major conjugate heat transfer characteristic. In section 4, it is shown that Biot number defining the ratio of body-fluid thermal resistances is the second parameter largely specified the heat transfer intensity. The final section 5 considers the universal expression for heat flux on a body surface as general boundary condition from which the known particular forms follow. It is shown that the estimation of the second term of this general condition with the first derivative of temperature head gives understanding whether or not the conjugate solution is required for some specific heat transfer problem. In the conclusion, a question "Should any heat transfer problem be considered using conjugate approach?" is discussed. As a whole, the article presents the modern conjugate heat transfer method for studying convective heat transfer substituting empirical approach based on heat transfer coefficient.

Effect of Nonisothermicity

Indeed, the conjugate heat transfer problem considers the thermal interaction between a body and a fluid flowing over or inside it. As a result of such interaction, a particular temperature distribution establishes on the body-fluid interface. This temperature field determines the heat flux distribution on the interface and virtually defines the intensity and properties of conjugate heat transfer. On the other hand, it is obvious that these properties of conjugate heat transfer and those of heat transfer from some nonisothermal surface are the same if in both cases, the temperature distributions are identical no matter how this distribution arose, as a result of conjugate procedure or by some other ways. Those considerations show that the question of conjugate heat transfer may be considered as a problem of heat transfer from arbitrary nonisothermal surface. From arbitrary because the temperature on the interface in typical conjugate problem is unknown in advance.

Such approach is realized in the author studies [25] and [26] using solutions of thermal boundary layer equation for laminar and turbulent flows. It is shown that the exact solution of a laminar thermal boundary layer equation for the plate with an arbitrary temperature distribution may be presented as a series of the consecutive derivations of the temperature head $\theta_w = T_w - T_\infty$

$$q_w = h_\bullet \left(\theta_w + g_1 x \frac{d\theta_w}{dx} + g_2 x^2 \frac{d^2\theta_w}{dx^2} + g_3 x^3 \frac{d^3\theta_w}{dx^3} + \ldots \right) = h_\bullet \left(\theta_w + \sum_{k=1}^{\infty} g_k x^k \frac{d^k\theta_w}{dx^k} \right) \tag{2}$$

where h_* is heat transfer coefficient on an isothermal surface. Coefficients g_k for laminar and turbulent flows rapidly decrease with the increasing numbers, so that the series converges fast, and retaining two or three first terms usually yields satisfactory results. For laminar flows at zero pressure gradient, only coefficient g_1 depends on Prandtl number for small values ($\Pr < 0.5$), while the next three coefficients in the whole range of Prandtl number ($0 < \Pr < \infty$) as well as the first coefficient g_1 for moderate and large values ($\Pr > 0.5$) are practically constant and equal to corresponding values for the case of $\Pr \to \infty$: $g_1 = 0.6123, g_2 = -0.1345, g_3 = 0.03, g_4 = 0.006$. For turbulent flows and zero pressure gradient the coefficients g_k depend on Prandtl and Reynolds numbers significantly decreasing with increasing both $\Pr$ and Re. They are smaller than those for laminar flows, and their maximum values are: $g_1 = 0.5$, $g_2 = -0.05$, $g_3 = 0.01$, $g_4 = -0.01$ for $\Pr = 0.01$ and $\mathrm{Re}_{\delta\bullet} = 10^3$ $\left(\mathrm{Re}_X \approx 3 \cdot 10^5\right)$. For large Reynolds numbers $\mathrm{Re}_{\delta\bullet} > 10^9$ $\left(\mathrm{Re}_X > 2.5 \cdot 10^{12}\right)$. , the largest coefficient is $g_1 \approx 0.1$, and for $\Pr > 100$ all coefficients $g_k \approx 0$, leading to negligible effect of nonisothermicity. Here, Re_{δ^*} is the Reynolds number defined through displacement thickness δ^* (more details in [24]).

Charts for Solving Simple Conjugate Problems

We begin from the basic classical problem of heat transfer between two fluids separated by a thin plate which imitates a heat exchanger. In common approach, the temperature head at one wall side is determined via overall coefficient h_Σ as follows

$$\theta_{w1} = \frac{T_{\infty 1} - T_{w1}}{T_{\infty 1} - T_{\infty 2}} = \frac{q_w}{h_\Sigma \left(T_{\infty 1} - T_{\infty 2}\right)} = \frac{1}{1 + h_{*_1} / h_{*_2} + h_{*_1} \Delta / \lambda_w} \tag{3}$$

where Δ and λ_w are the plate thickness and conductivity. In what follows, the conjugate solutions of the same problem for the plate at different thermal boundary conditions show how strong the correct results differ from those giving by old simple equation (3) still presented in college courses as a key approach in convective heat transfer.

Consider a thermally thin plate streamlined by two fluids with temperatures $T_{\infty 1}$ and $T_{\infty 2}$. The term thermally thin means that the transverse thermal resistance of the thin body is small in comparison with resistance of a fluid, and due to that, the temperature across the plate may be considered as practically constant. In this case, a two-dimensional conduction equation after integration across the plate thickness simplifies to the form

$$\frac{d^2 T_w}{dx^2} - \frac{q_{w1} + q_{w2}}{\lambda_w \Delta} + \frac{q_{\text{v.av}}}{\lambda_w} = 0, \quad \theta = \frac{T_w - T_{\infty 1}}{T_{\infty 2} - T_{\infty 1}}, \quad \xi = x / L, \quad \text{Bi}_{\bullet L} = \frac{h_{\bullet L} L^2}{\lambda_w \Delta} \tag{4}$$

Substituting series (2) with only the first three terms for heat fluxes q_{w1} and q_{w2} into this equation after applying variables (4) yields the differential equation determining the plate temperature [27]

$$D_0 \theta + D_{01} \xi \theta' + \left(D_{02} \xi^2 - \xi^{r/s}\right) \theta'' - \text{Bi}_{*L2} - \xi^{r/s} q_{\text{v}} = 0 \tag{5}$$

$$D_k = g_{k1} \text{Bi}_{*L1} + g_{k2} \text{Bi}_{*L2}, \quad g_{01} = g_{02} = 1, \quad q_{\text{v}} = \frac{\hat{q}_{\text{v.av}} L^2}{\lambda_w \left(T_{\infty 2} - T_{\infty 1}\right)}, \quad h_\bullet = h_{\bullet L} \left(\frac{x}{L}\right)^{-r/s}$$

Here, $\hat{q}_{\text{v}}$ is the dimensional average value of volumetric heat source, indices 1, 2 indicate the plate sides, and $\text{Bi}_{\bullet L}$ is a special form of Biot number which appears in derivation of equation (5), and which is defined as a product of usual Biot number $h_{*L} L / \lambda_w$ and ratio L / Δ. In obtaining equation (5) from the first relation (4), the following issues are taken into account: (i) the sum of dimensionless temperature heads defined by the second equation (4) is $T_{w1} + T_{w2} = \theta_1 + \theta_2 = \theta$, and due to that equation (5) contains only one function θ, (ii) the Biot numbers for both plate sides are different if the heat transfer isothermal coefficients h_* for both fluids are different, and therefore, two Biot numbers are present in equation (5) (iii) the exponent in the last formula (5) is given as a fraction r / s because its value depends on flow regime, pressure gradient and rheology type of fluid. For example, this exponent is 1/2 for laminar and 1/5 for turbulent flows, $(1 - m)/2$ for self-similar flows with external velocity $U = Cx^m$ [28], and its value also depends on exponent n for power law non-Newtonian fluids (see notes to Table 3).

Here, we consider the relatively simple case when the pressure gradient is zero $(m = 0)$, and flow regimes are the same on both sides of a plate resulting in only one exponent r / s containing in equation (5). Nevertheless, there are two Biot numbers in this equation because the isothermal heat transfer coefficients h_{*L} at the plate end for both streams are different if the velocities or physical properties of both streams are not the same leading to different Reynolds or/and Prandtl numbers. Other solutions of similar more complicated conjugate problems are considered in book [24].

In the simple case considered here, the equation (5) is transformed by employing a new variable z instead of $\xi = x / L$ to the form

$$\theta + g_1 z \frac{d\theta}{dz} + (g_2 z^2 - z^{r/s}) \frac{d^2\theta}{dz^2} - \sigma_{\mathrm{Bi}} - z^{r/s} \frac{q_{\mathrm{V}}}{z_L^2} = 0 \tag{6}$$

$$z = z_L (x/L), \qquad z_L = (\mathrm{Bi}_{*L1} + \mathrm{Bi}_{*L2})^{\frac{1}{2-r/s}} \qquad \sigma_{\mathrm{Bi}} = \frac{\mathrm{Bi}_{*L2}}{\mathrm{Bi}_{*L1} + \mathrm{Bi}_{*L2}}$$

It is seen that the plate temperature defined by equation (6) depends only on one variable z. Equation (6) also does not contains any boundary conditions of a particular problem. Therefore, function $\theta(z)$ is tabulated and used for solving different conjugate heat transfer problems. In order to distinguish the tabulated functions from others, we apply for these a special notation $\vartheta(z)$.

Four functions for laminar and turbulent flows are tabulated for some simple constant boundary conditions: ϑ_1 and ϑ_2 giving the solutions of homogeneous (without a heat source) equation (6) and ϑ_3 and ϑ_4 assigning particular solution of inhomogeneous equation (6) for the case of uniform or linear heat source $q_{\mathrm{V}} = A + B(x/L)$. The homogeneous equation (6) is modified to well-known hypergeometric equation. Then, the functions ϑ_1 and ϑ_2 are determined by two hypergeometric functions

$$\vartheta_1 = F\left(\alpha - \gamma + 1,\ \beta - \gamma + 1,\ 2 - \gamma,\ z^{2-r/s}\right), \qquad \vartheta_2 = z\,F\left(\alpha,\ \beta,\ \gamma,\ z^{2-r/s}\right) \tag{7}$$

where $\alpha + \beta = (1 + g_1/g_2)/(2 - r/s)$, $\alpha\beta = (1 + g_1)/g_2(2 - r/s)$ so that α and β are roots of quadratic equation and the third parameter is defined as $\gamma = (3 - r/s)/(2 - r/s)$. The following simple boundary conditions are used for tabulating functions

$$\vartheta_1(0) = 1,\ \vartheta_1'(0) = 0, \quad \vartheta_2(0) = 0,\ \vartheta_2'(0) = 1 \tag{8}$$

For the problems with thermal sources q_{V}, the temperature head is presented as a sum of a general ϑ_1 and ϑ_2 and a particular $\sigma_{\mathrm{Bi}} + \vartheta_q$ solutions of equation (6).

$$\theta = C_1\vartheta_1 + C_2\vartheta_2 + \sigma_{\mathrm{Bi}} + \vartheta_q \qquad \vartheta_q = A\vartheta_3 + B\vartheta_4 \tag{9}$$

$$A = \frac{\hat{A}L^2}{\lambda_w (T_{\infty 2} - T_{\infty 1}) z_L^2}, \qquad B = \frac{\hat{B}L^3}{\lambda_w (T_{\infty 2} - T_{\infty 1}) z_L^3}$$

The constants C_1 and C_2 in (9) are found using boundary condition given in the problem in question. The dimensionless local and total heat fluxes from a plate, and longitudinal heat flux along the plate are expressed via derivatives of functions (9) θ defined in terms of tabulated derivatives ϑ_1' and ϑ_2'

$$q_w = \frac{\hat{q}_w L^2}{\lambda_w \Delta T_R z_L^2 \Delta} = \frac{\theta''}{2\theta_0}, \qquad Q_w = \frac{2L\hat{Q}}{\lambda_w \Delta T_R z_L \Delta} = \frac{\theta'(z_L) - \theta'(0)}{\theta_0} \tag{10}$$

$$q_x = -\frac{\hat{q}_x L}{\lambda_w \Delta T_R z_L} = \frac{\theta'}{\theta_0}, \qquad \chi_t = \frac{h}{h_*} = 1 + g_1 x \frac{\theta'}{\theta} + g_2 x^2 \frac{\theta''}{\theta}$$

The last equation (10) determines the nonisothermicity coefficient which shows how much the heat transfer coefficient h gained in conjugate solution differs from isothermal coefficient h_*. Here, this coefficient is estimated applying only the first three terms of series (2) knowing that coefficients g_k for $k > 3$ are negligible small. In expressions (10), the dimensional values are marked by "cap", $\Delta T_R = T_R - T_\infty$ is the difference of reference temperature T_R and index 0 denotes values at the leading edge.

For laminar and turbulent flows, functions ϑ_1, ϑ_2, ϑ_3 and ϑ_4 and their derivatives are presented in Figures 1-4. For laminar flow, the tabulated functions are valid for zero pressure gradients and $\Pr > 0.5$ for which the coefficients g_k are independent of Prandtl number. For turbulent flow, the tabulated functions are applicable for zero pressure gradients, $\Pr \approx 1$ and $\mathrm{Re}_x = 10^6 - 10^7$. Examples of solutions with computing details and analyses are considered below. Some others may be found in [24].

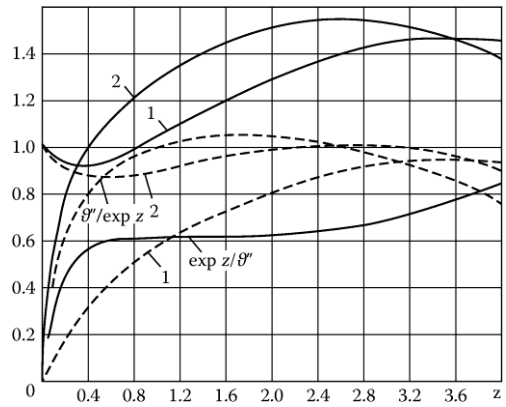

FIG. 1 CHART FUNCTIONS ϑ_1 AND ϑ_2 FOR LAMINAR FLOW, $\Pr > 0.5$, ------ ϑ_1, - - - - ϑ_2, $1 - \vartheta / \exp z$, $2 - \vartheta' / \exp z$, $\exp z / \vartheta''$, $\vartheta'' / \exp z$ -ON FIGURRE

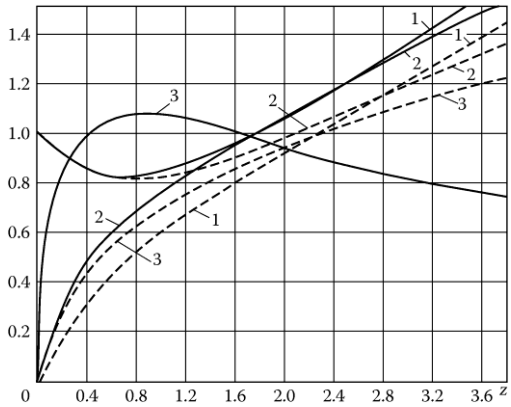

FIG 2 CHART FUNCTIONS ϑ_1 AND ϑ_2 FOR TURBULENT FLOW, $\Pr = 0.7$, $\mathrm{Re} = 10^6 ... 10^7$, ------ ϑ_1, - - - ϑ_2, $1 - \vartheta / \exp(3z/4)$, $2 - \vartheta' / \exp(3z/4)$, 3 ------ $\exp(3z/4) / \vartheta_1''$, - - - - - $\vartheta_2'' / \exp(3z/4)$

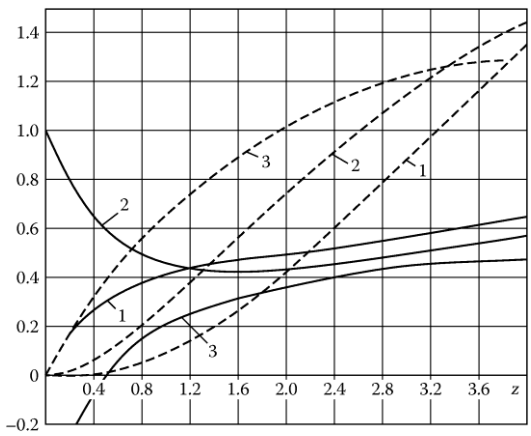

FIG. 3 CHART FUNCTIONS ϑ_3 AND ϑ_4 FOR LAMINAR FLOW. $\Pr > 0.5$, ------ ϑ_3, - - - - ϑ_4, $1 - \vartheta / \exp(3z/4)$, $2 - \vartheta' / \exp(3z/4)$, $3 - \vartheta'' / \exp(3z/4)$

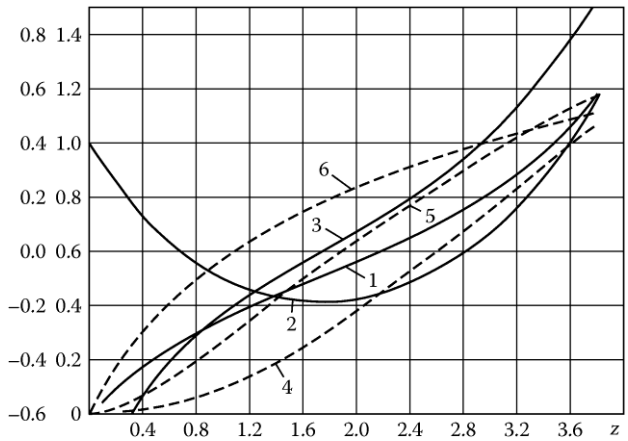

FIG.4 CHART FUNCTIONS ϑ_3 AND ϑ_4 FOR TUEBULENT FLOW. $\Pr = 0.7$, $\mathrm{Re} = 10^6 \ldots 10^7$, ----- ϑ_3, $---\vartheta_4$, $1-\vartheta_3/2$, $2-\vartheta_3'$, $3-\vartheta_3''$, $4-\left[-\vartheta_4/\exp\left(3z/4\right)\right]$, $5-\left[-\vartheta_4'/\exp\left(3z/4\right)\right]$, $6-\left[-\vartheta_4''/\exp\left(3z/4\right)\right]$

Example 1 A steel plate of length $0.25m$ and of thickness $0.01m$ is in a symmetrical air flow of velocity $3m/s$ and of temperature $300K$. The left-hand end is insulated, and the temperature of the other end is maintained at $T_w(L)$.

Because in this case, the temperature of the plate end T_{wL} is specified only, it is reasonable to take it as a reference temperature, and use dimensionless temperature head in the form $\theta = (T_w - T_\infty)/(T_{wL} - T_\infty)$. Applying boundary conditions $\theta(L) = 1$ for the right end, and $q_x(0) = 0$ for the isolated left end, one finds from first relations (9) and e third relation (10) two equations $C_1\vartheta_1(z_L) + C_2\vartheta_2(z_L) = 1$ and $C_1\vartheta_1'(0) + C_2\vartheta_2'(0) = 0$, respectively. Then, from the second equation follows that $C_1 = 0$ because according to (8) $\vartheta_1'(0) = 1$ and $\vartheta_2'(0) = 0$. Due to that, the first equation gives $C_2 = 1/\vartheta_1(z_L)$. Since $\mathrm{Re} = 5\cdot 10^4$, the flow is laminar, and the exponent in relations (6) is $r/s = 1/2$. Using this value, we estimate the Biot number (4)

$$\mathrm{Bi}_{*L} = \frac{h_L L^2}{\lambda_w \Delta} = \frac{\mathrm{Nu}_{*L}\lambda L}{\lambda_w \Delta} = \frac{0.295\cdot(5\cdot 10^4)^{1/2}\cdot 0.027\cdot 0.25}{0.65} = 0.66, \tag{11}$$

the third parameter (6) $z_L = (2\cdot 0.66)^{2/3} = 1.2$. Finally the temperature head and heat fluxes are defined by questions (9) and (10) $\theta = C_2\vartheta_1(z) = \vartheta_1(z)/\vartheta_1(z_L)$, $q_x = -\vartheta_1'(z)/\vartheta_1(z_L)$ and $q_w = \vartheta_1''(z)/2\vartheta_1(z_L)$. The required values of tabulated function and their derivatives are taken from Figure 1. The numerical results are given in Table 1.

TABLE 1

z	x/L	$\vartheta_1(z)$	$\vartheta_1'(z)$	$\vartheta_1''(z)$	θ	$-q_x$	q_w
0	0	1	0	∞	0.278	0	∞
0.2	0.167	1.12	0.949	2.75	0.311	0.264	0.382
0.4	0.334	1.37	1.48	2.66	0.388	0.411	0.369
0.6	0.501	1.72	2.04	3.02	0.478	0.567	0.429
0.8	0.668	2.19	2.70	3.62	0.608	0.750	0.503
1.0	0.835	2.81	3.50	4.42	0.780	0.969	0.614
1.2	1	3.60	4.48	5.12	1	1.244	0.753

The data from Tablet 1 are valid in both cases of increasing and decreasing temperature head because they are given in dimensionless values $(T_w - T_\infty)/(T_{wL} - T_\infty)$. To see the different effects of temperature head variation in those two cases, we compute the nonisothermicity coefficient using the last formula (10) with three terms of series (2). This procedure requires the relation for temperature head found above $\theta = \vartheta_1(z)/\vartheta_1(z_L)$ and two similar formulae for derivatives $\theta' = \vartheta_1'(z)/\vartheta_1(z_L)$ and $\theta'' = \vartheta_1''(z)/\vartheta_1(z_L)$. Using data from Table 1, we get: $\chi_t = 1.09, 1.22, 1.35, 1.46, 1.55, 1.64$ for growing (positive) and $\chi_t =$ 0.909, 0.777, 0.649, 0.538, 0.449, 0.361 for falling (negative) temperature heads.

It is seen that the temperature head variation strongly affects the heat transfer intensity. While in the case of the growing temperature head, the heat transfer coefficient increases and reaches at the end of the plate a value of about 65% greater than the isothermal coefficient $(\chi_t = 1.64)$, in the opposite case of falling temperature head, it strikingly decreases and becomes almost three times less than isothermal coefficient at the terminal edge $(\chi_t = 0.361)$. If in this case the plate was longer, the heat flux and heat transfer coefficient further would approach zero and then would change their directions leading to heat inversion- the phenomenon which is similar to separation.

As we will see from more following examples, such strongly different effects of increasing and decreasing temperature heads on the heat transfer coefficient values are the general properties of heat transfer. More precisely and detailed, we discuss this and other general properties of heat transfer in final sections and conclusion.

Comment 1 Here and below, we analyze chiefly the case of positive temperature head when the body temperature T_w is higher than that of the fluid T_∞. In the case when the body is cooler than the fluid, and the temperature head is negative $(T_w < T_\infty)$, these results are valid if one considers the temperature head as a negative value. Otherwise, if the absolute value of temperature head is employed in the second case, the opposite results are valid: a decreasing temperature head leads to growing heat transfer coefficient, and increasing temperature head results in falling heat transfer coefficient in comparison with that for an isothermal surface. That is because the derivative $\partial\theta/\partial x$ in the second term of relation (2) and last equation (10) changes the sign to the opposite in the case of negative temperature head. However, the same conclusions are valid in both cases if one considers in the case of negative temperature head it absolute value.

Example 2 Air at a temperature 313K flows with velocity $30\,m/s$ over one side of a copper plate $0.5\,m$ long and $0.02\,m$ in thickness. Another side of the plate is isolated. The temperatures of the leading and trailing ends are $T_{w0} = 593\,\mathrm{K}$ and $T_{wL} = 293\,\mathrm{K}$.

If the dimensionless temperature head is defined as $\theta = (T_w - T_\infty)/(T_{w0} - T_\infty)$, the boundary conditions are $\theta(0) = 1$ and $\theta(L) = \theta_L$. According to the first relation (9), these conditions give two equations $C_1\vartheta_1(0) + C_2\vartheta_2(0) = 1$ and $C_1\vartheta_1(z_L) + C_2\vartheta_2(z_L) = \theta_L$ which along with conditions (8) yielded from first equation $C_1 = 1$ and then from the second one $C_2 = \left[\theta_L - \vartheta_1(z_L)\right]/\vartheta_2(z_L)$. The Reynolds number $\mathrm{Re} = 0.88\cdot 10^6$ tells us that flow is turbulent, and hence, $r/s = 1/5$, and $\mathrm{Nu}_{*L} = 0.0255\,\mathrm{Re}^{4/5}$. Then, $\mathrm{Bi}_{*\mathrm{L}} = 2.53$, $z_L = 1.67$, and the temperature head according to (8) and just found constants C_1 and C_2 is $\theta = \vartheta_1(z) + \left[\theta_L - \vartheta_1(z_L)\right]\vartheta_2(z)/\vartheta_2(z_L)$. Finally, after taken functions ϑ from Figure 2, one finds $\theta = \vartheta_1(z) - 1.22\vartheta_2(z)$. The results are plotted in Figure 5 that shows the same dependence for the heat transfer coefficient the value of which intensively goes down, reaches zero close to the plate end and then the heat flux inversion occurs. The reason of such results as indicated above is the decreasing temperature head along a plate.

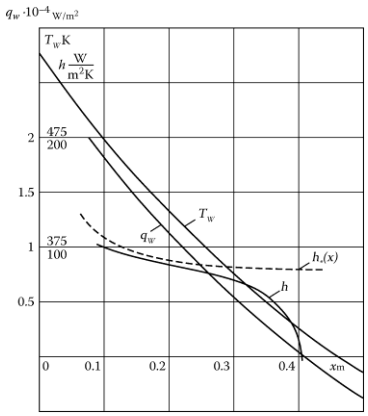

FIG.5 HEAT TRANSFER CHARACTERISTICS FOR A PLATE STREAMLINED ON ONE SIDE BY TURBULENT FLOW

Example 3 Consider the same problem for an aluminum plate of length $0.3m$ and with thickness of $0.002\ m$ streamlined by a flow of air with velocity $250\,m/s$ on an altitude of $20km$. Air temperature is $T_\infty = 223$K, a kinetic viscosity is $\nu = 1.65 \cdot 10^4 m^2/s$. The front end temperature is a stagnation temperature $T_{w0} = T_{\infty 0} = 254\,K$, and the other end is maintained at $T_{wL} = 323$K.

Because the Mach number in the problem in question is relatively high $\mathrm{M} = U/a = 250/20.1 \cdot \sqrt{223} = 0.833$ (here, $a = 20.1 \cdot \sqrt{223}$ is the speed of sound), it is necessary to take into account the effect of compressibility. It is known that in the case of not very high Mach number, this may be done by employing the adiabatic temperature T_{ad} instead of temperature T_∞. Therefore, in this case, the dimensionless temperature head is present in the form $\theta = (T_w - T_{wL})/(T_{ad} - T_{wL})$ where T_{wL} is used as a reference temperature and the stagnation (adiabatic) temperature $T_{w0} = T_{\infty 0}$ is applied instead of T_∞. Such form of a temperature head provides simple boundary conditions: $\theta(0) = 1$ and $\theta(L) = 0$. Then, in similar way by using equation (9) for θ along with relation (8), one gets two relations and defines constants $C_1 = 1$ and $C_2 = -\vartheta_1(z_L)/\vartheta_2(z_L)$ and after substituting constants into (9) obtains the solution $\theta = \vartheta_1 - [\vartheta_1(z_L)/\vartheta_2(z_L)]$. Reynolds number $\mathrm{Re} = 4.55 \cdot 10^5$ tells us that the flow is laminar giving $\mathrm{Nu}_* = 200$ and $\mathrm{Bi}_{*L} = 2.91$. Using these values and taking data for tabulated function from Figure 1, the last equation for temperature head is transformed to the form $\theta = \vartheta_1(z) - 1.60\vartheta_2(z)$. The results for heat fluxes are gained from equations (10) after substituting the difference $(T_{\infty 0} - T_{wL})$ for $(T_w - T_\infty)$. The numerical data presented in Tablet 2 indicate that in this case, the heat flux inversion $(q_w = 0)$ occurs close to plate end, at $x/L = 0.783$, leading farther to negative heat fluxes.

TABLE 2

z	x/L	$\vartheta_1(z)$	$\vartheta_1'(z)$	$\vartheta_1''(z)$	$\vartheta_2(z)$	$\vartheta_2'(z)$	$\vartheta_2''(z)$	θ	q_x	q_w
0	0`	1	0	∞	0	1	0	1	1.6	∞
0.4	0.196	1.37	1.48	2.66.	0.446	1.29	1.18	0.656	0.584	0.772
0.8	0.392	2.19	2.70	3.62	1.08	1.94	2.10	0.462	0.404	0.260
1.2	0.588	3.60	4.48	5.42	2.06	2.02	3.37	0.304	0.352	0.028
1.6	0.783	5.80	7.16	8.14	3.58	4.71	5.17	0.152	0.378	-0.132
2.04	1	10	11.7	12.6	6.26	7.61	8.04	0	0.476	-0.264

Example 4 Heat transfer from the plate heated from one end

This example shows clear-cut the role of temperature head variation because the heat transfer characteristics of such a plate significantly differ depending on the flow direction in two cases: from heated to unheated ends (the first case) and at an opposite direction, from unheated to heated ends (the second case). If one considering this

problem ignores the interface temperature head distribution, there would not be any differences in heat transfer characteristics for both flow directions which is incorrect.

To see the real situation, consider the last equation (10). It is clear that in the first case, when the flow starts from a heated edge, the temperature head decreases in the flow direction. Hence, in this case $d\theta_w / dx < 0$, and according to relation (10) the ratio (nonisothermicity coefficient) $\chi_t = h / h_*$ decreases along the plate. At the same time, the heat transfer coefficient of the isothermal surface h_* also lessens along the plate. Thus, the overall heat transfer coefficient h, defined as a product $\chi_t h_*$, strictly decreases along the plate. An opposite situation takes place in the second case when the flow starts from the coolest edge. In this situation, the temperature head increases in flow direction giving $d\theta_w / dx > 0$ so that according to the same equation (10), the product $\chi_t h_*$, grows along the plate. Since in this case, the heat transfer coefficient h_* for an isothermal surface decreases along the plate as well, the overall heat transfer coefficient $h = \chi_t h_*$ decreases or increases depending on ratio of the two multiplying factors in the last equation. This physical analysis is proved by following conjugate solution.

Let the temperature head of the heated end is θ_h, and the other end is isolated. Determining the temperature head for the case of symmetrical flow as $\theta = (T_w - T_\infty)/T_\infty$, we have the following boundary conditions: $\theta(0) = \theta_h$ and $\theta'(z_L) = 0$ in the first case and $\theta'(0) = 0$ and $\theta(z_L) = \theta_h$ in the second case. These conditions give: $C_1 = \theta_h$ and $C_2 = -\theta_h \ \vartheta_1'(z_L)/\vartheta_2'(z_L)$ and $C_2 = 0$ and $C_1 = \theta_h / \vartheta_1(z_L)$ for the first and second cases, respectively. Then, employing equations (9), (10) and (8) leads to the temperature heads, heat fluxes and gives the ratio of total heat flaxes in both cases

$$\frac{\theta}{\theta_h} = \vartheta_1 - \frac{\vartheta_1'(z_L)}{\vartheta_2'(z_L)}\vartheta_2, \qquad \frac{\theta}{\theta_h} = \frac{\vartheta_1}{\vartheta_1(z_L)}, \qquad \frac{Q_{w1}}{Q_{w2}} = \frac{\vartheta_1(z_L)}{\vartheta_2'(z_L)} \tag{12}$$

The results for laminar flow are plotted in Figure 6. It is seen that heat transfer characteristics differ substantially in both cases. In the first case when the temperature head decreases, the heat transfer coefficients are significantly less than the isothermal coefficients, and the heat flux sharply decreases along the plate, so that the situation is close to inversion at the plate end. Here, the heat transfer coefficient is 4.5 times less than an isothermal coefficient. In the second case, the temperature head increases in flow direction, and according to that, the heat transfer coefficients are greater than the isothermal ones, but not more than 1.8 times. Nevertheless, the total heat flux in this case is less than that in another case with the decreasing heat transfer coefficients. This seemingly strange outcome happened because in the first case there are large temperature heads and heat transfer coefficients at the start of flowing, while in the second case at the beginning when the heat transfer coefficient are large, the temperature heads are small and vice versa. As a result, the local heat flux has the minimum in this case in contrast to that for the first case (curves 3 in Fig. 6).

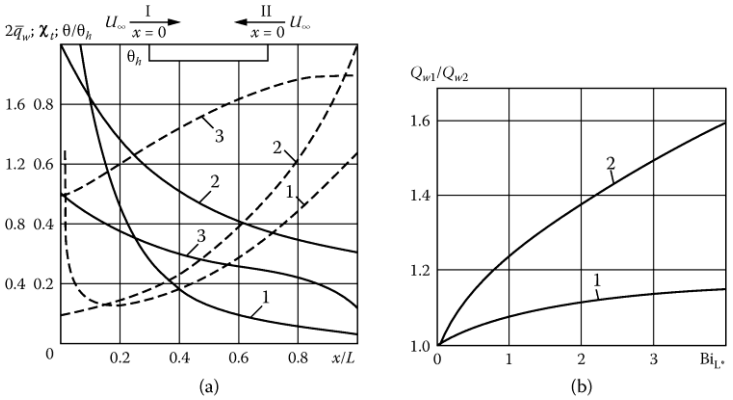

FIGS.6 HEAT TRANSFER CHARACTERISTICS FOR THE PLATE HEATED FROM ONE END. a) LOCAL CHARACTERISTICS $Bi_{*L} = 1.4$, I ------ FIRST CASE, II- - - - - SECOND CASE, $1 - 2\bar{q}_W$, $2 - \theta / \theta_h$, $3 - \chi_t$; b) RATIO OF TOTAL HEAT FLUXES REMOVED FROM PLATE 1- TUEBULENT FLOW AND 2-LAMINAR FLOW.

The value of the ratio of total heat fluxes Q_{w1}/Q_{w2} depends on Biot number and in the case of laminar flow riches significant values (Fig. 6(b)). For instance, for steel plate with $\Delta/L = 1/10$ past air (Bi_{*L}= 0.8) and water (Bi_{*L}= 4.5), this ratio is 1.2 and 1.65, respectively. In the case of turbulent flow, the difference between total flaxes is smaller (Fig. 6 (b)), but the distributions of the local heat fluxes along the plate in two opposite directions differ in essence as well which is easy to check using presented charts for conjugate problems solution.

Comment 2 This example is a model of a situation when a heated from one edge object is cooled moving through surroundings of air or water. If the heat is supplied at a leading edge, the temperature head decreases in flow direction, whereas if the heat is delivered through the trailing edge, the temperature head increases in flow direction as in the first and the second cases, respectively, in the just considered model. Since the removed total heat in the first case is greater than that in the second one, the average temperature of the body with leading heat source is less than in the case with the same heat source located at the trailing edge. As indicated above, this difference for large Biot numbers reaches 1.5-1.6 for laminar and about 1.2 for turbulent flows. The reason of this as it was revealed many times in this text is an entirely different effect of the temperature head variation resulting in substantial contrariety in heat transfer coefficients (curves 3 in Fig. 6).

Example 5 Heat transfer from a plate in flow past one side and isolated at another. Effect of initial heat fluxes

Let the temperature T_0 and the heat flux q_0 are given at the starting end of the plate. Using these boundary conditions, equation (9), the third equation (10) and conditions (8), we find the constants $C_1 = \theta_0, C_2 = \theta_0' = q_0\theta_0$ (since according to (10) $q_0 = \theta_0'/\theta_0$). Then, the solution for the temperature head is obtained as

$$\theta = \theta_0\left[\vartheta_1(z) + q_0\vartheta_2(z)\right] \tag{13}$$

Figure 7 shows the variation of the nonisothemicity coefficient χ_t and the temperature head for laminar (a) and turbulent (b) flows for the three cases: $q_0 = 10, 0$ and (-2).

In the first two cases, the temperature head increases along the plate, while in the third one, the temperature head first decreases and after reaching zero, its absolute value starts to increase. The same character of heat transfer variation as in other examples is observed. For an increasing temperature head, the heat transfer coefficients are greater than those for an isothermal surface but not more than 75% to 80% in the case of laminar flow and not more than 20% to 25% for the turbulent flow. In the third case in which the temperature head decreases, these coefficients are so much smaller that in some points where temperature head turns to zero, the heat transfer coefficient becomes meaningless (as it first was explained in [30]), and a curve $\chi_t(z)$ undergoes discontinuity (3 on Fig.7).

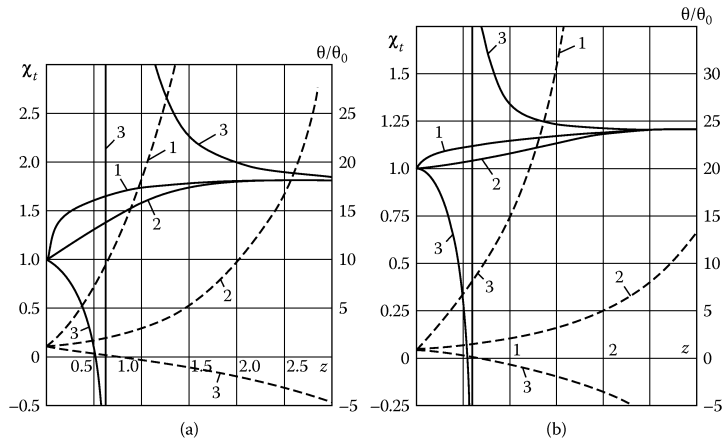

FIG.7 HEAT TRANSFER CHARACTERISTICS FOR THE PLATE STREAMLINED ON ONE SIDE BY LAMINAR (a) AND TURBULENT (b) FLOWS ------ χ_t, - - - - θ/θ_0, $1 - \bar{q}_0 = 10$, $2 - \bar{q}_0 = 0$, $3 - \bar{q}_0 = -2$.

Example 6 Heat transfer from a plate in flow past one side and isolated at another. Effect of boundary conditions

Here, we consider the same problem but with different boundary conditions. It is shown that the solution just obtained for boundary conditions specified at the leading edge is valid for some cases with other boundary conditions. In particular, if conditions are given at the terminal end, this is achieved by estimating an equivalent value of the leading heat flux q_0. For two cases when at the terminal end the temperature T_L or the heat flux q_L is specified instead of q_0, the problem solution is the same relation (13) as in the previous example if one uses for the starting value q_0 the two following expressions

$$q_0 = \frac{\theta_L / \theta_0 - \vartheta_1(z_L)}{\vartheta_2(z_L)}, \qquad q_0 = \frac{q_L - \vartheta_1'(z_L)}{\vartheta_2'(z_L)} \tag{14}$$

It is clear that in these cases, the heat transfer characteristics are the same as given on Figures 7 if the equivalent values q_0 are the same or may be obtained for other values of q_0 by approach described in Example 6.

Example 7 Heat transfer from plate in flow past two sides at different fluid temperatures.

Since there are two flows, the second formula (4) for the temperature head with the scale in the denominator $T_{\infty 2} - T_{\infty 1}$ should be employed. Assuming that temperature head at the leading edge for both sides of the plate equals to the difference of given flow temperatures $T_{\infty 2} - T_{\infty 1}$, we have $\theta_0 = 1$ and obtain expressions for heat fluxes along the plate and from both sides of the plate

$$q_x = \theta', \qquad q_{w1} = \theta'' + \sigma_{\mathrm{Bi}}\, z^{-r/s}, \qquad q_{w2} = q_{w1} - z^{-r/s} \tag{15}$$

The first equation is found from the third relation (10) knowing that $\theta_0 = 1$. The second equation follows from equation (6) (with $q_{\mathrm{v}} = 0$) because the first three terms in this equation determine the heat flux q_{w}, like in general case, the heat flux is determined by full series (2). The third equation (15) is obtained from the first equation (4) after transforming it to variable (6) $z = z_L(x/L)$ which is used for tabulated function. Then, solving the transforming equation for q_{w2} and applying the result (15) for q_{w1} gives the third equation (15).

Calculation was performed for turbulent flow, equal thermal resistances of both fluids ($\mathrm{Bi}_{*1} = \mathrm{Bi}_{*2}, \sigma_{\mathrm{Bi}} = 0.5$) and for the value of heat flux at starting edge $q_0 = -2$. Using this data, $\theta_0 = 1$ and the first equation (15) along with conditions (8), one finds the constants in equation (9) employing the same approach as in problems considered before. Then, taken the values of tabulated functions and their derivatives from Figure 2, the temperature heads for both sides are estimated regarding that $\theta_1 + \theta_2 = 1$ (see note (i) after equation (5)). Heat fluxes are obtained applying two last equations (15).

Figure 8 presents the results. The same pattern of heat transfer characteristics is observed: on the side with increasing temperature head, the nonisothermicity coefficient is a little more than unity (curve 2), while on the other side where at the beginning the temperature head decreases (curve 1), the heat transfer coefficient and the corresponding nonisothermicity coefficient χ_t sharply fall and after reaching zero go to $\pm\infty$ (curve 1) becoming discontinuous and meaningless as it is explained in previous examples.

Example 8 Heat transfer from a plate with inner heat sources.

The solution of this problem is found as a sum of general and particular solutions giving by function ϑ_1 and ϑ_2 for general part, as for other problems, and defined by functions ϑ_3 and ϑ_4 for the particular part of solution for uniform or linear sources. Calculations are performed for turbulent flow considering two cases: past one side and past two sides of a plate with linear heat source. The following conditions are specified: $\theta_0 = 1$, $q_0 = 0$, $A = 1$ and $B = 2$ (see equations (9)). Figure 9 shows that on one side of dual streamlined plate where the negative temperature head increases (dashed curve 2), the heat transfer coefficients do not much differ from those for an isothermal surface (the nonisothermicity coefficients do not much differ from unit). For one side streamlined plate and another side of dual streamlined plate, the temperature heads decrease (dashed curves 1 and 3) and the effect

of nonisothermicity is as significant as in the other cases with decreasing temperature heads despite of the turbulent flow regime.

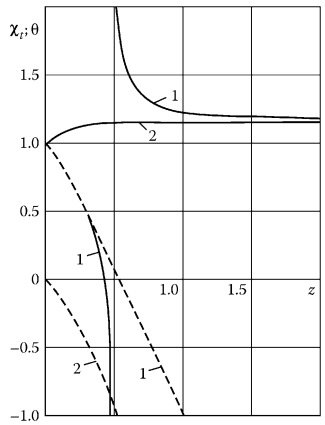

FIG. 8 VARIATION OF TEMPERATURE HEAD AND NOMISONHERMICITY COEFFICIENT ALONG THE PLATE STREAMLINED ON BOTH SIDES BY TURBULENT FLOW, $\sigma_{\mathrm{Bi}} = 0.5, \quad \theta_0 = 1, \quad \bar{q}_0 = -2$, ------ χ_t, ---- θ, 1, 2-DIFFREENT DIDES OF A PLATE

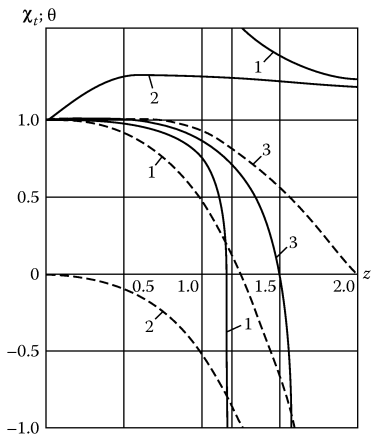

FIG.9 HEAT TRANSFER CHARACTERISTICS FOR THE PLATE WITH INNER HEAT SOURCES STREAMLINED BY TURBULENT FLOW, ---- --- χ_t, ---- $\underline{\theta}$, 1, 2- DIFFERENT SIDES OF A PLATE, $\sigma_{\mathrm{Bi}} = 0.5$, 3- ONE SIDE STREAMLINED PLATE $\left(\sigma_{\mathrm{Bi}} = 0\right)$

Temperature Head Variation-Major Conjugate Heat Transfer Characteristic

Presented analysis of different particular problems demonstrated how much the conjugate method differs from a common approach showing the essential role of temperature head variation (nonisothermicity effect) along the body-fluid interface, which is ignored in common means. Proceeding from this point, we formulate below the general properties of heat transfer that follow from general expression (2) for heat flux on a body surface (which is body-fluid interface) at arbitrary temperature head distribution.

Because the expression (2) presents the heat flux as a series of successive derivatives of the temperature head, this relation is used for investigating the effect of temperature head distribution on the heat transfer intensity. Physically, such series can be considered as a sum of perturbations of the uniform surface temperature. The case when the all derivatives are zero, and in series (2) only the first term $h_* \theta_w$ retains, corresponds to an isothermal surface which may be considered as undisturbed temperature head. The series with two first terms containing the only first derivative presents the linear disturbed temperature field. The series consisting of two derivatives describes the quadratic distributed temperature field, and so on, finally resulting in series with infinite terms giving the arbitrary temperature field distribution.

Calculation shows [24] that the coefficients g_k of series (2) rapidly decrease. Due to that, the contribution of each series term diminishes as the number of derivative grows. Moreover, comparison shows that the first coefficient g_1 is significantly larger than others in all studied cases, and even the largest among others, the second coefficient g_2, is less than the first one from three to ten times in different cases (see Table 3). This result indicates that the first derivative (i. e. temperature head gradient) basically defines the effect of the surface temperature head variation or in other words, the effect of the nonisothermicity of the body surface (or body-fluid interface)

TABLE 3 RELATION BETWEEN COEFFICIENTS g_1 AND (- g_2)

	1	**2**	**3**	**4**	**5**	**6**	**7**	**8**	**9**	**10**	**11**
g_1	1	0.6123	0.380	1/2	2.4	≈0.5	≈0.1	≈0.2	≈0.8	≈0.4	1.25
$\lvert g_2 \rvert$	1/6	0.1345	0.135	3/16	0.8	≈0.05	≈0.01	≈0.04	≈0.2	≈0.06	0.15
$\frac{\lvert g_2 \rvert}{g_1}$	1/6	0.22	0.36	3/8	1/3	≈0.1	≈0.1	≈0.2	≈0.25	≈0.15	0.12

Note to Table 3: the numbers on the top indicate the flow type and conditions associated with obtained data: Laminar layer: arbitrary θ_w $-1-\mathrm{Pr}\to 0$, $2-\mathrm{Pr}\to\infty$, arbitrary q_w $-3-\mathrm{Pr}\to\infty$, $4-\mathrm{Pr}\to 0$, unsteady laminar thermal layer $5-\mathrm{Pr}=1$, turbulent layer: $6-\mathrm{Pr}\to 0$, $\mathrm{Re}_{\delta^*}=10^3$, $7-\mathrm{Re}_{\delta^*}=10^9$, $8-\ \mathrm{Pr}=1$, $\mathrm{Re}_{\delta^*}=10^3$, non-Newtonian power law fluid with exponents: $9-n=1.8$, $10-n=0.2$, $11-\mathrm{Pr}\approx 1$, moving surface.

We have seen from considered examples that increasing and decreasing temperature heads strongly different affect the value of heat transfer coefficient. While in the case of growing temperature head, the heat transfer coefficient increases and reaches values moderately greater than that of isothermal surface, in the opposite case of falling temperature head, it decreases sharply becoming times less than isothermal heat transfer coefficient and may attain even zero and get negative resulting in inversion phenomenon.

More clear and assured, this can be seen from the general expression (2) or from the last relation (10) for nonisothermisity factor. Because the first coefficient g_1 in these expressions is positive, the increasing temperature heads (positive gradients) always lead to an increase of heat transfer intensity, while the decreasing temperature heads (negative gradients) ever cause a decrease of the heat transfer intensity. Or more precisely: if the temperature head increases in the flow direction or in time, the heat transfer coefficient is greater than isothermal coefficient, whereas a decreasing of the temperature head along the flow direction or in time yields a decrease of the heat transfer coefficient compared with the isothermal one.

At the same time, a simple analysis shows that an identical change of increasing and decreasing temperature heads results in significantly different variations in the heat transfer coefficients. The reason of this is that the same absolute difference in the temperature head and in corresponding heat transfer coefficient yields much greater change in the values of relative variation in the cases of a falling than in a growing temperature heads. Moreover, as it can be seen from the same formulae (2) and (10) in the case of decreasing temperature head (negative first derivative), the heat flux and heat transfer coefficient becomes zero if the negative temperature gradient is large or surface is sufficiently long. Even in turbulent flows, where the nonisothermicty effects are relatively small, the falling temperature head may result in zero heat transfer coefficient. This is true for all Reynolds and Prandtl numbers except the case of turbulent flows with high Prandtl numbers (say more than 100), when the nonisothermicity effect is negligible.

The temperature head gradient plays the same role in heat transfer as the pressure gradient acts in flow (gradient analogy [24]). The favorable positive temperature head gradient acts similar to positive velocity (or negative pressure) gradient, while the unfavorable negative temperature head gradient works analogous to negative

velocity (or positive pressure) gradient. In the last case, in heat transfer may develop inversion of heat flux, when the heat flux becomes zero (or heat transfer coefficient) and then changed its direction [29]. This phenomenon is similar to flow separation occurring in flows with adverse negative velocity gradients. Despite the similarity, there is a principle difference between those two processes: after separation, the flow changes its structure, so that boundary layer does not exist anymore, whereas in heat inversion only direction of heat flux changes without breaking the flow pattern.

Thus, the general expression (2) for heat flux (in conformity with conjugate solutions) shows that temperature head (or temperature at T_∞ = const.) variation along the body surface basically determines the intensity and characteristics of heat transfer acting as favorable variation in the case of increasing temperature head in flow direction or in time and working as unfavorable variation usually resulting in singularities in opposite case when the temperature head decreases in flow direction or in time.

Biot Number as a Second Important Parameter

The other parameter defined the intensity of conjugate heat transfer is the ratio of thermal resistances of the body and flowing fluid. In the case of the given temperature head variation, this ratio largely specifies the absolute value of heat transfer change caused by the surface nonisothermicity. This can be shown by using the same expression (2) for heat flux or the last equation (10) for nonisothermicity coefficient along with the conjugate conditions. By taking into account that, the nonisothermicity effect is basically determined by the second term of the series (2), one gets from conjugate conditions (equalities of temperatures and heat flaxes on the interface) the following relation

$$\lambda_w \left.\frac{\partial T}{\partial y}\right|_{y=0} = h_* g_1 x \frac{\partial \theta_w}{\partial x} \quad \text{or} \quad \frac{1}{\mathrm{Bi}} \left.\frac{\partial T}{\partial (y/\Delta)}\right|_{y=0} = g_1 x \frac{\partial \theta_w}{\partial x}, \quad \mathrm{Bi}_\bullet = \frac{h_* \Delta}{\lambda_w} \tag{16}$$

The left side of equation (16) is the heat flux at the interface gained by using the Fourier law for a body, and the right side of this equation is the second term of expression (2) (or of nonisothermicity coefficient (10)) determined the heat flux at the interface in a fluid.

Equation (16) shows that the value of the temperature head gradient $\partial\theta_w / \partial x$ is inversely proportional to Biot number for an isothermal surface which is a ratio of the thermal resistances of a body (Δ / λ_w) and a fluid $(1/h_*)$. It follows from equation (16) that in both limiting cases $\mathrm{Bi}_* \to \infty$ and $\mathrm{Bi}_* \to 0$, the corresponding conjugate problem degenerates, because in these cases, only one resistance is finite, while another either is infinite as in the first case or becomes zero as in the second one. In the first case, a conjugate problem transforms into a problem with isothermal surface, because according to (16) the temperature gradient in this case is zero. This case corresponds to a situation when the body of infinite thickness (or negligible conductivity) is streamlined by the fluid with finite heat transfer coefficient or when a body of finite conductivity and thickness is streamlined by the fluid with infinite heat transfer coefficient. In the other case, a conjugate problem transforms into a problem of a body streamlined by a fluid that changes temperature in a stepwise manner, because according to (16), the temperature head gradient is infinite in this case. This case corresponds to a situation when the body of finite thickness and conductivity is streamlined by the fluid with zero heat transfer coefficient, or the body with infinite conductivity (or negligible thickness) is streamlined by fluid with finite heat transfer coefficient.

Because in both limiting cases, the conjugate problem decays, one concludes that the greatest effect of nonisothermicity should be expected when the both resistances are of the same order, so that Biot number is close to unity. The Biot number can be presented in various forms suitable for one or another particular conjugate problem. In such a case, the Biot number characterizes the relation between the resistances of the body and fluid as well, but the quantitative results can be different from unit. This is also the reason why there are several similar other criteria characterizing the relation of body-fluid thermal resistances. For example, Luikov in an early work suggested the Brun number [31] $\mathrm{Br} = (\Delta / x)(\lambda / \lambda_w)(\mathrm{Pe})^{1/3}$, or later Cole proposed similar criterion $(\lambda / \lambda_w)(\mathrm{Pe})^{1/3}$ [32].

However, it is easy to see that those relations are, in fact, various Biot numbers.

General Boundary Condition and Common Approach Accuracy

Series (2) may be also considered as a sum of boundary condition perturbation [33]. The case when all derivatives are zero corresponds to the boundary condition with isothermal heat transfer coefficient which may be considered as undisturbed boundary conditions. The series containing only the first derivative presents the linear perturbed boundary condition. The series with two derivatives describes the quadratic perturbed boundary condition and so on. In a general case, the series consist of infinite number of derivatives and describes arbitrary boundary condition. From such considerations, one concludes that expression (2) can be treated as a general boundary condition describing different types of surface temperature distribution.

In the case of an isothermal surface, in series (2), it retains only the first term, and it becomes the boundary condition of the third kind. This boundary condition is still often employed despite existing effective numerical methods. Two reasons are responsible for that: the simplicity of his approach and the fact that there are some problems in which the nonisothermicity slightly affects the final results. In view of this fact, it is important to know an accuracy of common simple approach to see whether the conjugate solution is required. If the solution obtained by common approach using boundary condition of the third kind is known, the error caused by such approximation can be estimated by computing the second term of the general boundary condition (2). Comparing the value of the second term with the known approximate solution gives an understanding of common method accuracy and tells us whether a conjugate solution is required. Simpler the error may be estimated by computing the second term of expression (10) for the nonisothermicity coefficient which gives a value of relative error in fraction. Below we present some examples.

Example 9 Heat transfer from fluid to fluid in a flow past two sides of a thin plate.

In common approach, the temperature head at one wall side is determined via overall coefficient h_Σ by equation (3). If the flow regimes on both sides are the same, the ratio h_{*1}/h_{*2} in this equation does not depend on x. Taking this into account and knowing that the Biot number for isothermal surface is a power-law function: $\mathrm{Bi}_{*}. \sim x^{-n}$, one presents the denominator in equation (3) in the form $D_1 + D_2 x^{-n}$ with constant coefficients. Then, equation (3) becomes

$$\theta_{w1} = \frac{1}{D_1 + D_2 x^{-n}} \qquad \sigma = g_1 \frac{x}{\theta_w}\frac{d\theta_w}{dx} = \frac{g_1 n D_1}{D_1 x^n + D_2} \tag{17}$$

As indicated above, the error σ caused by common approach due to ignoring the effect of nonisothermicity is estimated through the second term of the last equation (10) which in the case of the temperature head (17) is determined by second relation (17) obtained after differentiating the first expression (17) for θ_{w1}.

The maximum value of error (17) is $\sigma_{\max} = g_1 n$ at $x = 0$ when the dominator in (17) is minimal. Thus, for laminar flow ($n = 1/2$) the greatest error is $g_1/2$, and for turbulent flow ($n = 1/5$) it is $g_1/5$. For laminar flow the coefficient g_1 is practically constant for $\mathrm{Pr} > 0.5$ and according to Table 3 equals $g_1 = 0.62$, the maximum error in this case is $\approx 30\%$. For turbulent flow at $\mathrm{Pr} = 1$, the coefficient $g_1 = 0.2$ (Table 3, row 8) and it decreases when Pr increases. Therefore, in this range of Prandtl number, the maximum error is $\approx 4\%$. However, for $\mathrm{Pr} = 0.01$, the coefficient $g_1 = 0.5$, and hence, the error is $\approx 10\%$.

Thus, in this problem for laminar flow, the error may be moderate, while for turbulent flow, when $\mathrm{Pr} > 1$, the use of the common approach does not lead to significant errors. These estimates are in agreement with corresponding conjugate problem solutions. For laminar flow, conjugate solution gives the maximum error from 20 to 25%. For turbulent flow, the maximum error according to conjugate solution is about 7%. These results are obtained in conjugate solution considering the plate as a thin with linear temperature distribution across the thickness which is the same assumption as that using in derivation of formula (3) (details in [24]).

Note that the errors in this problem are moderate in laminar and small in turbulent flows because the temperature head increases in flow direction on both sides of the plate.

Example 10 Heat transfer from a symmetrically streamlined thermally thin plate.

In this example, we estimate the error for the problem conjugate solution of which is obtained in example 1. The averaged conduction equation (4) and its common solution under boundary condition of the third kind with isothermal heat transfer coefficient are

$$\frac{d^2\theta_w}{d\xi^2} - 2\bar{\mathrm{B}}\mathrm{i}_{*\mathrm{L}}\theta_w = 0, \quad \theta_w = \frac{T_w - T_\infty}{T_{wL} - T_\infty} = \frac{ch\left(\sqrt{2\bar{\mathrm{B}}i_{*L}}\,\xi\right)}{ch\left(\sqrt{2\bar{\mathrm{B}}i_{*L}}\right)}, \quad \bar{\mathrm{B}}\mathrm{i}_{\bullet L} = \frac{\bar{h}_{\bullet L}L^2}{\lambda_w\Delta} \tag{18}$$

Here, a bar at the top of the parameters indicates the averaged values, like, for example, the averaged along the plate heat transfer coefficient $\bar{h}_{*L} = 2h_{*L}$. The first equation (18) is obtained after substituting the heat flux $q_w = \bar{h}_*\theta_w$ for heat fluxes in equation (4) since in common approach usually the average isothermal heat transfer coefficient is used (see introduction). The solution of equation (18) is obtained applying the hyperbolic cosine function because the second derivative of the hyperbolic cosine is proportional to this function itself as it requires a solution of differential equation (18).

Calculating the second term of the last expression (10) using solution (18) yields an error caused by this solution due to neglecting interface temperature distribution. After differentiating thesecond equation (18), one gets error and then, putting $th\left(\sqrt{2\bar{\mathrm{B}}\mathrm{i}_{*L}}\,\xi\right)_{\max} = 1$, obtains the maximal value of error

$$\sigma = g_1\frac{x}{\theta_w}\frac{d\theta_w}{dx} = g_1\sqrt{2\bar{\mathrm{B}}i_{*L}}\,\frac{x}{L}th\left(\sqrt{2\bar{\mathrm{B}}\mathrm{i}_{*\mathrm{L}}}\,\frac{x}{L}\right), \quad \sigma_{\max} = g_1\sqrt{2\bar{\mathrm{B}}\mathrm{i}_{*L}} = g_1\sqrt{\frac{2\bar{\mathrm{N}}\mathrm{u}_{*L}L\lambda}{\lambda_w\Delta}} \tag{19}$$

The last equation (19) follows from a previous after using Nusselt number $\mathrm{Nu}_{*L} = hL/\lambda$ instead of Biot number. Calculation yields: $\mathrm{Re}_L = 5\cdot 10^4$ (laminar flow), $\bar{\mathrm{N}}\mathrm{u}_{*L} = 2\mathrm{Nu}_{*L} = 132$, $\mathrm{Bi}_{*L} = 1.32$, $g_1 = 0.62$ and $\sigma_{\max} \approx 1$. Hence, the solution of this problem with the boundary condition of the third kind is unacceptable, and conjugate solution is required.

The conjugate solution of this problem is given in Table 1. Calculation shows that the temperature head distribution obtained by common simple solution (18) differs significantly from conjugate results with the largest deviation at the leading edge of 36% giving 0.379 instead of 0.278. This problem as well as previous problem in the case of laminar flow (with an error of about 30%) are examples with increasing along the plate temperature head when the conjugate solution is required.

Example 11 Heat transfer from continuous plate (strip) of polymer

A strip of polymer at temperature T_0 is extruded from a die and passed at velocity U_W through a bath with cold water ($\mathrm{Pr} = 6.1$) at temperature T_∞. The solution of this problem with boundary condition of the third kind is presented in paper [33] and in the book [24]. The along the strip dimensionless temperature head distribution is presented in the form $\theta_W(\tilde{x})$, with variables $\theta_W = (T_W - T_\infty)/(T_0 - T_\infty)$ and $\tilde{x} = x\alpha_W/\Delta^2 U_W$, where α_w is the thermal diffusivity. It is shown that in this case, the dimensionless temperature head depends on the ratio $(c_p\rho\lambda)_W/(c_p\rho\lambda)$ which is 8.51 in considered example. The derivative $d\theta_W/d\tilde{x}$ required for error estimation is found by numerical differentiation of the corresponding curve $\theta_W(\tilde{x})$. Estimation of the second term of the last equation (10) shows that the error grows as the distance from the die increases and finally reaches the maximal value $\sigma_{\max} \approx 2.6$. It is evident that the real results may be obtained only by solving the conjugate problem. The reason of that is a decreasing temperature head resulting in highly overestimating temperature of cooling strip [33], [24].

Presented here examples demonstrated that the error estimation by calculating the second term of series (2) for heat flux or of the second term of the last equation (10) for nonisothermicity coefficient helps to understand whether the conjugate solution for particular problem is required or the common simple approach is satisfactorily accurate.

Conclusion

Should Any Heat Transfer Problem Be Considered as a Conjugate?

The theory and analysis of examples show that the level of conjugation (the difference between conjugate and traditional solutions) of a particular convective heat transfer problem depends on many factors basic of which are:

- Variation of the temperature head in flow direction or in time. The decreasing temperature head affects the heat transfer characteristics much more strongly than an increasing temperature head.
- Relation between thermal resistances of the body and fluid at isothermal conditions characterized by Biot number. The level of conjugation is greater for the case of comparable resistances and usually small when one of thermal resistances is negligible
- Parameters and conditions determining the coefficients in the basic expression (2) for heat flux on nonisothermal surface: (i) flow regime- the effect of conjugation in laminar flows is greater than that in turbulent flows, (ii) state of heat transfer- the effect of conjugation at unsteady heat transfer is higher than that for steady- state temperature regime, (iii) Prandtl number- the higher is the Prandtl number, the smaller the effect of conjugation, (iv) Reynolds number- the effect of conjugation decreases with growing the Reynolds number, (v) type of coolant- for some non-Newtonian fluids, the effect of conjugation is greater (for $n > 1$) but for others is smaller (for $n < 1$) than for Newtonian liquids, (vi) shape of the surface- for example, increasing surface curvature leads to increasing the conjugation effect, (vii) type of boundary layer- for instance, a conjugation effect in a flow on continuously moving sheet is greater than that in flow past fixed plate.
- Distribution of the pressure gradient. The effect of conjugation is usually higher in the flows with unfavorable gradients.
- A scheme of heat transfer. For example, the effect of conjugation is greater for the heat transfer between countercurrent flowing fluids than that for concurrent flowing fluids under the same conditions.

In Table 4 below, the factors affecting the conjugation effect are listed and arranged so that next to the right issue, each represents a subject with lower effect of conjugation. For instance, because turbulent flow is located to the right of the laminar flow, this means that the conjugation effect in the problems with turbulent flows is less than that in corresponding problems with laminar flows.

TABLE 4 EFFECT OF DIFFERENT FACTORS ON THE PROBLEM CONJUGATION

Decreasing temperature heads		Increasing temperature heads
Comparable thermal resistances		Incomparable thermal resistances
Laminar flows	Transient flows	Turbulent flows
High Prandtl numbers	Mean Prandtl numbers	Low Prandtl number
Low Reynolds numbers	Mean Reynolds numbers	High Reynolds numbers
Unsteady heat transfer		Steady heat transfer
Unfavorable pressure gradients	Zero pressure flows	Favorable pressure gradients
Non-Newtonian fluids ($n > 1$), Newtonian fluids ($n = 1$), Non-Newtonian fluids ($n < 1$)		
Continuity moving sheet		Streamlined fixed plate
Small surface curvature		High surface curvature

It is obvious that in reality, the choice of the method for solution largely depends on the aim of a particular heat transfer problem and on the desired accuracy of results. Therefore, such qualitative considerations can be used for preliminary approximate estimation, whereas the exact information of the conjugate effect can be obtained only by

solving a particular conjugate problem. Nevertheless, the investigation results make it possible to formulate two general conclusions regarding question formulated in heading:

1. Convective heat transfer problems containing a temperature head decreasing in flow direction or in time should be, as a rule, considered as a conjugate because in this case, the effect of conjugation is usually significant.
2. For the turbulent flow of the fluids with high (say higher than 100) Prandtl numbers, the convective heat transfer problems may be solved using a traditional approach with boundary condition of the third kind, because for such fluids, the effect of conjugation is negligible.

For other cases, the error arising by using the traditional approach may be estimated by computing the second term $g_1 \frac{x}{\theta_w} \frac{d\theta_w}{dx}$ of equation (10) for nonisothermisity coefficient applying the known traditional solution. The value of this term helps to understand whether the conjugate solution is required. Examples of such estimations are given in the part 5 of this text.

REFERENCES

[1] Perelman, T. L. 1961. On conjugated problems of heat transfer, Int. J. Heat Mass Transfer, 3: 293-303.

[2] Dorfman, A. S. 1970. Heat transfer from liquid to liquid in a flow past two sides of a plate. High Temperature 8: 515-20.

[3] Viskanta, R. and Abrams, M. 1971. Thermal interaction of two streams in boundary layer flow separated by a plate. Int. J. Heat Mass Transfer, 14: 1311-21.

[4] Kanna, P. R., Taler, J., Anbumalar, V., Kumar, A. V . S., Pushparaj, A. and Christopher, D. S., 2015, Conjugate heat transfer from sudden expansion using nanofluid, Num. Heat Transfer, Part A, 67 (1): 75-99.

[5] Ito, Y., Inocura, N. and Nagasaki, T., 2014, Conjugate heat transfer in air-to refrigerant airfoil heat exchanger, J. Heat Transfer-Transactions ASME 135 (8): 081703.

[6] Jians, Y., Zheng, Q., Yue, G., Dong, P., Gao, J. and Yu,F., 2014, Conjugate heat transfer simulation of turbine blade high efficiency cooling method with mist injection, Proceedings of the Institution of Mechanical Engineering Part C-J. mech. Engi. Sci., 228 (15): 2738-2749

[7] Piro, M. H. A. and Leitch, B. W., 2014, Conjugate heat transfer simulation of advanced research reactor fuel, Nucl. Engin. Design 274: 30-43.

[8] Ali, M. M., Mamun, A. A. and Maleque, M. A., 2014, Radiation and heat generation effects on viscous Joule heating MGD-conjugate heat transfer for a vertical flat plate, Canadian J. Physics 92 (6): 509-521.

[9] Tosetti, M., Maggiore, P., Cavagnino, A. and Vaschetto, S., 2014, Conjugate heat transfer analysis of integrated brashless generators for more electric engines, IEEE Transactions Industry Applic. 50 (4): 2467-2475.

[10] Shen, C., Sun, F. X. and Xia, X. L., 2013, Analysis on transient conjugate heat transfer in gap-cavity-gap structure heated by high speed airflow, Int. J. Heat Mass Transfer 67: 1030-1038.

[11] Horikiri, K., Kana, Y. and Yao, J., 2014, Modeling conjugate flow and heat transfer in a ventilated room for indoor thermal comfort assessment, Building Environment 77: 135-147.

[12] Dorfman A. S. 2004, Transient heat transfer between a semi-infinite hot plate and a flowing cooling liquid film. ASME J. Heat Transfer, 126: 149-154.

[13] Baiocco, P. and Bellomi, P. 1996 A coupled thermo-ablative and fluid dynamic analysis for numerical application to solid propellant rockets. AIAA 96-1811, 31st. AIAA Thermophysics Conference, June 17-20, New Orleans, LA

[14] Khan, F. A., Fisher, C. and Straatman, A. G., 2015, Numerical model for non-equilibrium heat and mass exchange in conjugate fluid/solid/porous domains with application to evaporative cooling and drying, Int. J. Heat Mass Transfer 80:513-528.

[15] Oumarou, N., Kocaefe, D. and Kocaefe, Y., 2014, 3D-modelingof conjugate heat and mass transfer: effects of storage conditions and species on wood high temperature treatment, Int. J. Heat Mass Transfer 79: 945-953.

[16] Mansour, M. K., 2014, Effect of natural convection on conjugate heat transfer characteristics in liquid minichannel during phase change material melting, Proceedings Inst. Mech. Engin. Part C-J. Mech. Engin. Sci. 228 (3): 491-513.

[17] Eaves, N. A., Thomson, M. J. and Dworkin, S. B., 2013, The effect of conjugate heat transfer on soot formation modeling at elevated pressures, Combust. Sci Technol. 185(12): 1799-1819.

[18] Defraeye, T., Blocken, B. and Carmeliet, J., 2012, Analysis of convective heat and mass transfer coefficients for convective drying of a porous flat plate by conjugate modeling, Int. J. Heat Mass Transfer 55 (1-3): 112-124.

[19] Van Belleghem, M., De Backer, L. and Janssens, A. and De Paepe, M., 2012, Conjugate modeling of convective drying phenomena in porous building materials, 6th European Thermal Sci. Conf. (Eurotherm 2012), J. Physics Conf. Series 395: 012142.

[20] Nam, J. H. and Song, C. S. 2007 Numerical simulation of conjugate heat and mass transfer during multi-dimensional freeze drying of slab-shaped food products. . Int. J. Heat Mass Transfer, 50:4891-4900.

[21] Dolinskiy, A. A., Dorfman, A. S. and Davidenko, B. V. 1991 Conjugate heat and mass transfer in continuous processes of convective drying. Int. J. Heat Mass Transfer 34: 2883-89.

[22] Abdoli, A., Dulikravich, G. S., Bajaj, C., Stowe, D. F. and Jahania, M. S., 2014, Human heart conjugate cooling simulation: unsteady thermo-fluid-stress analysis, Int. J. Num. Metods Biomed. Engin. 30 (11): 1372-1386.

[23] Mondaca, M., Rojano, F., Choi, C. Y. and Gebremedhin, K. G., 2013, A conjugate heat and mass transfer model to evaluate the efficiency of conductive cooling for dairy cattle, Transactions ASABE 56 (6): 1471-1482.

[24] Dorfman, A. S., 2010, Conjugate Problems in Convective Heat Transfe, CRC Press Taylor & Francis, Boca Raton.

[25] Dorfman A. S. and Schapiro, D., 2011, Simulation of combustion- acoustic interaction using a conjugate method, Int. J. Thermal Sci. 50 (6): 1062-1072.

[26] Dorfman, A. S. 1971. Exact solution of the equation for a thermal boundary layer for an arbitrary surface temperature distribution, High Temperature, 9: 870-878.

[27] Dorfman, A. S. and Lipovetskaya, O. D., 1976, Heat transfer of arbitrary nonisothermic surface with gradient turbulent flow of an incompressible liquid within a wide range of Prandtl and Reynolds numbers, High Temperature, 14: 86-92.

[28] Dorfman, A. S., 1975. Temperature-distribution singularities on the separation surface during heat transfer between a plate and the liquid flowing around It, High Temperature 13: 97-100.

[29] Schlichting, H., 1979 Boundary layer Theory, McGraw-Hill, New York.

[30] Eckert, E. R.G. and Drake, R.M., 1959, Heat and Mass Transfer. McGraw-Hill.

[31] Chapman, D. and Rubesin, M., 1949, Temperature and velocity profiles in the compressible laminar boundary layer with arbitrary distribution of surface temperature, J. Aeronaut. Sci. 16: 547-565.

[32] Luikov, A. V., 1974, Conjugate heat transfer problems, Int. J. Heat Mass Transfer 17: 257-265

[33] Cole, K. D., 1997, Conjugate heat transfer from a small heated strip, Int. J. Heat Mass Transfer 40 (11): 2709-2719.

[34] Dorfman, A. S., 1985, A new type of boundary condition in convective heat transfer problems, Int. J. Heat Mass Transfer 28 (6): 1197-1203.

Hygrothermoelastic Postbuckling Response of Graphite Epoxy Material Composite Plates with Random System Properties:

SFEM Micromechanical Model Approach Investigation

Rajesh Kumar*

Professor, School of Mechanical Engineering, JIT, Jimma University, Ethiopia

rajeshtripathi63@gmail.com

Abstract

The present study investigated the hygrothermoelastic postbuckling response of graphite epoxy composite plates with random system properties such as coefficients of thermal expansion, coefficients of hygroscopic expansion, foundation stiffness parameters, geometric properties and lamina material properties by modeling as basic random variables and using SFEM micromechanical model approach. The basic formulation is based on a higher-order shear deformation plate theory in von Karman nonlinear kinematics. A direct iterative based C^0 non-linear FEM in conjunction with Taylor series based mean-centered first order regular perturbation technique is used to obtain mean and standard deviation of post buckling load of laminated composite at micro level. The environmental effects, boundary conditions, plate aspect ratios, elastic foundation stiffness parameters, fiber orientations and effects of temperature rises, degree of moisture concentrations, are investigated. The results are verified with published literature and independent Monte Carlo simulation.

Keywords

Hygrothermoelastic Post Buckling; Random System Properties; Elastic Foundations; Laminated Composite Plates; Regular Perturbation Technique

Introduction

Elastically supported laminated composite plates have been used in a great variety of engineering applications including aerospace vehicles, aircraft runways, launching sites of missile and spacecraft, foundation engineering etc. The applications have been increased in many folds for the aerospace and other engineering fields due to combined features of high strength to weight ratio, excellent corrosion resistance and good fatigue characteristics. The varying environmental conditions due to moisture absorption and temperature have an adverse effect on the stiffness and strength of the composites. As, the matrix is more susceptible to the hygrothermal condition than the fiber, the deformation is observed to be more in the transverse direction of the composite. The rise in moisture and temperature reduces the elastic moduli and degrades the strength of the materials as well as induces internal initial stresses, which may affect the stability as well as the safety of the structures.

As a result, a careful evaluation of environmental exposure is required to find the nature and extent of their adverse effects upon performance design in composite analysis and uncertainties in system behavior. Micro-mechanical stochastic modeling yields more accurate and exact prediction of system behavior has been proved to be superior design. Large numbers of parameters are associated with manufacturing and fabrication composite components as compared with conventional material. Such as material and geometric properties, fiber orientations, lamina lay-up sequence design and curing parameters. Effects of these parameters must be considered in accurate prediction of system behavior of composite so that reliability of the structure during its operating life can be assessed accurately. Thus, there is a need to quantify structural system uncertainties in the response. This may be appropriately handled by modeling system properties in probabilistic sense only. Uncertainties in the system

2325-6796/16/02 085-27, © 2016 DEStech Publications, Inc.
doi: 10.12783/fae.2016.0502.02

properties lead to uncertainties in the response behavior of the structure. For accurate study of structural behavior, the random variation in the system properties should be incorporated in the analysis. Otherwise, the predicted response may differ significantly from the observed values and the structures may not be safe.

In available literature much of the published work based on deterministic analysis using macro mechanical model on hygrothermal buckling analysis exists, including notably published work of Whitney and Ashton [1], Flaggs et al. [2], Lee and Yen [3], Ram and Sinha [4], hygrothermal buckling analysis using micro- mechanical model based on deterministic analysis Shen [5]. Hygrothermal effects on the structural behavior of thick laminates have been analyzed using higher order theory. This is a deterministic analysis by Patel et al. [6]. In deterministic analysis, the system parameters are taken to be deterministic and variations in the system parameters are ignored, which results in a conservative design and reduces the potential of the composites. It is, therefore, necessary that the system properties are taken as random variables. Limited work has been done assuming system properties as random and their effects on the performance of composites. Nakagiri et al [7] have studied all edges simply supported of a laminate with stochastic finite element method taking fiber orientation, layer thickness and a number of layers as random variables. Englested and Reddy [8] contributed metal matrix composites based on probabilistic micro mechanics non-linear analysis. Singh at al. [9] studied the buckling of composite cylindrical panels with uncertain material properties using probabilistic approach. Effects of random system properties on initial buckling of composite plates resting on elastic foundation using stochastic finite element method has been studied by Lal et al. [10]. Post buckling of laminated composite plate on elastic foundation with random system properties based on HSDT in conjunction with FOPT has been studied by Singh et al. [11]. Chen at al. [12] outlined the probabilistic method to evaluate the effects of uncertainties in geometric and material properties. Relatively little work is available on hygrothermal linear buckling analysis of the structures made of composites with random system parameters using macro-mechanical model Singh and Verma [13]. Pandey et al. [14] studied the thermo elastic stability analysis of laminated composite plates resting on nonlinear elastic foundations using analytical approach. Singh et al. [15-16] studied the effects of random system properties on initial buckling and thermal buckling using stochastic finite element method. Onkar et al.[17-18] studied the buckling problem using stochastic finite element problems. Lal et al.[19] studied the effects on the thermal buckling response of laminated composite plates using stochastic finite element method. Verma et al.[20] investigated thermal buckling problem with random material and geometric properties. Pandey et al. [35] investigated the Hygrothermoelastic Postbuckling Response of Laminated Composite Plates using the quadratic extrapolation technique and fast converging finite double Chebyshev series for linearization and spatial discretization of the governing nonlinear equations of equilibrium, respectively.

The work dealing with Hygrothermal buckling response of laminated composite plates with random material properties, Micro-mechanical model was investigated by Rajesh Kumar et al. [36]. Rajesh Kumar et al. investigated Hygrothermal buckling analysis of laminated composite plates with random system properties and resting on Elastic foundations [37]. Hygrothermally Induced Postbuckling Response of Non-linear Elastically Supported Laminated Composite Plates with Uncertain System Properties: Stochastic Finite Elemental Macro mechanical Model has been studied by Rajesh Kumar et al. [38]. Rajesh Kumar et al. investigated Hygrothermoelastic Buckling Response of Laminated Composite Plates with Random System Properties, Macro and Micro Mechanical Model [39].

However, the works dealing with Hygrothermal buckling analysis of composite plates resting on elastic foundations parameters using micro mechanical model and Hygrothermal post buckling analysis of the laminated composite plate with random system properties i.e. material properties, geometric properties- and nonlinear foundation parameters have not been reported in the literature to the best of the authors' knowledge. The work dealing with hygrothermal post buckling analysis of the laminated composite plate with random system properties i.e. material properties, geometric properties and nonlinear elastic foundations parameters using macro mechanical model has been published by Rajesh Kumar et al. [38]. The present study is further extended work of [38] and contributes to provide a tool for analysis of structural system uncertainties in elevated hygrothermal environments using micromechanical finite element model, especially applicable for aerospace engineering and other fields.

Formulations

A rectangular arbitrary laminated composite plate of length *a*, width *b* and total thickness *h* has been, defined in (*X*, *Y*, *Z*) system with *X* and *Y* axes located in the middle plane and its origin placed at the corner of the plate. Let $(\bar{u}, \bar{v}, \bar{w})$ be the displacement parallel to the (*X*, *Y*, *Z*) respectively as shown in Fig. 1. The thickness coordinate Z of the top and bottom surfaces of any k_{th} layer are denoted by $Z_{(k-1)}$ and $Z_{(k)}$, respectively. The fiber of the k_{th} layer is oriented with angle θ_k to the X- axes. The plate is assumed to be attached to the foundation so that no separation takes place in the process of deformation. The load – displacement relation between the plate and the supporting foundations is given as

$$P = K_1 w - K_2 \nabla^2 w \tag{1}$$

where P is the foundation reaction per unit area, $\nabla^2 = \partial^2/\partial x^2 + \partial^2/\partial y^2$ and K_1 and K_2 are linear Winkler (normal) foundation, linear Pasternak (shear layer) foundation parameters, respectively and w is the transverse displacement of the plate. This model is simply known as Winkler type when $K_2 = 0$.

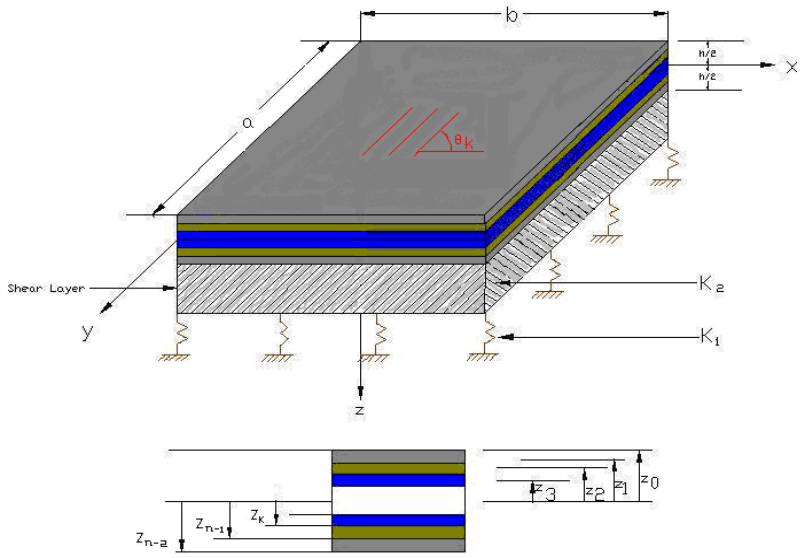

FIG.1 GEOMETRY OF LAMINATED COMPOSITE PLATE WITH ELASTIC FOUNDATION

Displacement field- Strain Displacement Relations, Stress-Strain Relation- Energy Equations The Strain Energy due to Elastic Foundation, Potential Energy due to Hygrothermal Stresses, Finite Element Formulations are studied in [13, 21, 22, 23, 24, 25, 26, 34, 35, 36,37,38,39] .

A composite plate with arbitrary lamination is considered with the co-ordinates X, Y along the in-plane directions and Z along the thickness direction as shown in Fig 1.

$$\begin{aligned} \bar{u} &= u + f_1(z)\psi_x + f_2(z)\theta_x; \\ \bar{v} &= v + f_1(z)\psi_y + f_2(z)\theta_y; \\ \bar{w} &= w; \end{aligned} \tag{2}$$

where

u, *v*, and *w* are corresponding displacements of a point on the mid plane. ψ_x and ψ_y are the rotations of normal to the mid plane about the y-axis and x-axis respectively, with $\theta_x = w,_x$ and $\theta_y = w,_y$ where, comma (,) denotes partial differential.

$$f_1(z) = C_1 z - C_2 z^3;\ f_2(z) = -C_4 z^3 \text{ with } C_1 = 1, C_2 = C_4 = 4h^2/3.$$

The displacement vector for the modified models is

$$\{\Lambda\} = \begin{bmatrix} u & v & w & \theta_y & \theta_x & \psi_y & \psi_x \end{bmatrix}^T, \tag{3}$$

The strain-displacements relations with von Karman type geometric nonlinear elasticity are expressed as-

$$\begin{aligned}
\varepsilon_{xx} &= \varepsilon_1 = \bar{u},_x + \varepsilon_1^0 + z(k_1^0 + z^2 k_1^2) + \frac{1}{2}\bar{w}^2,_x \\
\varepsilon_{yy} &= \varepsilon_2 = \bar{v},_x + \varepsilon_2^0 + z(k_2^0 + z^2 k_2^2) + \frac{1}{2}\bar{w}^2,_y \\
\gamma_{xy} &= \varepsilon_6 = \bar{u},_y + \bar{v},_x = \varepsilon_6^0 + z(k_6^0 + z^2 k_6^2) + \bar{w},_{xx} + \bar{w},_{yy} \\
\gamma_{yz} &= \varepsilon_4 = \bar{v},_z + \bar{w},_y = \varepsilon_4^0 + z^2 k_4^2 \\
\gamma_{xz} &= \varepsilon_5 = \bar{u},_z + \bar{w},_x = \varepsilon_5^0 + z^2 k_5^2
\end{aligned} \tag{4}$$

Where,

$$\begin{aligned}
&\varepsilon_1^0 = u,_x, \quad k_1^0 = \psi_x,_x, \quad k_1^2 = -4/3h^2\left(\psi_x,_x + w,_{xx}\right) \\
&\varepsilon_2^0 = v,_x, \quad k_2^0 = \psi_y,_y, \quad k_2^2 = -4/3h^2\left(\psi_y,_y + w,_{yy}\right) \\
&\varepsilon_6^0 = u,_y + v,_x, \quad k_6^0 = \psi_x,_y + \psi_y,_x, \quad k_6^2 = -4/3h^2(\psi_x,_y + \psi_y,_x + 2w,_{xy}) \\
&\varepsilon_4^0 = \psi_y + w,_y, \quad k_4^2 = -4/h^2\left(\psi_x + w,_y\right) \\
&\varepsilon_5^0 = \psi_x + w,_x, \quad k_5^2 = -4/h^2\left(\psi_x + w,_x\right)
\end{aligned}$$

where comma (,) denotes the partial differential. The mid plane strain vector $\{\bar{\varepsilon}\}$ for the model is

$$\{\bar{\varepsilon}_1\} = \left(\varepsilon_1^0 \;\; \varepsilon_2^0 \;\; \varepsilon_6^0 \;\; k_1^0 \;\; k_2^0 \;\; k_6^0 \;\; k_1^2 \;\; k_2^2 \;\; k_6^2 \;\; \varepsilon_4^0 \;\; \varepsilon_5^0 \;\; k_4^2 \;\; k_5^2\right)^T \tag{5}$$

The constitutive law of hygrothermal elasticity for the materials under consideration associates the stresses with strains in a plane stress state for the *k*th lamina oriented as an arbitrary angle with respect to the reference axis for an orthotropic layer which is given by [22,23].

$$\{\sigma\}_k = \left[\bar{Q}\right]_k \{\varepsilon\}_k \text{ or } \begin{Bmatrix} \sigma_{xx} \\ \sigma_{yy} \\ \sigma_{xy} \\ \sigma_{yz} \\ \sigma_{xz} \end{Bmatrix}_k = \begin{bmatrix} \bar{Q}_{11} & \bar{Q}_{12} & \bar{Q}_{16} & 0 & 0 \\ \bar{Q}_{12} & \bar{Q}_{22} & \bar{Q}_{26} & 0 & 0 \\ \bar{Q}_{16} & \bar{Q}_{26} & \bar{Q}_{66} & 0 & 0 \\ 0 & 0 & 0 & \bar{Q}_{44} & \bar{Q}_{45} \\ 0 & 0 & 0 & \bar{Q}_{45} & \bar{Q}_{55} \end{bmatrix}_k - \begin{Bmatrix} \varepsilon_{xx} - \alpha_{xx}\Delta T - \beta_{xx}\Delta C \\ \varepsilon_{yy} - \alpha_{yy}\Delta T - \beta_{yy}\Delta C \\ \varepsilon_{xy} - \alpha_{xy}\Delta T - \beta_{xy}\Delta C \\ \varepsilon_{yz} \\ \varepsilon_{zx} \end{Bmatrix}_k [X, Y, Z] \tag{6}$$

where $\{\bar{Q}\}_k$, $\{\sigma\}_k$ and $\{\varepsilon\}_k$ are transformed stiffness matrix, stress and strain vectors of the kth lamina, respectively and (α_x, α_y)and (β_{xx}, β_{yy}) are the thermal and hygroscopic expansion coefficients along x, y, z, direction; (α_{xy}, β_{xy}) are shear coefficients in x,y plane respectively. These can be obtained from the thermal and moisture coefficients in the longitudinal (α_1,β_1,) and transverse (α_2, β_2) directions of the fibers using transformation matrix. T (X, Y, Z) is the uniform temperature and moisture field distribution.

Substituting Eq. (3) into Eq. (5) and integrating through thickness gives a relationship between stress resultants and mid-plane strain which are given as [22].

$$\begin{Bmatrix} N_i \\ M_i \\ P_i \end{Bmatrix} = \begin{bmatrix} A_{ij} & B_{ij} & E_{ij} \\ B_{ij} & D_{ij} & F_{ij} \\ E_{ij} & F_{ij} & H_{ij} \end{bmatrix} \begin{Bmatrix} \varepsilon_j^0 \\ k_j^0 \\ k_j^2 \end{Bmatrix} - \begin{Bmatrix} N_i^{HT} \\ M_i^{HT} \\ P_i^{HT} \end{Bmatrix} \quad \text{(i, j=1, 2, 6)} \tag{7a}$$

$$\begin{Bmatrix} Q_2 \\ Q_1 \end{Bmatrix} = \begin{bmatrix} A_{4j} & D_{4j} \\ A_{5j} & D_{5j} \end{bmatrix} \begin{Bmatrix} \varepsilon_j^0 \\ k_j^2 \end{Bmatrix}; \begin{Bmatrix} R_2 \\ R_1 \end{Bmatrix} = \begin{bmatrix} D_{4j} & F_{4j} \\ D_{5j} & F_{5j} \end{bmatrix} \begin{Bmatrix} \varepsilon_j^0 \\ k_j^2 \end{Bmatrix} \quad \text{(j=4, 5)} \tag{7b}$$

where

stress resultants per unit length are

$$\{N_i\} = \left[N_{ix} \quad N_{iy} \quad N_{ixy}\right]^T, \; \{M_i\} = \left[M_{ix} \quad M_{iy} \quad M_{ixy}\right]^T \text{ and } \{P_i\} = \left[P_{ix} \quad P_{iy} \quad P_{ixy}\right]^T \tag{8}$$

expressed in terms of mid plane strains and curvatures [23,24].

The hygrothermal stress and moments resultants per unit length due to temperature and moisture change are calculated and the equivalent hygrothermal loads are defined as [3].

$$N_i^{HT} = [N]^T + [N]^C,\ M_i^{HT} = [M]^T + [M]^C,\ P_i^{HT} = [P]^T + [P]^C \tag{9}$$

For the plate subjected to uniform temperature and moisture rise (U.T) which can be expressed as:

$$[T, C] = \{T_0, C_0\} \tag{10}$$

The potential energy (Π_1) of the laminated composite plates can be expressed as

$$\Pi_1 = \frac{1}{2}\iint_R \begin{bmatrix} (N_i + M_i + P_i)\varepsilon_{xx} + (N_i + M_i + P_i)\varepsilon_{yy} \\ + (N_i + M_i + P_i)\gamma_{xy} + \bar{Q}_1\gamma_{xz} + \bar{Q}_2\gamma_{yz} \end{bmatrix} dx\, dy \tag{11}$$

Due to uniform change in temperature and moisture, pre buckling stresses, i.e., in plane hygrothermal compressive stress resultants in the plate are generated. These resultants are the reasons for the buckling. The potential energy (Π_2) due to the in plane hygrothermal stress resultants is expressed as:

$$\begin{aligned} \Pi_2 &= \frac{1}{2}\int_A \left[N_x (w,_x)^2 + N_y (w,_y)^2 + 2N_{xy}(w,_x)(w,_y) \right] dA \\ &= \frac{1}{2}\int_A \begin{Bmatrix} w,_x \\ w,_y \end{Bmatrix}^T \begin{bmatrix} N_x & N_{xy} \\ N_{xy} & N_y \end{bmatrix} \begin{Bmatrix} w,_x \\ w,_y \end{Bmatrix} dA \end{aligned} \tag{12}$$

where, N_x, N_y and N_{xy} are in plane hygrothermal compressive stress resultants per unit length. In the present study, a C^0 nine-noded isoparametric finite element with 7 DOFs per node is employed. For this type of element, the displacement vector and the element geometry are expressed as

$$\{\Lambda\} = \sum_{i=1}^{NN} \varphi_i \{\Lambda\}_i; \qquad x = \sum_{i=1}^{NN} \varphi_i x_i; \quad \text{and} \qquad (13) \qquad y = \sum_{i=1}^{NN} \varphi_i y_i$$

where φ_i is the interpolation function for the ith node, $\{\Lambda\}_i$ is the vector of unknown displacements for the ith node, NN is the number of nodes per element and x_i and y_i are Cartesian Coordinates of the ith node.

The linear mid plane strain vector as given in Eq. (5) can be expressed in terms of mid plane displacement field; and then energy is computed for each element and then summed over all the elements to get the total potential energy of the system. Eq. (13) can be written as

$$\Pi_1 = \sum_{e=1}^{NE} \Pi_1^{(e)} \tag{14}$$

where, NE is the number of elements and $\Pi^{(e)}$ is the elemental total potential energy which can be expressed as

$$\begin{aligned} \Pi_2 &= \sum_{e=1}^{NE} \left[\frac{1}{2} \{\Lambda^{(e)}\}^T \left[K^{*(e)} \right] \{\Lambda\}^{(e)} - \{\Lambda^{(e)}\}^T \left[F_{HT}^{(e)} \right] \right] \\ &= \frac{1}{2}\{q\}^T [K]\{q\} - \{q\}^T \left[F^{HT} \right] \\ &\text{with } [K] = [K_g] + [K_s] \end{aligned} \tag{15}$$

where, global buckling stiffness matrix [K_g], shear stiffness matrix[K_s], global displacement vector {q} are defined as appendix and hygrothermal load vector [F^{HT}] is force vector.

Using finite element model Eq. (13), Eq. (12) can also be written as

$$\Pi_2 = \sum_{e=1}^{NE} \Pi_2^{(e)}$$

$$= \frac{1}{2}\sum_{e=1}^{NE}\{\Lambda\}^{T(e)}\lambda\left[K_g\right]^{(e)}\{\Lambda\}^{(e)}\,dA \tag{16}$$

where, λ and $\left[K_g\right]$ are defined as the thermal buckling load parameters and the global geometric stiffness matrix, respectively. Adopting Gauss quadrature integration numerical rule, the element linear and geometric stiffness matrix respectively can be obtained by transforming expression in x, y coordinate system to natural coordinate system:ξ, η.

Micromechanical Approach

The material properties of the fiber composite at different moisture concentration and temperature are evaluated using micromechanical model. Since the effect of temperature and moisture concentration is dominant in matrix material. The degradation of the fiber composite material properties is estimated by degrading the matrix property only. The matrix mechanical property retention ratio is expressed as [35].

$$F_m = \left[\frac{T_{gw} - T}{T_{g0} - T_0}\right]^{\frac{1}{2}} \tag{17}$$

where T=To+ΔT and T is the temperature at which material property is to be predicted; To is the reference temperature, ΔT=increase in temperature from reference temperature, Tgw and Tgo are glass transition temperature for wet and reference dry conditions, respectively. The glass transition temperature for wet material is determined as [35].

$$T_{gw} = \left(0.005C^2 - 0.10C + 1.0\right)T_{g0} \tag{18}$$

where, C=Co is the weight percent of moisture in the matrix material. Co=0 weight percent and C is the increase in moisture content. The elastic constants are obtained from the following equations [35].

$$E_{11} = E_{f1}V_f + F_m E_m V_m$$

$$E_{22} = \left(1-\sqrt{V_f}\right)F_m E_m + \frac{F_m E_m \sqrt{V_f}}{1-\sqrt{V_f}\left(1-\frac{F_m E_m}{E_{f2}}\right)} \tag{19}$$

$$G_{12} = \left(1-\sqrt{V_f}\right)F_m G_m + \frac{F_m G_m \sqrt{V_f}}{1-\sqrt{V_f}\left(1-\frac{F_m G_m}{G_{f12}}\right)} \tag{20}$$

$$\nu_{12} = \nu_{f12}V_f + \nu_m V_m \tag{21}$$

where "V" is the volume fraction and subscripts "f" and "m" are used for fiber and matrix, respectively. The effect of increased temperature and moisture concentration on the coefficients of thermal expansion (α) and hygroscopic expansion (β) is opposite from the corresponding effect on strength and stiffness. The matrix hygrothermal property retention ratio is approximated as

$$F_h = \frac{1}{F_m} \tag{22}$$

Coefficients of thermal expansion are expressed as [35].

$$\alpha_{11} = \frac{E_{f1}V_f\alpha_{f1} + F_m E_m V_m F_h \alpha_m}{E_{f1}V_f + F_m E_m V_m} \tag{23}$$

$$\alpha_{22} = \left(1+\nu_{f12}\right)V_f\alpha_{f2} + \left(1+\nu_m\right)V_m F_h \alpha_m - \nu_{12}\alpha_{11} \tag{24}$$

Similarly, coefficients of hygroscopic expansion are expressed as [35].

$$\beta_{11} = \frac{E_{f1}V_f\beta_{f1} + F_m E_m V_m F_h \beta_m}{E_{f1}V_f + F_m E_m V_m} \tag{25}$$

$$\beta_{22} = \left(1+\nu_{f12}\right)V_f\beta_{f2} + \left(1+\nu_m\right)V_m F_h \beta_m - \nu_{12}\beta_{11} \tag{26}$$

The elastic constants are obtained from the following equations given in [5].

$$E_{11} = VfEf + VmEm \tag{27}$$

$$\frac{1}{E_{22}} = \frac{Vf}{Ef} + \frac{Vm}{Em} - VfVm\frac{Vf^2\frac{Em}{Ef} + \upsilon m^2\frac{Ef}{Em} - 2\upsilon f\upsilon m}{VfEf + VmEm} \tag{28}$$

$$\frac{1}{G_{12}} = \frac{Vf}{Ef} + \frac{Vm}{Gm} \tag{29}$$

$$\upsilon_{12} = Vf\upsilon f + Vm\upsilon m \tag{30}$$

where "V" is the volume fraction and subscripts "f" and "m" are used for fiber and matrix, respectively. The effect of increased temperature and moisture concentration on the coefficients of thermal expansion (α) and hygroscopic expansion (β) is opposite from the corresponding effect on strength and stiffness.

Coefficients of thermal expansion are expressed as [5].

$$\alpha_{11} = \frac{VfEf\alpha f + VmEm\alpha m}{VfEf + VmEm} \tag{31}$$

$$\alpha_{22} = (1+\upsilon f)Vf\alpha f + (1+\upsilon m)Vm\alpha m - \upsilon_{12}\alpha_{11} \tag{32}$$

Similarly, coefficients of hygroscopic expansion are expressed as [5].

$$\beta_{11} = \frac{VfEfcfm\beta f + VmEm\beta m}{E_{11}(Vf\rho fcfm + Vm\rho m)}\rho \tag{33}$$

$$\beta_{22} = \frac{Vf(1+\upsilon f)cfm\beta f + Vm(1+\upsilon m)\beta m}{(Vf\rho fcfm + Vm\rho m)}\rho - \upsilon_{12}\beta_{11} \tag{34}$$

other constants are related as [5].

$$\rho = Vf\rho f + Vm\rho m \tag{35}$$

$$Vm + Vf = 1 \tag{36}$$

The Equation of Motion and Its Solution Techniques

Governing Equation, Steps For the Direct Iterative Technique and solution Technique are given in [27, 28, 29, 30, 31, 32, 35, 36, 37, 38, 39].

The governing equation for hygrothermal buckling of laminated composite plate can be derived using Variational principle [27] which is the generalization of the principle of virtual displacement. For the prebuckling analysis, the first variation of total potential energy $\Pi = (\Pi_1 + \Pi_2)$ must be zero.

$$[K]\{q\} = \left[F^{HT}\right] \tag{37}$$

For the critical buckling state corresponding to the neutral equilibrium condition, the second variation of total potential energy (Π) must be zero. Following this conditions, ones can be obtained as standard eigenvalue problem

$$[K]\{q\} = \lambda\left[K_g\right]\{q\}$$

The Eq. 37 can be rewritten as:

$$\left|[K] + \lambda\left[K_g\right]\right| = 0 \tag{21}$$

where

[K], and [K_g] are the stiffness matrix and geometric stiffness matrix respectively.

The pre buckling equations are solved to compute the stress state in the plate subjected a hygrothermal loads corresponding to unit temperature and moisture rise, neglecting the geometric stiffness matrix. Based on this stress state, the geometric stiffness matrix is constructed. To compute the critical temperature and moisture at which buckling occurs are solved.

The stiffness matrix [K] and geometric stiffness matrix [K_g] are random in nature, being dependent on the system geometric and hygrothermo-elastic properties. Therefore, the eigenvalues and eigenvectors also become random. The Eq. (37) can be solved with the help probabilistic FEM combined with direct iterative in conjunction with perturbation technique or Monte Carlo simulation (MCS) to compute the mean and variance of the hygrothermal buckling load.

Results and Discussions

The direct iterative based stochastic finite element method [DISFEM] is used to illustrate the hygrothermally induced post buckling response considering different random system parameters of laminated composite plate i.e. symmetric and antisymmetric as shown in Fig.2.

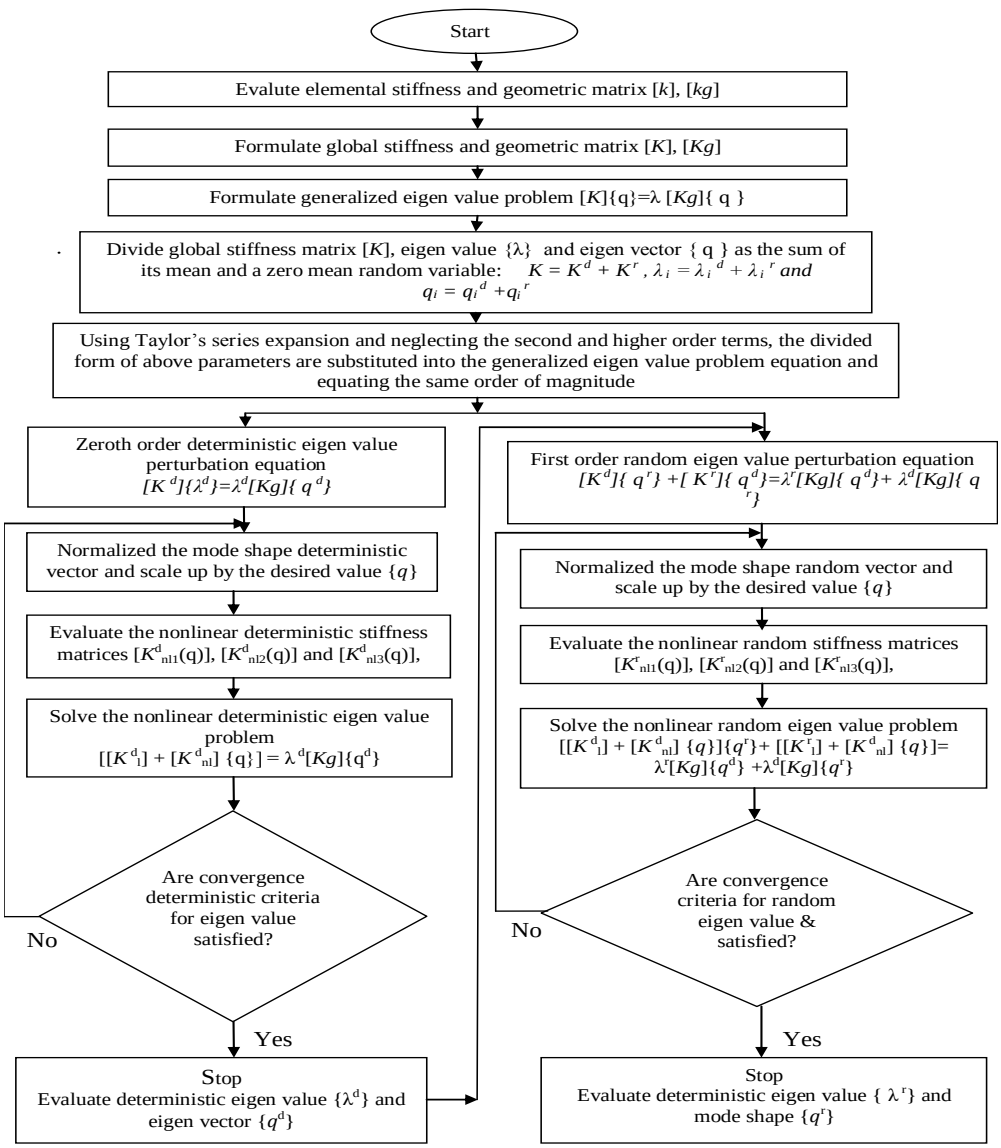

FIG. 2 COMPUTATIONAL MODEL FOR STOCHASTIC ANALYSIS

In this section, the mean post buckling load and effect of randomness in the system properties on the postbuckling load of geometrically non-linear laminated composite plate resting on nonlinear elastic foundations has been investigated in hygrothermal environments. The present methodology for mean and coefficient of variation of post buckling load in hygrothermal environment is verified with available results in literature and independent MCS. The lamina coefficients of hygroscopic expansion, thermal expansion and foundation stiffness parameters including geometric and material properties are modeled as basic random variables (RVs) as stated earlier. However, the results are only presented taking coefficient of variation (COV) of the system property equal to 0.10

[31] as the nature of the SD (standard deviation) variation which is linear and passing through the origin. Hence, the presented results would be sufficient to extrapolate the results for other COV value keeping in mind the limitation of the first order perturbation technique (FOPT) [11,25]. The thickness of all the lamina is assumed to be constant and of same material without varying individual property of materials used. The results obtained have been compared with MCS and those available in the literature. For the present study, a nine nodded serendipity element, which results in 63 degree of freedom (DOFs) per element modified form HSDT based C^0 finite element model, has been used for discretizing the laminate. Based on convergence, an (8x8) mesh has been used throughout for evaluation of the results. Programme in Mat lab is developed for the computational analysis. Results have been computed by employing the full (3x3) integration rule for bending stiffness matrices, hygrothermal load vector and the geometric stiffness matrices and the reduced (2x2) integration rule for computing the shear stiffness matrices to avoid shear locking in the thin plates.

All edges simply supported (SSSS (S1)):

$$u = w = \theta_y = \psi_y = 0, at\ x = 0, a; \quad v = w = \theta_x = \psi_x = 0\ at\ y = 0, b\ ;$$

All edges simply supported (SSSS (S2)):

$$v = w = \theta_y = \psi_y = 0, at\ x = 0, a; \quad u = w = \theta_x = \psi_x = 0\ at\ y = 0, b\ ;$$

All edges clamped (CCCC):

$$u = v = w = \psi_x = \psi_y = \theta_x = \theta_y = 0, at\ x = 0, a \quad and\ y = 0, b;$$

The plate geometry used is characterized by aspect ratios (a/b) = 1and 2, side to thickness ratios (a/h) =5, 10, 30, 40, 60, 80 and 100. The mean values of coefficients of hygroscopic expansion, coefficients of thermal expansion, geometric properties, material constants and foundation stiffness parameters are used for computation. We consider now a second steps as the elastic constants, thermal expansion coefficients and coefficients of hygroscopic expansion of each layers which are assumed to be linear function of temperature and moisture. The only exception is the Poisson's ratio, which can reasonably be assumed as constant due to weakly dependency on temperature and moisture change. The coefficient of hygroscopic expansion β_{11}in longitudinal direction is considered to be zero because moisture contents have negligible effects on fiber and have effects on matrix in transverse direction. Because the coefficients of variation of material and geometric properties varying from 0 to 20% with a/h= 10, 20, 30, 40, 50, 80 and 100 subjected to uniform temperature and moisture rise have been considered. The lamina material properties such as E_{11}, E_{22}, G_{12}, G_{13}, G_{23}, α_1, α_2, β_2 and h are modeled as basic RVs. E_{11}, and E_{22} are longitudinal and transverse elastic modulii, respectively, G_{12}, G_{13}, G_{23} are shear modulii, α_1 and α_2 are longitudinal and transverse coefficients of thermal expansion, β_1 and β_2 are longitudinal and transverse coefficients of hygroscopic expansion and h is the total thickness of the composite laminate considered for the analysis. The input random variables b_i for post buckling is related and sequenced as

$$b_1 = E_{11},\ b_2 = E_{22},\ b_3 = G_{12},\ b_4 = G_{13},\ b_5 = G_{23},$$

$$b_6 = V_{12},\ b_7 = \alpha_1,\ b_8 = \alpha_2,\ b_9 = \beta_2 \text{ and } b_{10} = h.$$

The input random variables for plate resting on elastic foundations are related as

$$b_1 = E_{11},\ b_2 = E_{22},\ b_3 = G_{12},\ b_4 = G_{13},\ b_5 = G_{23},$$

$$b_6 = V_{12},\ b_7 = \alpha_1,\ b_8 = \alpha_2,\ b_9 = \beta_2,\ b_{10} = k_1,\ b_{11} = k_2.$$

The non dimensionalised foundation parameters used for the analysis can be illustrated as

$$k_1 = K_3 a^4 / E_{22}^d h^3; \;\; k_2 = K_2 a^4 / E_{22}^d h^3 \;;$$

For the temperature and moisture dependent material properties (TD), the relation among elastic constants is given as:

$$\begin{aligned}
E_{11} &= E_{10}\left(1 + E_{111}T_1 + E_{111}C_1\right), \\
E_{22} &= E_{20}\left(1 + E_{211}T_1 + E_{211}C_1\right) \\
G_{12} &= G_{120}\left(1 + G_{121}T_1 + G_{121}C_1\right), \\
G_{13} &= G_{130}\left(1 + G_{131}T_1 + G_{131}C_1\right) \\
G_{23} &= G_{230}\left(1 + G_{231}T_1 + G_{231}C_1\right), \\
\alpha_1 &= \alpha_{10}\left(1 + \alpha_{11}T_1\right), \alpha_2 = \alpha_{20}\left(1 + \alpha_{21}T_1\right), \\
\beta_1 &= \beta_{10}\left(1 + \beta_{11}C_1\right), \beta_2 = \beta_{20}\left(1 + \beta_{21}C_2\right)
\end{aligned}$$

where, temperature and moisture dependent material properties are defined as

$$\begin{aligned}
E_{111} &= -0.5 \times 10^{-3} \\
E_{221} &= G_{121} = G_{131} = G_{231} = -0.2 \times 10^{-3} \\
\alpha_{11} &= \alpha_{21} = 0.5 \times 10^{-3} \\
\beta_{11} &= \beta_{21} = 0.5 \times 10^{-3}
\end{aligned}$$

All layers are of equal thickness for the temperature and moisture independent material properties (TID) E_{11}, E_{21}, G_{121}, G_{131}, G_{231}, α_{11}, α_{21}, β_{11} and β_{21} quantities are taken equal to zero.

Material Properties for the study are given in [5].

T_0=25; C_0=0; V_f =0.6; E_f=230.0*1e9; G_f=9.0*1e9;

cf_m=0; ρc=1.5; G_m= 0.10 & 0.155*G_f; V_f =0.203;

α_f=-0.54*1e-6; ρ_f=1750; cf_m=0; V_m= 0.34;

γ_m=45*1e-6; ρ_m=1200; β_m=2.68*1e-3; β_f=0; T=T_0+ΔT; C=C_0+ΔC; E_m= (3.51-0.003*T-0.142*C)*1e9; V_m=1-V_f; G_x= (V_f/G_f) + (V_m/G_m); G_{12}=1/G_x; G_{13}=G_{12}; G_{23}=0.5*G_{12};

V_{21}=V_{12}*E_2/E_1; α_{12} = 0; α_0=1e-6; β_{12} = 0; β_0=0.00;

Table 1(*a*) and 1(*b*) are compared for validation of mean buckling and post buckling analysis. Tables 2, 3(*a*), 3(*b*), 3(*c*), 3(*d*), 4(*a*), 4(*b*), 4(*c*), 5(*a*), 5(*b*), 5(*c*), 6(*a*), 6(*b*),6(*c*), 7(*a*), 7(*b*),7(*c*), 8(*a*), 8(*b*), 8(*c*) and 8(*d*) give results generated for various combinations of random variables with geometric parameters for second order statistics for post buckling and buckling load of laminated composite plate resting on elastic foundations in hygrothermal environment: The numerical values and relationship between the mean values of the material properties for graphite epoxy composite with change in temperature and moisture.

Validation Study: Mean and Standard Deviations without Foundations

In order to validate the proposed outlined approach, the results for the mean and standard deviation are compared with those available in the literature and an independent Monte Carlo simulation technique.

1) Mean Hygrothermal Buckling and Post Buckling Analysis

Table 1 (a), 1(b) show the comparison of buckling loads Nx (KN) for perfect $(\pm 45^0{}_2)_T$ laminated square plates (a/h=10) , a/b=1.0, where dimensionless plate length a=0.05, plate width b=0.05, T_0=25^{0}C, C_0=0, simple support S2 under four sets of environmental conditions. Uniaxial compression, Total temperature $T=T_0+\Delta T$ where T_0 =Initial temperature and ΔT is rise in temperature, total moisture concentration $C=C_0+\Delta C$ where C_0 is initial moisture contents in percentage and ΔC is rise in moisture with those available results [5]. The results are in good agreements. It can be observed that foundation parameters have significant effects as shown by bounds of buckling load and post buckling strength. The material properties of the composite plate are: E_1/E_2 =25; G_{12}=0.5E_2; G_{23}=0.2E_2; E_{20}=1*1e5; v_{12}=0.25; E_{10}=m_1*E_{20}; G_{120}=m_2*E_{20}; G_{130}=G_{120}; G_{230}=m3*E_{20}; v_{21}=v_{12}*E_{20}/E_{10}; α_{110} =1*1e-6; α_{210} =10.0*1e-6; α_{12} = 0; αo =1e-6;. The non- dimensional foundation parameters can be given: as; K_1= k_1*D_{11} / a^4, K_2= k_2*D_{11}/ a^2 and (T_{cr} = T_1* α_0*1000). The results obtained are in good agreements and validated with the available literature results of [14].

Table1(c), shows the comparison of dimensionless buckling load of symmetric and antisymmetric cross-ply[0^0/90^0]2T laminated composite square plate subjected to uniaxial compression is estimated for different fiber-volume fraction *Vf* (= 0.4, 0.5, 0.6)and moisture concentration(ΔC %), Plate thickness ratio (*a/h*) = 10. It can be seen that the present results using C0 non-linear finite element method are in good agreements with Cbeivshev based analytical solution of [36]. It is seen that the buckling load decreases with the increase in moisture concentration due to degradation in material properties at higher moisture concentration.

TABLE 1(A) COMPARISON OF BUCKLING LOADS NX (KN) FOR PERFECT $(\pm 45^0{}_2)_T$ LAMINATED SQUARE PLATES (A/H=10) , A/B=1.0, WHERE DIMENSIONLESS PLATE LENGTH A=0.05, PLATE WIDTH B=0.05, T_0=25^{0}C, C_0=0%, SIMPLE SUPPORT S2 UNDER FOUR SETS OF ENVIRONMENTAL CONDITIONS. UNIAXIAL COMPRESSION, TOTAL TEMPERATURE T=T_0+ΔT WHERE T_0 =INITIAL TEMPERATURE AND ΔT IS RISE IN TEMPERATURE, TOTAL MOISTURE CONCENTRATION C=C_0+ΔC WHERE C_0 IS INITIAL MOISTURE CONTENTS IN PERCENTAGE AND ΔC IS RISE IN MOISTURE.

Lay-up	Environment Conditions	Buckling Load Nx (KN)					
		Shen [5]			Present [HSDT]		
		V_f=0.5	V_f=0.6	V_f=0.7	V_f=0.5	V_f=0.6	V_f=0.7
$(\pm 45^0{}_2)_T$	ΔT=0^{0}C, ΔC=0%	142.740	169.708	203.014	141.1574	171.2263	214.1426
	ΔT=100^{0}C, Δ C=1%	136.434	162.605	195.165	130.7277	159.3173	199.8785
	ΔT=200^{0}C, ΔC=3%	129.726	154.992	186.698	122.2797	149.2539	187.0655
	ΔT=300^{0}C, ΔC=5%	122.545	146.784	177.511	116.7270	142.6928	178.7516

TABLE 1(B) COMPARISON OF POST BUCKLING LOADS NX (KN) FOR PERFECT $(\pm 45^0{}_2)_T$ LAMINATED SQUARE PLATES (A/H=10) , A/B=1.0, WHERE DIMENSIONLESS PLATE LENGTH A=0.05, PLATE WIDTH B=0.05, T_0=25^{0}C, C_0=0%, SIMPLE SUPPORT S2 UNDER FOUR SETS OF ENVIRONMENTAL CONDITIONS. UNIAXIAL COMPRESSION, TOTAL TEMPERATURE T=T_0+ΔT WHERE T_0 =INITIAL TEMPERATURE AND ΔT IS RISE IN TEMPERATURE, TOTAL MOISTURE CONCENTRATION C=C_0+ΔC WHERE C_0 IS INITIAL MOISTURE CONTENTS IN PERCENTAGE AND ΔC IS RISE IN MOISTUREPERCENTAGE. FIBER VOLUME FRACTION (V_F=0.6).

W_{max}/h	Post Buckling Load Nx (KN)							
	Shen [5]				Present [HSDT]			
	ΔT=0^{0}C, ΔC=0.00	ΔT=100^{0}C, ΔC=0.01	ΔT=200^{0}C, ΔC=0.03	ΔT=300^{0}C, ΔC=0.05	ΔT=0^{0}C, ΔC=0.00	ΔT=100^{0}C, ΔC=0.01	ΔT=200^{0}C, ΔC=0.03	ΔT=300^{0}C, ΔC=0.05
0.0	169.7308	162.6052	154.9923	146.7844	171.2263	161.3355	154.1767	150.2451
0.1	170.0337	162.9066	155.2690	147.0355	173.0117	166.2605	156.0044	153.3669
0.2	171.0109	163.8121	156.1001	147.0355	173.7823	166.6820	156.2569	153.7263
0.3	172.6439	165.3253	157.4890	149.0504	174.5664	166.9032	157.9553	154.2129
0.4	174.9390	167.4520	159.4412	150.8225	177.3027	167.6058	159.660	155.0469
0.5	177.9051	170.2007	161.9646	153.1134	180.2628	168.3383	161.9241	155.2371
0.6	181.5356	173.5822	165.0693	155.9322	181.1877	171.1708	163.8541	156.4457
0.7	185.8984	177.6096	168.7674	159.2904	184.1877	175.7278	166.49 0	158.6815
0.8	190.9563	182.2982	173.0735	163.2014	190.4932	176.2758	170.6950	163.0031
0.9	196.7476	187.6662	178.0042	167.6808	192.2369	181.1966	173.1806	165.7838

TABLE 1(C) COMPARISON OF DIMENSIONLESS BUCKLING LOAD OF SYMMETRIC AND ANTISYMMETRIC CROSS-PLY $[0^0/90^0]_{2T}$ LAMINATED COMPOSITE SQUARE PLATE SUBJECTED TO UNIAXIAL COMPRESSION IS ESTIMATED FOR DIFFERENT FIBER-VOLUME FRACTION *VF* (= 0.4, 0.5, 0.6) AND MOISTURE CONCENTRATION(ΔC %). PLATE THICKNESS RATIO (*A*/*H*) = 10.

Vf	ΔC %	Pandey et al. [36]	Present HSDT
0.4	0	14.178	16.545
	1	13.253	14.747
	3	11.712	12.111
0.5	0	17.405	19.823
	1	16.183	17.826
	3	14.703	14.835
0.6	0	20.913	23.669
	1	19.742	21.524
	3	18.304	18.219

2) Validation Result for Random Material Properties

The present results of random hygrothermal buckling load of laminated composite plate Without Foundation (k1=00, k2=00) and plate resting on Pasternak (k_1=100, k_2=10) elastic foundation obtained from present perturbation approach have been compared and validated with an independent MCS approach. Fig. 3 plots the normalized standard deviation, coefficient of variation (SD/mean) of the hygrothermal buckling load versus the coefficient of variation (SD/mean) of the random material constant for an all edges simply supported SSSS (S2), *a*/*h*=20, volume fraction Vf=0.6, angle ply antisymmetric $(\pm 45^0)_{2T}$ square laminated composite plate, ΔT= 100 ^{0}C, ΔC= 0.010, with hygrothermo-mechanical properties varying from 0 to 20% [34]. It is assumed that one of the material properties (i.e., E_{11}) changes at a time keeping other as a deterministic, with their mean value of the material properties. The present results are obtained by using first-order perturbation approach based on HSDT and the independent MCS approach. For the MCS approach, the samples are generated using Mat Lab to fit the desired mean and SD. These samples used in response are solved repeatedly, adopting conventional eigen value procedure, to generate a sample of the hygrothermal buckling load. The number of samples used for MCS approach is 12,000 based on satisfactory convergence of the results. The normal distribution has been assumed for random number generations in MCS. However, the present perturbation approach used in the study does not put any limitation with regard to probability distribution of the system property. This is an advantage over the MCS. From the figure, it is clear that close correlation is achieved between two results.

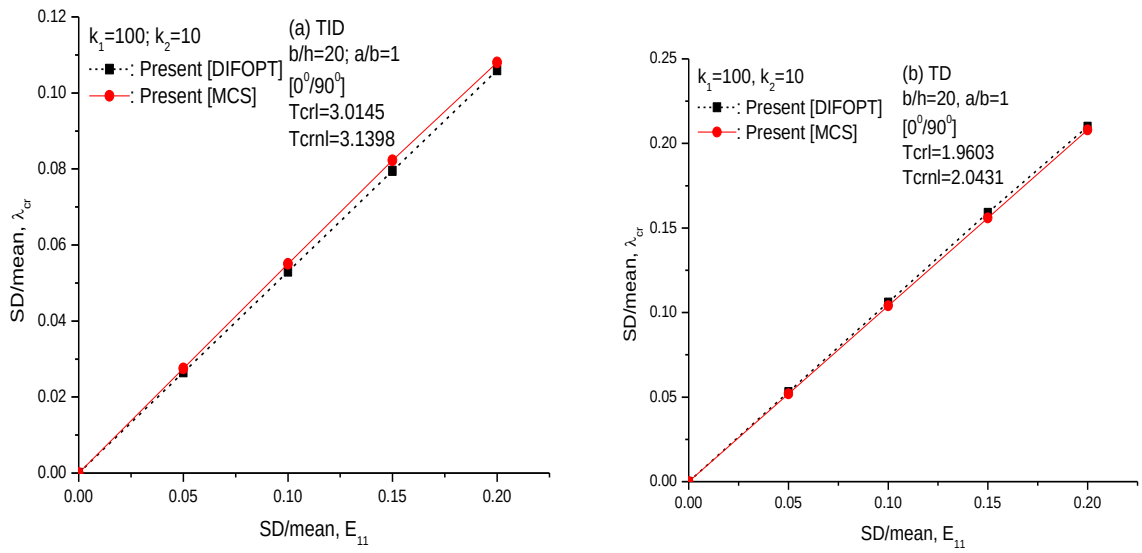

FIG. 3 VALIDATION OF PRESENT DIRECT ITERATIVE STOCHASTIC FIRST ORDER PERTURBATION TECHNIQUE.(DISFOPT) RESULTS WITH INDEPENDENT MCS RESULTS FOR: (A) TEMPERATURE AND MOISTURE INDEPENDENT MATERIAL PROPERTIES (TID) (B) TEMPERATURE AND MOISTURE DEPENDENT MATERIAL PROPERTIES (TD).

Parametric Analysis of Second Order Statistics without Foundations

Table 2 shows the effects of the variation of individual input random variables b_i, {(i =1 to 11) = 0.10} on the expected mean (T_{crl}) and dimensionless coefficient of variation (λ_{crl}) of the hygrothermal buckling load N_x (KN) for perfect angle ply $(\pm 45^0{}_2)_T$ square plates resting on Winkler (k_1=100, k_2=00), Pasternak (k_1=100, k_2=10) elastic foundations, (a/h=10), fiber volume fraction (V_f=0.6), initial temperature T_0=25^{0}C, initial moisture contents in percentage C_0=0, Simple Support (S2) under environmental conditions. The expected mean hygrothermal buckling loads are given in brackets (KN). T_{crl} - Linear solution. It is observed that mean hygrothermal buckling load increases drastically when plate is supported on Pasternak elastic foundation, the coefficient of variation for material property E_{11} is of significance as compared with other random variables for with and without rise in temperature and moisture.

TABLE 2 EFFECTS OF INDIVIDUAL INPUT RANDOM VARIABLES B_I, {(I =1 TO 11) = 0.10} ON THE EXPECTED MEAN (T_{CRL}) AND DIMENSIONLESS COEFFICIENT OF VARIATION (λ_{CRL}) OF THE HYGROTHERMAL BUCKLING LOAD N_X (KN) FOR PERFECT ANGLE PLY $(\pm 45^0{}_2)_T$ SQUARE PLATES RESTING ON WINKLER (K_1=100, K_2=00), PASTERNAK (K_1=100, K_2=10) ELASTIC FOUNDATIONS, (A/H=10), FIBER VOLUME FRACTION (V_F=0.6), INITIAL TEMPERATURE T_0=25^{0}C , INITIAL MOISTURE CONTENTS IN PERCENTAGE C_0=0%, SIMPLE SUPPORT (S2) BOUNDRY CONDITIONS UNDER ENVIRONMENTAL CONDITIONS . THE MEAN HYGROTHERMAL BUCKLING LOADS ARE GIVEN IN BRACKETS (KN). T_{CRL} - LINEAR SOLUTION.

b_i	(k_1=100, k_2=00)		(k_1=100, k_2=10)	
	COV, λ_{crl}		COV, λ_{crl}	
	ΔT=0^{0}C, ΔC=0%	ΔT=100^{0}C, ΔC=1%	ΔT=0^{0}C, ΔC=0%	ΔT=100^{0}C, ΔC=1%
E_{11} (i=1)	(T_{crl}=186.3044) (λ_{crl}= 0.0325)	(T_{crl}=173.3735) (λ_{crl}= 0.0330)	(T_{crl}=276.7238) (λ_{crl}= 0.1360)	(T_{crl}= 256.9799) (λ_{crl}= 0.1364)
E_{22} (i=2)	0.0190	0.0011	0.0127	7.562e-04
G_{12}(i=3)	7.575e-04	7.705e-04	5.089e-04	5.176e-04
G_{13} (i=4)	0.0502	0.0501	0.0339	0.0340
G_{23} (i=5)	0.0251	0.0251	0.0169	0.0170
V_{12} (i=6)	0.0028	2.0061e-04	0.0019	1.342e-04
α_{11} (i=7)	2.139e-05	1.527e-04	1.440e-05	1.030e-04
α_{22} (i=8)	4.671e-04	0.0021	3.145e-04	0.0014
β_{22} (i=9)	0	4.282e-04	0	2.889e-04
k_1 (i=10)	0.0048	0.0048	0.0032	0.0032
k_2 (i=11)	0	0	0.0327	0.0325

Table 3 (a) & (b) illustrares effects of boundary conditions and input random variables bi{i=1…9, 7-8, 9 and 10, 11= 0.10} on the buckling loads N_x (KN) for perfect angle ply $(\pm 45^0{}_2)_T$ square plate resting on Winkler (k_1=100, k_2=0) and Pasternak (k_1=100, k_2=10) elastic foundations, plate thickness ratio (a/h=20) ,V_f=0.6, T_0=25^{0}C, C_0=0 under Environmental Conditions. It is seen that the mean hygrothermal load is higher for clamp support as compared with other support for with and without rise in temperature and moisture. The coefficient of variation of hygrothermal load is also varied for different combinations of random variables for Winkler elastic foundations. The mean hygrothermal load for Pasternak elastic foundations further increases and it is higher for clamp support as compared with other support for with and without rise in temperature and moisture. The coefficient of variation of hygrothermal load is also varied for different combinations of random variables for Pasternak elastic foundations.

Table 3(c) shows the effects of boundary conditions and input random variables bi{i=1…9, 7-8, .9 and 10 = 0.10} on the expected mean (T_{crnl}) and dimensionless coefficient of variation (λ_{crnl}) of the hygrothermal post-buckling load N_x (KN) for perfect angle ply $(\pm 45^0{}_2)_T$ square laminated composite plate, plate thickness ratio (a/h=30), fiber volume fraction (V_f=0.6), initial temperature T_0=25^{0}C, initial moisture C_0=0, temperature and moisture independent material properties(TID), under environmental conditions. It is seen that without increase of temperature and moisture if amplitude ratio increased, then expected mean post-buckling load increases for different support, it increases more for clamped support.COV decreases in general for all support. On increase of temperature and moisture contents, there is further decrease in expected mean and COV further decrease, it shows appreciable change for clamped support conditions for various combinations of input random variables as shown in table.

TABLE 3 (A) EFFECT OF BOUNDARY CONDITIONS AND INPUT RANDOM VARIABLES BI{I=1…9, 7-8, .9 AND 10, 11= 0.10} ON THE EXPECTED MEAN (T_{CRL}) AND DIMENSIONLESS COEFFICIENT OF VARIATION (λ_{CRL}) OF THE HYGROTHERMAL BUCKLING LOAD N_X (KN) FOR PERFECT ANGLE PLY $(\pm 45^0{}_2)_T$ SQUARE LAMINATED COMPOSITE PLATE RESTING ON WINKLER (K1=100, K2=0) ELASTIC FOUNDATION, PLATE THICKNESS RATIO (A/H=20) , FIBER VOLUME FRACTION (V_F=0.6), INITIAL TEMPERATURE T_0=25^{0}C, INITIAL MOISTURE C_0=0% UNDER ENVIRONMENTAL CONDITIONS.

BCs	(k1=100, k2=00)									
	ΔT=0^{0}C, ΔC=0%					ΔT=100^{0}C, ΔC=1%				
	Mean, T_{crl}	COV, λ_{crl}				Mean, T_{crl}	COV, λ_{crl}			
		bi					bi			
		(i=1...9)	(i=7.-8)	(i=9)	(i=10,11)		(i=1.. 9)	(i=7.-8)	(i=9)	(i=10,11)
SSSS S1	51.950	0.0755	8.45e-04	0	0.0050	49.872	0.0713	0.0039	7.765e-04	0.0050
SSSS S2	51.033	0.0754	8.60e-04	0	0.0051	49.069	0.0712	0.0040	7.892e-04	0.0050
CCCC	61.865	0.0658	7.101e-04	0	0.0030	59.345	0.0617	0.0033	6.526e-04	0.0030
CSCS	55.170	0.0729	7.96e-04	0	0.0046	53.217	0.0676	0.0036	7.277e-04	0.0045

TABLE 3 (B) EFFECT OF BOUNDARY CONDITIONS AND INPUT RANDOM VARIABLES BI{I=1…9, 7-8, .9 AND 10, 11= 0.10} ON THE EXPECTED MEAN (T_{CRL}) AND DIMENSIONLESS COEFFICIENT OF VARIATION (λ_{CRL}) OF THE HYGROTHERMAL BUCKLING LOAD N_X (KN) FOR PERFECT ANGLE PLY $(\pm 45^0{}_2)_T$ SQUARE LAMINATED COMPOSITE PLATE RESTING ON PASTERNAK (K1=100, K2=10) ELASTIC FOUNDATION, PLATE THICKNESS RATIO (A/H=20) , FIBER VOLUME FRACTION (V_F=0.6), INITIAL TEMPERATURE T_0=25^{0}C, INITIAL MOISTURE C_0=0%, UNDER ENVIRONMENTAL CONDITIONS.

BCs	(k1=100, k2=10)									
	ΔT=0^{0}C, ΔC=0%					ΔT=100^{0}C, ΔC=1%				
	Mean, T_{crl}	COV, λ_{crl}				Mean, T_{crl}	COV, λ_{crl}			
		bi					bi			
		(i=1- 9)	(i=7.-8)	(i=9)	(i=10,11)		(i=1- 9)	(i=7.-8)	(i=9)	(i=10,11)
SSSS S1	64.793	0.1246	6.780e-04	0	0.0202	62.155	0.1236	0.0031	6.231e-04	0.0202
SSSS S2	63.880	0.1254	6.877e-04	0	0.0205	61.360	0.1243	0.0032	6.311e-04	0.0204
CCCC	73.987	0.1028	5.937e-04	0	0.0165	70.940	0.1017	0.0027	5.459e-04	0.0165
CSCS	67.830	0.1156	6.476e-04	0	0.0188	65.323	0.1139	0.0030	5.928e-04	0.0187

TABLE 3 (C) EFFECT OF BOUNDARY CONDITIONS AND INPUT RANDOM VARIABLES BI{I=1…9, 7-8, .9 AND 10 = 0.10} ON THE EXPECTED MEAN (T_{CRNL}) AND DIMENSIONLESS COEFFICIENT OF VARIATION (λ_{CRNL}) OF THE HYGROTHERMAL POST-BUCKLING LOAD N_X (KN) FOR PERFECT ANGLE PLY $(\pm 45^0{}_2)_T$ SQUARE LAMINATED COMPOSITE PLATE, PLATE THICKNESS RATIO (A/H=30) , FIBER VOLUME FRACTION (V_F=0.6), INITIAL TEMPERATURE T_0=25^{0}C, INITIAL MOISTURE C_0=0%, TEMPERATURE AND MOISTURE INDEPENDENT MATERIAL PROPERTIES(TID), UNDER ENVIRONMENTAL CONDITIONS.

BCs	W_{max}/h	TID									
		ΔT=0^{0}C, ΔC=0.00					ΔT=100^{0}C, ΔC=0.01				
		Mean T_{crnl}	COV, λ_{crnl}				Mean T_{crnl}	COV, λ_{crnl}			
			bi					bi			
			(i=1,..10)	i=(7,8)	(i=9)	(i=10)		(i=1.,10)	i=(7, 8)	(i=9)	(i=10)
SSSS(S1)	0.3	19.977	0.097	0.0015	0	0.034	19.624	0.078	0.0067	0.0013	0.035
	0.6	21.963	0.075	0.0013	0	0.034	21.412	0.075	0.0062	0.0012	0.036
	0.9	24.143	0.072	0.0012	0	0.035	23.614	0.071	0.0056	0.0011	0.037
	T_{crl}	17.818	0.088	0.0016	0	0.038	17.383	0.087	0.0076	0.0015	0.038
SSSS(S2)	0.3	19.514	0.080	0.0015	0	0.042	19.287	0.076	0.0068	0.0014	0.039
	0.6	21.516	0.075	0.0014	0	0.034	21.160	0.074	0.0062	0.0012	0.036
	0.9	23.702	0.072	0.0012	0	0.035	23.405	0.072	0.0056	0.0011	0.040
	T_{crl}	17.704	0.087	0.0017	0	0.037	17.295	0.088	0.0076	0.0015	0.039
CCCC	0.3	26.231	0.075	0.0011	0	0.037	26.062	0.070	0.0051	0.0010	0.038
	0.6	29.884	0.075	9.82e-04	0	0.043	29.614	0.073	0.0045	8.88e-04	0.047
	0.9	33.199	0.072	8.84e-04	0	0.053	32.856	0.072	0.0040	8.80e-04	0.049
	T_{crl}	25.937	0.077	0.0011	0	0.038	25.242	0.074	0.0052	8.76e-04	0.040

TABLE 3 (D) EFFECT OF BOUNDARY CONDITIONS AND INPUT RANDOM VARIABLES BI{I=1…9, 7-8, .9 AND 10 = 0.10} ON THE EXPECTED MEAN (T_{CRNL}) AND DIMENSIONLESS COEFFICIENT OF VARIATION (λ_{CRNL}) OF THE HYGROTHERMAL POST-BUCKLING LOAD N_x (KN) FOR PERFECT ANGLE PLY $(\pm 45^0{}_2)_T$ SQUARE LAMINATED COMPOSITE PLATE, PLATE THICKNESS RATIO (A/H=30) , FIBER VOLUME FRACTION (V_F=0.6), INITIAL TEMPERATURE T_0=25^{0}C, INITIAL MOISTURE C_0=0%, TEMPERATURE AND MOISTURE DEPENDENT MATERIAL PROPERTIES(TD), UNDER ENVIRONMENTAL CONDITIONS.

BCs	W_{max}/h	TD									
		$\Delta T=0^0C$, $\Delta C=0.00$					$\Delta T=100^0C$, $\Delta C=0.01$				
		Mean T_{crnl}	COV, λ_{crnl} bi				Mean T_{crnl}	COV, λ_{crnl} bi			
			(i=1,..10)	i=(7,8)	(i=9)	(i=10)		(i=1.,10)	i=(7, 8)	(i=9)	(i=10)
SSSS(S1)	0.3	19.152	0.080	0.0015	0	0.040	18.875	0.081	0.0072	0.0013	0.040
	0.6	21.640	0.076	0.0014	0	0.038	20.388	0.074	0.0066	0.0012	0.035
	0.9	23.487	0.072	0.0013	0	0.038	21.502	0.073	0.0063	0.0011	0.039
	T_{crl}	17.625	0.087	0.0017	0	0.038	16.428	0.088	0.0082	0.0015	0.039
SSSS(S2)	0.3	19.095	0.080	0.0015	0	0.042	18.152	0.077	0.0075	0.0014	0.039
	0.6	20.873	0.075	0.0014	0	0.034	20.684	0.073	0.0065	0.0012	0.036
	0.9	23.546	0.071	0.0013	0	0.036	21.316	0.073	0.0064	0.0012	0.039
	T_{crl}	17.513	0.080	0.0017	0	0.037	16.348	0.087	0.0083	0.0015	0.038
CCCC	0.3	25.733	0.073	0.0011	0	0.038	24.667	0.071	0.0055	9.99e-04	0.039
	0.6	27.691	0.070	0.0011	0	0.039	26.871	0.074	0.0050	9.17e-04	0.045
	0.9	34.261	0.083	8.62e-04	0	0.062	33.258	0.087	0.0041	7.41e-04	0.068
	T_{crl}	25.695	0.073	0.0011	0	0.038	24.041	0.075	0.0056	7.14e-04	0.040

The effects of boundary conditions and input random variables bi{i=1…9, 7-8, .9 and 10 = 0.10} on the expected mean (T_{crnl}) and dimensionless coefficient of variation (λ_{crnl}) of the hygrothermal post-buckling load N_x (KN) for perfect angle ply $(\pm 45^0{}_2)_T$ square laminated composite plate, plate thickness ratio (a/h=30) , fiber volume fraction (V_f=0.6), initial temperature T_0=25^{0}C, initial moisture C_0=0, temperature and moisture dependent material properties(TD), under environmental conditions has been shown in Table 3(d). It is noticed that temperature and moisture dependent material properties(TD) used plates show further decrease of expected mean when there is no increase of temperature and moisture, only amplitude ratio is increased the expected mean increases and COV decreases for different combinations of input variables as compared with TID condition. On increase of temperature and moisture the expected mean decreases as compared with that without temperature and moisture condition. Amplitude ratio always increases the mean values where as COV shows appreciable change.

Table 4 (a) & (b) show the effects of plate thickness ratio(a/h) and input random variables bi{i=1…9, 7-8, 9 and 10,11= 0.10} on the hygrothermal buckling loads N_x (KN) for angle ply $(\pm 45^0{}_2)_T$, square laminated composite plate resting on Winkler (k1=100, k2=0) and Pasternak (k1=100, k2=10) elastic foundations, V_f=0.6, T_0=25^{0}C, C_0=0, Simple Support (S2) under environmental conditions. It is observed that the mean hygrothermal buckling loads is higher for moderately thick plate and decreases drastically for thin plates resting on Winkler elastic foundation: however, coefficient of variations for different combinations of random variables is also varied in with and without rise in temperature and moisture. It is interesting that mean hygrothermal buckling loads rises rapidly for moderately thick plate and decreases drastically for thin plates resting on Pasternak elastic foundation in similar environmental conditions.

Table 4 (c) shows the effects of plate thickness ratios (a/h), amplitude ratios(W_{max}/h) and input variables bi{ i= 1…10,7-8,9,10=0.10} on the expected mean (T_{crnl}) and dimensionless coefficient of variations(λ_{crnl}) of hygrothermally induced post-buckling loads Nx (KN)for angle ply antisymmetric $(\pm 45^0)_{2T}$ laminated composite plates, fiber volume fraction (V_f=0.6), initial temperature (T_0=25^{0}C), initial moisture (C0=0.0), simple support(S2), temperature and moisture dependent material properties(TD),under environmental conditions. T_{crl} linear solution. It is noticed that there is drastic decrease of expected mean for thin plates even without change of temperature and moisture. Amplitude ratio further decreases the mean value where as COV increases for different combinations of input variables. Aspect ratio further decreases expected mean when there is rise in temperature and moisture. COV further changes significantly foe different combinations of input random variables. Thin plates are more influenced by combined effect od aspect ratio, amplitude ratio and environmental conditions.

TABLE 4 (A) EFFECT OF PLATE THICKNESS RATIO (A/H) AND INPUT RANDOM VARIABLES BI{I=1…9, 7-8, 9 AND 10,11= 0.10} ON EXPECTED MEAN (T_{CRL}) AND DIMENSIONLESS COEFFICIENT OF VARIATION (λ_{CRL}) OF THE HYGROTHERMAL BUCKLING LOAD N_X (KN) FOR ANGLE PLY $(\pm 45^0{}_2)_T$, SQUARE LAMINATED COMPOSITE PLATE RESTING ON WINKLER (K1=100, K2=0) ELASTIC FOUNDATION, FIBER VOLUME FRACTION (V_F=0.6), INITIAL TEMPERATURET_0=25^0C, INITIAL MOISTURE PERCENTAGE C_0=0%, SIMPLE SUPPORT (S2) BOUNDRY CONDITIONS UNDER ENVIRONMENTAL CONDITIONS. ΔT IS RISE IN TEMPERATURE, ΔC IS RISE IN MOISTURE PERCENTAGE. T= T_0+ ΔT AND C= C_0+ ΔC.

a/h	(k1=100, k2=00)									
	ΔT=0^0C, ΔC=0%					ΔT=100^0C, ΔC=1%				
	Mean, (T_{crl})	COV, λ_{crl} bi				Mean, (T_{crl})	COV, λ_{crl} bi			
		(i=1- 9)	(i=7.-8)	(i=9)	(i=10,11)		(i=1- 9)	(i=7.-8)	(i=9)	(i=10,11)
5	463.27	0.0706	3.700e-04	0	0.0045	405.24	0.0705	0.0017	3.38e-04	0.0044
30	19.87	0.0791	0.0015	0	0.0039	19.32	0.0787	0.0068	0.0014	0.0042
80	1.2571	0.1210	0.0088	0	0.6521	1.24	0.1275	0.0404	0.0081	0.0125
100	0.65	0.1218	0.0136	0	0.0126	0.64	0.1366	0.0623	0.0124	0.0123

TABLE 4 (B) EFFECT OF PLATE THICKNESS RATIO (A/H) AND INPUT RANDOM VARIABLES BI{I=1…9, 7-8, 9 AND 10,11= 0.10} ON EXPECTED MEAN (T_{CRL}) AND DIMENSIONLESS COEFFICIENT OF VARIATION (λ_{CRL}) OF THE HYGROTHERMAL BUCKLING LOAD N_X (KN) FOR ANGLE PLY $(\pm 45^0{}_2)_T$, SQUARE LAMINATED COMPOSITE PLATE RESTING ON PASTERNAK (K1=100, K2=10) ELASTIC FOUNDATION, FIBER VOLUME FRACTION (V_F=0.6), T_0=25^0C, C_0=0%, SIMPLE SUPPORT (S2) BOUNDRY CONDITIONS UNDER ENVIRONMENTAL CONDITIONS. ΔT IS RISE IN TEMPERATURE, ΔC IS RISE IN MOISTURE PERCENTAGE. T= T_0+ ΔT AND C= C_0+ ΔC.

a/h	(k1=100, k2=10)									
	ΔT=0^0C, ΔC=0%					ΔT=100^0C, ΔC=1%				
	Mean, (T_{crl})	COV, λ_{crl} bi				Mean, (T_{crl})	COV, λ_{crl} bi			
		(i=1- 9)	(i=7.-8)	(i=9)	(i=10,11)		(i=1- 9)	(i=7.-8)	(i=9)	(i=10,11)
5	1116.60	0.2087	1.534e-04	0	0.0582	972.7616	0.2096	7.065e-04	1.40e-04	0.0580
30	23.695	0.1206	0.0012	0	0.0164	23.0442	0.1205	0.0057	0.0011	0.0164
80	1.5733	0.1598	0.0070	0	0.0210	1.5459	0.1603	0.0324	0.0065	0.0201
100	0.8145	0.1629	0.0109	0	0.0214	0.8024	0.1684	0.0501	0.0100	0.0207

TABLE 4(C). EFFECTS OF PLATE THICKNESS RATIOS (A/H), AMPLITUDE RATIOS(W_{MAX}/H) AND INPUT VARIABLES BI{ I= 1…10,7-8,9,10=0.10} ON THE NONLINEAR EXPECTED MEAN (T_{CRNL}) AND DIMENSIONLESS COEFFICIENT OF VARIATIONS(λ_{CRNL}) OF HYGROTHERMALLY INDUCED POST-BUCKLING LOADS NX (KN)FOR ANGLE PLY ANTISYMMETRIC $(\pm 45^0)_{2T}$ LAMINATED COMPOSITE PLATES, FIBER VOLUME FRACTION (V_F=0.6), INITIAL TEMPERATURE T_0=25^0C, INITIAL MOISTURE C_0=0%, SIMPLE SUPPORT(S2), TEMPERATURE AND MOISTURE DEPENDENT MATERIAL PROPERTIES(TD), UNDER ENVIRONMENTAL CONDITIONS. T_{CRL} LINEAR SOLUTION.

a/h	W_{max}/h	TD									
		ΔT=0^0C, ΔC=0.00					ΔT=100^0C, ΔC=0.01				
		Mean T_{crnl}	COV, λ_{crnl} bi				Mean T_{crnl}	COV, λ_{crnl} bi			
			(i=1,.10)	i=(7,8)	(i=9)	(i=10)		(i=1,.,10)	i=(7, 8)	(i=9)	(i=10)
5	0.3	435.289	0.069	3.960e-04	0	0.0093	386.543	0.001	0.0019	3.391e-04	0.0023
	0.6	441.899	0.069	3.901e-04	0	0.0113	388.865	0.001	0.0019	3.371e-04	0.0028
	0.9	470.607	0.070	3.851e-04	0	0.0138	390.530	0.069	0.0018	3.357e-04	0.0035
	T_{crl}	(427.256)	0.068	4.034e-04	0	0.0058	(372.476)	0.067	0.0019	3.519e-04	0.0042
10	0.3	173.374	0.062	5.053e-04	0	0.0151	158.492	0.063	0.0024	4.438e-04	0.0230
	0.6	180.269	0.064	4.861e-04	0	0.0167	164.277	0.065	0.0024	4.282e-04	0.0234
	0.9	191.097	0.066	4.585e-04	0	0.0188	171.214	0.066	0.0023	4.108e-04	0.0247
	T_{crl}	(170.047)	0.063	5.153e-04	0	0.0166	(155.498)	0.063	0.0025	4.514e-04	0.0229
40	0.3	09.285	0.087	0.0024	0	0.0345	08.846	0.084	0.0846	0.0021	0.0402
	0.6	10.486	0.076	0.0021	0	0.0333	10.073	0.079	0.0795	0.0018	0.0373
	0.9	12.435	0.074	0.0018	0	0.0381	11.729	0.075	0.0759	0.0016	0.0369
	T_{crl}	(07.930)	0.090	0.0028	0	0.0387	(07.441)	0.092	0.0921	0.0025	0.0391
60	0.3	03.100	0.086	0.0048	0	0.0414	03.085	0.084	0.0864	0.0040	0.0414
	0.6	03.450	0.080	0.0043	0	0.0321	03.369	0.084	0.0844	0.0037	0.0321
	0.9	04.291	0.078	0.0035	0	0.0359	04.044	0.080	0.0807	0.0031	0.0359
	T_{crl}	(02.496)	0.094	0.0059	0	0.0389	(02.356)	0.098	0.0988	0.0053	0.0389
100	0.3	0.795	0.084	0.0112	0	0.0329	0.757	0.757	0.1013	0.0099	0.0342
	0.6	0.800	0.080	0.0111	0	0.0326	0.792	0.792	0.0951	0.0095	0.0295
	0.9	0.963	0.081	0.0092	0	0.0321	0.905	0.905	0.0719	0.0083	0.0278
	T_{crl}	(0.562)	0.097	0.0158	0	0.0385	(0.532)	0.532	0.1209	0.0141	0.0389

Table 5 (a) & (b) show the effects of aspect ratio (a/b) and input random variables bi{i=1…9, 7-8, 9 and 10,11= 0.10} on the buckling loads N_x (KN) for angle ply $(\pm 45^0{}_2)_T$ laminated composite plates resting on Winkler (k_1=100, k_2=0) and Pasternak (k_1=100, k_2=10) elastic foundations, plate thickness ratio (a/h=40), V_f=0.6, T_0=25^{0}C, C_0=0, Simple Support under Environmental Conditions. It is seen that under given environmental conditions and plate resting on Winkler elastic foundations the mean hygrothermal buckling load increases when the aspect ratio is increased; whereas the coefficient of variation for different combinations of random variables is decreased. However, when the plate is resting on Pasternak elastic foundation, the mean and coefficient of variations values further vary in similar environmental conditions.

Effects of aspect ratios (a/b), amplitude ratios(W_{max}/h) and input variables bi{ i= 1…10,7-8,9,10=0.10} on the expected mean (T_{crnl}) and dimensionless coefficient of variations(λ_{crnl}) of hygrothermally induced post-buckling loads Nx (KN)for angle ply antisymmetric $(\pm 45^0)_{2T}$ laminated composite plates, plate thickness ration (a/h=40), fiber volume fraction (V_f=0.6), initial temperature (T_0=25^{0}C), initial moisture (C_0=0.0), simple support(S2), temperature and moisture independent material properties(TID),under environmental conditions. T_{crl} linear solution is shown in Table 5 (c). Combined effects of aspect ratio and amplitude ratio without temperature and moisture rise have significance on expected mean specially when aspect ratio is one and half times. There is no much change in COV for different combinations of input random variables. On increase of temperature and moisture there is marginally decrease in expected mean and input variables.

TABLE 5 (A) EFFECT OF ASPECT RATIO (A/B) AND INPUT RANDOM VARIABLES BI{I=1…9, 7-8, 9 AND 10,11= 0.10} ON THE EXPECTED MEAN (T_{CRL}) AND DIMENSIONLESS COEFFICIENT OF VARIATION (λ_{CRL}) OF THE HYGROTHERMAL BUCKLING LOAD N_X (KN) FOR ANGLE PLY $(\pm 45^0{}_2)_T$ LAMINATED COMPOSITE PLATES RESTING ON WINKLER (K1=100, K2=0) ELASTIC FOUNDATION, PLATE THICKNESS RATIO (A/H=40), FIBER VOLUME FRACTION (V_F=0.6), T_0=25^{0}C, C_0=0, SIMPLE SUPPORT UNDER ENVIRONMENTAL CONDITIONS.

(a/b)	(k1=100, k2=0)									
	ΔT=0^{0}C, ΔC=0%					ΔT=100^{0}C, ΔC=1%				
	Mean, (T_{crl})	COV, λ_{crl} bi				Mean, (T_{crl})	COV, λ_{crl} bi			
		(i=1- 9)	(i=7.-8)	(i=9)	(i=10,11)		(i=1- 9)	(i=7.-8)	(i=9)	(i=10,11)
0.5	8.9775	0.1199	0.0025	0	0.0143	8.6398	0.1183	0.0115	0.0023	0.0132
1.0	9.3148	0.1178	0.0024	0	0.0134	9.0880	0.1146	0.0109	0.0022	0.0123
1.5	13.3157	0.0963	0.0025	0	0.0065	12.9227	0.0965	0.0114	0.0023	0.0065
2.0	19.3966	0.0844	0.0023	0	0.0034	18.6460	0.0842	0.0104	0.0021	0.0033

TABLE 5 (B) EFFECT OF ASPECT RATIO (A/B) AND INPUT RANDOM VARIABLES BI{I=1…9, 7-8, 9 AND 10,11= 0.10} ON THE EXPECTED MEAN (T_{CRL}) AND DIMENSIONLESS COEFFICIENT OF VARIATION (λ_{CRL}) OF THE HYGROTHERMAL BUCKLING LOAD N_X (KN) FOR ANGLE PLY $(\pm 45^0{}_2)_T$ LAMINATED COMPOSITE PLATES RESTING ON PASTERNAK (K1=100, K2=10) ELASTIC FOUNDATION, PLATE THICKNESS RATIO (A/H=40), FIBER VOLUME FRACTION (V_F=0.6), T_0=25^{0}C, C_0=0%, SIMPLE SUPPORT UNDER ENVIRONMENTAL CONDITIONS.

(a/b)	(k1=100, k2=10)									
	ΔT=0^{0}C, ΔC=0%					ΔT=100^{0}C, ΔC=1%				
	Mean, (T_{crl})	COV, λ_{crl} bi				Mean, (T_{crl})	COV, λ_{crl} bi			
		(i=1- 9)	(i=7.-8)	(i=9)	(i=10,11)		(i=1- 9)	(i=7.-8)	(i=9)	(i=10,11)
0.5	10.9401	0.1359	0.0020	0	0.0175	0.5808	0.1385	0.0094	0.0019	0.0177
1.0	11.1321	0.1206	0.0020	0	0.0148	10.8939	0.1219	0.0091	0.0018	0.0149
1.5	16.1082	0.1397	0.0020	0	0.0182	15.6168	0.1402	0.0094	0.0019	0.0181
2.0	22.6125	0.1213	0.0019	0	0.0145	21.7223	0.1216	0.0089	0.0018	0.0144

TABLE 5 (C) EFFECTS OF ASPECT RATIOS (A/B), AMPLITUDE RATIOS(W_{MAX}/H) AND INPUT VARIABLES BI{ I= 1…10,7-8,9,10=0.10} ON THE EXPECTED MEAN (T_{CRNL}) AND DIMENSIONLESS COEFFICIENT OF VARIATIONS(λ_{CRNL}) OF HYGROTHERMALLY INDUCED POST-BUCKLING LOADS NX (KN)FOR ANGLE PLY ANTISYMMETRIC ($\pm 45^0$)$_{2T}$ LAMINATED COMPOSITE PLATES, PLATE THICKNESS RATION (A/H=40), FIBER VOLUME FRACTION (V_F=0.6), INITIAL TEMPERATURE T_0=25^{0}C, INITIAL MOISTURE PERCENTAGE C_0=0%, SIMPLE SUPPORT(S2), TEMPERATURE AND MOISTURE INDEPENDENT MATERIAL PROPERTIES(TID), UNDER ENVIRONMENTAL CONDITIONS. T_{CRL} LINEAR SOLUTION.

a/b	W_{max}/h	TID									
		$\Delta T=0^0C$, $\Delta C=0.00$					$\Delta T=100^0C$, $\Delta C=0.01$				
		Mean T_{crnl}	COV, λ_{crnl} bi				Mean T_{crnl}	COV, λ_{crnl} bi			
			(i=1,..10)	i=(7,8)	(i=9)	(i=10)		(i=1,.,10)	i=(7, 8)	(i=9)	(i=10)
0.5	0.3	08.726	0.080	0.0025	0	0.053	08.190	0.102	0.0122	0.0024	0.0637
	0.6	10.162	0.079	0.0022	0	0.036	09.922	0.080	0.0100	0.0020	0.038
	0.9	10.817	0.079	0.0020	0	0.036	10.433	0.089	0.0095	0.0019	0.057
	T_{crl}	(07.683)	0.094	0.0029	0	0.047	(07.431)	0.099	0.0134	0.0027	0.053
1.0	0.3	09.620	0.083	0.0023	0	0.037	09.283	0.081	0.0107	0.0021	0.0355
	0.6	10.718	0.077	0.0021	0	0.033	10.288	0.078	0.0097	0.0019	0.0353
	0.9	12.535	0.075	0.0018	0	0.038	12.359	0.075	0.0087	0.0016	0.0401
	T_{crl}	(08.020)	0.091	0.0028	0	0.038	(07.885)	0.091	0.0126	0.0025	0.0391
1.5	0.3	30.578	0.079	0.0021	0	0.036	29.850	0.080	0.0096	0.0024	0.0396
	0.6	41.343	0.072	0.0016	0	0.035	36.717	0.074	0.0076	0.0020	0.0397
	0.9	48.035	0.072	0.0014	0	0.040	45.657	0.073	0.0063	0.0019	0.0449
	T_{crl}	(24.737)	0.087	0.0021	0	0.038	(23.631)	0.089	0.0122	0.0027	0.0420
2.0	0.3	23.363	0.076	0.0017	0	0.035	22.850	0.077	0.0086	0.0017	0.0386
	0.6	27.949	0.070	0.0016	0	0.034	26.905	0.071	0.0073	0.0014	0.0374
	0.9	32.551	0.068	0.0013	0	0.034	31.388	0.069	0.0062	0.0012	0.0378
	T_{crl}	(18.745)	0.083	0.0023	0	0.036	(18.142)	0.084	0.0108	0.0021	0.0391

Table 6 (a) &(b) show the effects of lamina layup and input random variables bi{i=1…9, 7-8, 9 and 10,11= 0.10} on the buckling loads N_x (KN) for angle ply square laminated composite plates resting on Winkler (k_1=100, k_2=00) and Pasternak (k_1=100, k_2=10) elastic foundations, plate thickness ratio (a/h=50), V_f=0.6, T_0=25^{0}C, C_0=0, Simple Support under environmental conditions. It is observed that mean hygrothermal buckling load decreases for cross ply antisymmetric plate as compared with other lamina lay-up for when the plate is resting on Winkler elastic foundations under given environmental conditions; however, the coefficients of variation of hygrothermal buckling load also vary for different combinations of random variables. The mean and coefficient of variation of hygrothermal buckling load further vary for different combinations of random variables and the plate is resting on Pasternak elastic foundation

Table 6(c), shows the effects of total number of plies, amplitude ratios (W_{max}/h) and input variables bi{ i= 1…10,7-8,9,10=0.10} on the expected mean (T_{crnl}) and dimensionless coefficient of variations (λ_{crnl}) of hygrothermally induced post-buckling loads Nx(KN) for laminated composite plates with plate, thickness ratio (a/h=40), fiber volume fraction (V_f=0.6), initial temperature T_0=25^{0}C, initial moisture C_0=0.0, simple support(S_2), temperature and moisture independent material properties (TID) under environmental conditions. It is seen that that there is slight increase in expected mean for different lamina lay-up and without change in temperature and moisture. When amplitude ratio is increased, then expected mean increases and COV also decrease and increases for different combinations of input random variables. On further increase in temperature and moisture contents, there are:marginally changes in the values.

TABLE 6 (A) EFFECT LAMINA LAY UP AND INPUT RANDOM VARIABLES BI{I=1…9, 7-8, 9 AND 10,11= 0.10} ON THE EXPECTED MEAN (T_{CRL}) AND DIMENSIONLESS COEFFICIENT OF VARIATION (λ_{CRL}) OF THE HYGROTHERMAL BUCKLING LOAD N_X (KN) FOR LAMINATED COMPOSITE PLATES RESTING ON WINKLER (K1=100, K2=00) ELASTIC FOUNDATION, PLATE THICKNESS RATIO (A/H=50), FIBER VOLUME FRACTION (V_F=0.6), T_0=25^{0}C, C_0=0%, SIMPLE SUPPORT UNDER ENVIRONMENTAL CONDITIONS.

Lay- up	(k1=100, k2=00)									
	ΔT=0^{0}C, ΔC=0%					ΔT=100^{0}C, ΔC=1%				
	Mean, (T_{crl})	COV, λ_{crl} bi				Mean, (T_{crl})	COV, λ_{crl} bi			
		(i=1- 9)	(i=7.-8)	(i=9)	(i=10,11)		(i=1- 9)	(i=7.-8)	(i=9)	(i=10,11)
$(\pm45^0)_S$	4.2965	0.1133	0.0041	0	0.0139	4.2519	0.1091	0.0187	0.0037	0.0119
$(\pm45^0{}_2)_T$	4.9298	0.1201	0.0036	0	0.0134	4.8384	0.1200	0.0165	0.0033	0.0129
$(0^0/90^0)_S$	4.7936	0.0946	0.0037	0	0.0434	4.7489	0.0961	0.0168	0.0034	0.0431
$(0^0/90^0)_T$	3.6537	0.1147	0.0048	0	0.0344	3.6169	0.1169	0.0221	0.0044	0.0340

TABLE 6 (B) EFFECT LAMINA LAY UP AND INPUT RANDOM VARIABLES BI{I=1…9, 7-8, 9 AND 10,11= 0.10} ON THE EXPECTED MEAN (T_{CRL}) AND DIMENSIONLESS COEFFICIENT OF VARIATION (λ_{CRL}) OF THE HYGROTHERMAL BUCKLING LOAD N_X (KN) FOR LAMINATED COMPOSITE PLATES RESTING ON PASTERNAK (K1=100, K2=10) ELASTIC FOUNDATION, PLATE THICKNESS RATIO (A/H=50), FIBER VOLUME FRACTION (V_F=0.6), T_0=25^{0}C, C_0=0%, SIMPLE SUPPORT UNDER ENVIRONMENTAL CONDITIONS.

Lay- up	(k1=100, k2=10)									
	ΔT=0^{0}C, ΔC=0%					ΔT=100^{0}C, ΔC=1%				
	Mean, (T_{crl})	COV, λ_{crl} bi				Mean, (T_{crl})	COV, λ_{crl} bi			
		(i=1- 9)	(i=7.-8)	(i=9)	(i=10,11)		(i=1- 9)	(i=7.-8)	(i=9)	(i=10,11)
$(\pm45^0)_S$	5.4917	0.1384	0.0032	0	0.0192	5.3440	0.1403	0.0149	0.0030	0.0194
$(\pm45^0{}_2)_T$	6.0523	0.1224	0.0029	0	0.0142	5.9360	0.1280	0.0134	0.0027	0.0150
$(0^0/90^0)_S$	8.9032	0.1029	0.0020	0	0.0517	8.8035	0.1033	0.0091	0.0018	0.0516
$(0^0/90^0)_T$	6.1351	0.1435	0.0029	0	0.0453	6.0469	0.1442	0.0132	0.0026	0.0448

TABLE 6(C). EFFECTS OF TOTAL NUMBER OF PLIES, AMPLITUDE RATIOS (W_{MAX}/H) AND INPUT VARIABLES BI{ I= 1…10,7-8,9,10=0.10} ON THE EXPECTED MEAN (T_{CRNL}) AND DIMENSIONLESS COEFFICIENT OF VARIATIONS (λ_{CRNL}) OF HYGROTHERMALLY INDUCED POST-BUCKLING LOADS NX(KN) FOR LAMINATED COMPOSITE PLATES WITH PLATE, THICKNESS RATIO (A/H=40), FIBER VOLUME FRACTION (V_F=0.6), INITIAL TEMPERATURE T_0=25^{0}C, INITIAL MOISTURE C_0=0%, SIMPLE SUPPORT(S_2), TEMPERATURE AND MOISTURE INDEPENDENT MATERIAL PROPERTIES (TID) UNDER ENVIRONMENTAL CONDITIONS.

Lay-up	W_{max}/h	TID									
		ΔT=0^{0}C, ΔC=0.00					ΔT=100^{0}C, ΔC=0.01				
		Mean T_{crnl}	COV, λ_{crnl} bi				Mean T_{crnl}	COV, λ_{crnl} bi			
			(i=1,..10)	i=(7,8)	(i=9)	(i=10)		(i=1.,10)	i=(7, 8)	(i=9)	(i=10)
$(0^0/90^0)s$	0.3	07.563	0.070	0.0029	0	0.031	07.455	0.072	0.0029	0.0027	0.0325
	0.6	11.401	0.075	0.0019	0	0.035	11.212	0.075	0.0019	0.0018	0.0369
	0.9	14.395	0.076	0.0015	0	0.031	14.119	0.076	0.0015	0.0014	0.0333
	T_{crl}	(04.773)	0.087	0.0046	0	0.035	(04.709)	0.090	0.0046	0.0042	0.0336
$(0^0/90^0)_{3S}$	0.3	06.644	0.073	0.0033	0	0.034	06.558	0.074	0.0152	0.0030	0.0360
	0.6	10.354	0.070	0.0021	0	0.026	10.126	0.070	0.0098	0.0020	0.0278
	0.9	14.395	0.069	0.0015	0	0.036	14.411	0.061	0.0069	0.0014	0.0348
	T_{crl}	(04.773)	0.090	0.0051	0	0.043	(04.860)	0.090	0.0235	0.0047	0.0446
$(\pm45^0)_{2T}$	0.3	07.921	0.067	0.0012	0	0.027	07.877	0.068	0.0055	8.03e-04	0.0270
	0.6	10.499	0.064	8.83e-04	0	0.029	10.462	0.064	0.0042	6.04e-04	0.0291
	0.9	13.327	0.062	6.95e-04	0	0.029	13.256	0.061	0.0033	4.77e-04	0.0298
	T_{crl}	(04.879)	0.087	0.0019	0	0.033	(04.860)	0.087	0.0090	1.30e-04	0.0333
$(\pm45^0)_{2S}$	0.3	09.620	0.083	0.0023	0	0.037	09.283	0.081	0.0107	0.0021	0.0355
	0.6	10.718	0.077	0.0021	0	0.033	10.288	0.078	0.0097	0.0019	0.0353
	0.9	12.535	0.075	0.0018	0	0.038	12.359	0.075	0.0081	0.0016	0.0401
	T_{crl}	(08.020)	0.091	0.0028	0	0.038	(07.885)	0.091	0.0126	0.0025	0.0391

Table 7 (a) &(b) show the effect of matrix and fiber volume fraction (Vf) and input random variables bi{i=1…9, 7-8, 9 and 10,11= 0.10} on the buckling loads N_x (KN) for angle ply $(\pm 45^0{}_2)_T$ square laminated composite plate resting on Winkler (k_1=100, k_2=0) and Pasternak (k_1=100, k_2=10) elastic foundations, plate thickness ratio (a/h=60), T_0=25^{0}C, C_0=0, Simple Support(S2) under Environmental Conditions. It is noticed that on varying the volume fraction the mean and coefficient of variation of hygrothermal buckling load changes when the plate is resting on Winkler elastic foundation under given environmental conditions with different combinations of input random variables. These values further increase when the plate is resting on Pasternak elastic foundation under similar environmental conditions and different combinations of input random variables.

Effects of fiber volume fractions (V_f), amplitude ratios (W_{max}/h) and input variables bi{ i= 1…10,7-8,9,10=0.10} on the mean (T_{crnl}) and dimensionless coefficient of variations(λ_{crnl}) of hygrothermally induced post-buckling loads Nx (KN)for angle ply antisymmetric $(\pm 45^0)_{2T}$ laminated composite plates with plate thickness ratio (a/h=40), initial temperature T_0=25^{0}C, initial moisture C_0=0.0, simple support(S2) temperature and moisture independent material properties (TID) under environmental conditions have been shown in Table 7 (c). It is noticed that combined effect of fiber volume fractions, amplitude ratio with random input variables, without rise in temperature and moisture have slight increase of expected mean and decrease of COV. It is higher when there is more fiber volume fraction. On increase of temperature and moisture, the expected mean values decrease and COV increases for different combinations of input random variables.

TABLE 7 (A) EFFECT OF FIBER VOLUME FRACTIONS (VF) AND INPUT RANDOM VARIABLES BI{I=1…9, 7-8, 9 AND 10,11= 0.10} ON THE EXPECTED MEAN (T_{CRL}) AND DIMENSIONLESS COEFFICIENT OF VARIATION (λ_{CRL}) OF THE HYGROTHERMAL BUCKLING LOAD N_X (KN) FOR ANGLE PLY $(\pm 45^0{}_2)_T$ SQUARE LAMINATED COMPOSITE PLATE RESTING ON WINKLER (K1=100, K2=0) ELASTIC FOUNDATION, PLATE THICKNESS RATIO (A/H=60), T_0=25^{0}C, C_0=0%, SIMPLE SUPPORT(S2) UNDER ENVIRONMENTAL CONDITIONS.

(Vf)	(k1=100, k2=00)									
	ΔT=0^{0}C, ΔC=0%					ΔT=100^{0}C, ΔC=1%				
	Mean, (T_{crl})	COV, λ_{crl} bi				Mean, (T_{crl})	COV, λ_{crl} bi			
		(i=1- 9)	(i=7.-8)	(i=9)	(i=10,11)		(i=1- 9)	(i=7.-8)	(i=9)	(i=10,11)
0.50	2.4310	0.1205	0.0062	0	0.0131	2.3897	0.1233	0.0284	0.0045	0.0127
0.55	2.6672	0.1205	0.0056	0	0.0131	2.6242	0.1227	0.0256	0.0046	0.0127
0.60	2.9109	0.1207	0.0051	0	0.0132	2.8662	0.1222	0.0232	0.0046	0.0128
0.65	3.1650	0.1200	0.0046	0	0.0132	3.1183	0.1215	0.0212	0.0047	0.0128
0.70	3.4337	0.1193	0.0042	0	0.0132	3.3843	0.1207	0.0194	0.0047	0.0128

TABLE 7 (B) EFFECT OF FIBER VOLUME FRACTIONS (VF) AND INPUT RANDOM VARIABLES BI{I=1…9, 7-8, 9 AND 10,11= 0.10} ON THE EXPECTED MEAN (T_{CRL}) AND DIMENSIONLESS COEFFICIENT OF VARIATION (λ_{CRL}) OF THE HYGROTHERMAL BUCKLING LOAD N_X (KN) FOR ANGLE PLY $(\pm 45^0{}_2)_T$ SQUARE LAMINATED COMPOSITE PLATE RESTING ON PASTERNAK (K1=100, K2=10) ELASTIC FOUNDATION, PLATE THICKNESS RATIO (A/H=60), T_0=25^{0}C, C_0=0%, SIMPLE SUPPORT(S2) UNDER ENVIRONMENTAL CONDITIONS.

(Vf)	(k1=100, k2=10)									
	ΔT=0^{0}C, ΔC=0%					ΔT=100^{0}C, ΔC=1%				
	Mean, (T_{crl})	COV, λ_{crl} bi				Mean, (T_{crl})	COV, λ_{crl} bi			
		(i=1- 9)	(i=7.-8)	(i=9)	(i=10,11)		(i=1- 9)	(i=7.-8)	(i=9)	(i=10,11)
0.50	3.0256	0.1340	0.0050	0	0.0160	2.9614	0.1427	0.0229	0.0036	0.0171
0.55	3.3206	0.1330	0.0045	0	0.0158	3.2526	0.1420	0.0207	0.0037	0.0170
0.60	3.6285	0.1331	0.0041	0	0.0158	3.5556	0.1419	0.0187	0.0037	0.0171
0.65	3.9538	0.1338	0.0037	0	0.0161	3.8741	0.1427	0.0171	0.0038	0.0174
0.70	4.3026	0.1376	0.0034	0	0.0170	4.2138	0.1443	0.0156	0.0038	0.0180

TABLE 7 (C). EFFECTS OF FIBER VOLUME FRACTIONS (V_F), AMPLITUDE RATIOS (W_{MAX}/H) AND INPUT VARIABLES BI{ I= 1…10,7-8,9,10=0.10} ON THE MEAN (T_{CRNL}) AND DIMENSIONLESS COEFFICIENT OF VARIATIONS(λ_{CRNL}) OF HYGROTHERMALLY INDUCED POST-BUCKLING LOADS NX (KN)FOR ANGLE PLY ANTISYMMETRIC ($\pm 45^0)_{2T}$ LAMINATED COMPOSITE PLATES WITH PLATE THICKNESS RATIO (A/H=40), INITIAL TEMPERATURE T_0=25^{0}C, INITIAL MOISTURE C_0=0%, SIMPLE SUPPORT(S2) TEMPERATURE AND MOISTURE INDEPENDENT MATERIAL PROPERTIES (TID) UNDER ENVIRONMENTAL CONDITIONS.

V_f	W_{max}/h	TID									
		$\Delta T=0^0C$, $\Delta C=0.00$					$\Delta T=100^0C$, $\Delta C=0.01$				
		Mean T_{crnl}	COV, λ_{crnl} bi				Mean T_{crnl}	COV, λ_{crnl} bi			
			(i=1,..10)	i=(7,8)	(i=9)	(i=10)		(i=1,.,10)	i=(7, 8)	(i=9)	(i=10)
0.50	0.3	08.095	0.081	0.0028	0	0.0423	07.952	0.083	0.012	0.0020	0.0374
	0.6	08.943	0.075	0.0025	0	0.0337	08.728	0.079	0.011	0.0018	0.0405
	0.9	10.377	0.072	0.0022	0	0.0373	10.269	0.076	0.009	0.0016	0.0405
	T_{crl}	(06.690)	0.090	0.0034	0	0.0386	(06.563)	0.092	0.015	0.0024	0.0393
0.55	0.3	08.667	0.080	0.0026	0	0.0339	08.545	0.082	0.082	0.0021	0.0355
	0.6	09.841	0.077	0.0023	0	0.0357	09.660	0.078	0.078	0.0021	0.0396
	0.9	12.281	0.074	0.0018	0	0.0418	12.017	0.076	0.076	0.0015	0.0435
	T_{crl}	(07.342)	0.091	0.0030	0	0.0386	(07.211)	0.092	0.092	0.0015	0.0392
0.60	0.3	09.620	0.083	0.0023	0	0.0372	09.283	0.081	0.010	0.0021	0.0355
	0.6	10.718	0.077	0.0021	0	0.0339	10.288	0.078	0.009	0.0019	0.0353
	0.9	12.535	0.075	0.0018	0	0.0381	12.359	0.075	0.008	0.0016	0.0401
	T_{crl}	(08.735)	0.091	0.0028	0	0.0387	(07.885)	0.091	0.012	0.0025	0.0391
0.65	0.3	11.594	0.077	0.0019	0	0.0363	11.352	0.079	0.005	0.0019	0.0381
	0.6	13.490	0.074	0.0016	0	0.0386	13.241	0.076	0.007	0.0017	0.0403
	0.9	14.766	0.074	0.0015	0	0.0414	14.476	0.075	0.006	0.0015	0.0429
	T_{crl}	(08.735)	0.090	0.0025	0	0.0388	(08.596)	0.091	0.011	0.0025	0.0390

Table 8(a) & (b) show the effects of environmental conditions and input random variables bi{i=1…9, 7-8, 9 and 10,11= 0.10} on the buckling of a angle ply $(\pm 45^0{}_2)_T$ square laminated composite plate resting on Winkler (k_1=100, k_2=0) and Pasternak (k_1=100, k_2=10) elastic foundations with plate thickness ratio (a/h=50), ,V_f=0.6, T_0=25^{0}C, C_0=0, Simple Support(S2). It is noticed that mean hygrothermal load and coefficient of variations vary on changing environmental conditions for plate resting on Winkler elastic foundation with input random variables. The mean hygrothermal load and coefficient of variations values further increase for plates resting on Pasternak elastic foundation under similar environmental conditions with input random variables.

Effects of environmental conditions, amplitude ratios (W_{max}/h) and input random variables bi{i=1…10, 7-8, 9, 10 = 0.10} on the expected mean (T_{crnl}) and dimensionless coefficient of variation (λ_{crnl}) of hygrothermally induced post buckling load Nx (KN) of a perfect angle ply $(\pm 45)_{2T}$ square laminated composite plate, plate thickness ratio (a/h=50), fiber volume fraction (Vf=0.6), initial temperature T_0=25^{0}C, initial moisture percentage C_0 =0%, temperature and moisture independent material properties (TID) and simple support(S2) are shown in Table 8 (c). It is seen that environmental effects with amplitude ratio and different combinations of input random variables there is increase in expected mean and decrease in COV but for temperature has significant effects. Amplitude ratio increases the mean values which decrease the COV.

Effects of environmental conditions, amplitude ratios (W_{max}/h) and input random variables bi{i=1…10, 7-8, 9, 10 = 0.10} on the expected mean (T_{crnl}) and dimensionless coefficient of variation (λ_{crnl}) of hygrothermally induced post buckling load Nx (KN) of a perfect angle ply $(\pm 45)_{2T}$ square laminated composite plate, plate thickness ratio (a/h=50), fiber volume fraction (Vf=0.6), initial temperature (T_0=25^{0}C), initial moisture percentage (C_0 =0%), temperature and moisture dependent material properties (TD) and simple support(S2) are shown in Table 8 (d). It is noticed that there is significant change of expected mean for different combinations of environmental conditions combined with amplitude ratios and input random variables. The COV has meaningful variations for different combinations of input random variables compared to TID conditions.

TABLE 8 (A) THE EFFECTS OF ENVIRONMENTAL CONDITIONS AND INPUT RANDOM VARIABLES BI{I=1…9, 7-8, 9 AND 10,11= 0.10} ON EXPECTED MEAN (T_{CRL}) AND DIMENSIONLESS COEFFICIENT OF VARIATION (λ_{CRL}) OF THE HYGROTHERMAL BUCKLING LOAD N_X (KN) OF ANGLE PLY $(\pm 45^0{}_2)_T$ SQUARE LAMINATED COMPOSITE PLATE RESTING ON WINKLER (K1=100, K2=0) ELASTIC FOUNDATION WITH PLATE THICKNESS RATIO (A/H=50 FIBER VOLUME FRACTION (V_F=0.6), T_0=25^{0}C, C_0=0%, SIMPLE SUPPORT(S2).

Environmental Conditions.	Mean, (T_{crl})	(k1=100, k2=0)			
		COV, λ_{crl}			
		bi			
		(i=1- 9)	(i=7.-8)	(i=9)	(i=10,11)
ΔT=0^{0}C, ΔC=0%	4.9298	0.1201	0.0036	0	0.0139
ΔT=100^{0}C, ΔC=1%	4.8384	0.1200	0.0165	0.0033	0.0129
ΔT=200^{0}C, ΔC=3%	4.7360	0.1227	0.0271	0.0099	0.0127
ΔT=300^{0}C, ΔC=5%	4.6518	0.1263	0.0356	0.0166	0.0126

TABLE 8 (B) THE EFFECTS OF ENVIRONMENTAL CONDITIONS AND INPUT RANDOM VARIABLES BI{I=1…9, 7-8, 9 AND 10,11= 0.10} ON EXPECTED MEAN (T_{CRL}) AND DIMENSIONLESS COEFFICIENT OF VARIATION (λ_{CRL}) OF THE HYGROTHERMAL BUCKLING LOAD N_X (KN) OF ANGLE PLY $(\pm 45^0{}_2)_T$ SQUARE LAMINATED COMPOSITE PLATE RESTING ON PASTERNAK (K1=100, K2=10) ELASTIC FOUNDATION WITH PLATE THICKNESS RATIO (A/H=50 FIBER VOLUME FRACTION (V_F=0.6), T_0=25^{0}C, C_0=0%, SIMPLE SUPPORT(S2).

Environmental Conditions.	Mean, (T_{crl})	(k1=100, k2=10)			
		COV, λ_{crl}			
		bi			
		(i=1- 9)	(i=7.-8)	(i=9)	(i=10,11)
ΔT=0^{0}C, ΔC=0%	6.0523	0.1224	0.0029	0	0.0142
ΔT=100^{0}C, ΔC=1%	5.9360	0.1280	0.0134	0.0027	0.0150
ΔT=200^{0}C, ΔC=3%	5.8056	0.1316	0.0221	0.0081	0.0152
ΔT=300^{0}C, ΔC=5%	5.6978	0.1348	0.0290	0.0136	0.0153

TABLE 8 (C) EFFECTS OF ENVIRONMENTAL CONDITIONS, AMPLITUDE RATIOS (W_{MAX}/H) AND INPUT RANDOM VARIABLES BI{I=1…10, 7-8, 9, 10 = 0.10} ON THE EXPECTED MEAN (T_{CRNL}) AND DIMENSIONLESS COEFFICIENT OF VARIATION (λ_{CRNL}) OF HYGROTHERMALLY INDUCED POST BUCKLING LOAD NX (KN) OF A PERFECT ANGLE PLY $(\pm 45)_{2T}$ SQUARE LAMINATED COMPOSITE PLATE, PLATE THICKNESS RATIO (A/H=50), FIBER VOLUME FRACTION (VF=0.6), INITIAL TEMPERATURE T_0=25^{0}C, INITIAL MOISTURE PERCENTAGE C_0 =0%,
TEMPERATURE AND MOISTURE INDEPENDENT MATERIAL PROPERTIES (TID) AND SIMPLE SUPPORT(S2).

Environmental Conditions	W_{max}/h	TID				
		Mean T_{crnl}	COV, λ_{crnl}			
			bi			
			(i=1,..10)	i=(7,8)	(i=9)	(i=10)
ΔT=0^{0}C ΔC=0.0	0.3	5.780	0.0809	0.0031	0	0.0357
	0.6	6.881	0.0782	0.0026	0	0.0375
	0.9	7.779	0.0777	0.0023	0	0.0400
	T_{crl}	(4.264)	0.0934	0.0031	0	0.0391
ΔT=100^{0}C ΔC=0.01	0.3	5.689	0.0824	0.0140	0	0.0373
	0.6	6.779	0.0791	0.0118	0	0.0390
	0.9	7.535	0.0780	0.0106	0	0.0413
	T_{crl}	(4.209)	0.0951	0.0190	0	0.0291
ΔT= 200^{0}C ΔC=0.03	0.3	5.344	0.0870	0.0242	0	0.0368
	0.6	6.668	0.0819	0.0194	0	0.0400
	0.9	7.412	0.0805	0.0175	0	0.0423
	T_{crl}	(4.143)	0.0988	0.0312	0	0.0400
ΔT= 300^{0}C ΔC=0.05	0.3	5.517	0.0897	0.0303	0	0.0392
	0.6	6.580	0.0850	0.0254	0	0.0407
	0.9	7.316	0.0832	0.0229	0	0.0431
	T_{crl}	(4.090)	0.1052	0.0409	0	0.0406
ΔT= -100^{0}C ΔC=0.01	0.3	4.525	0.0934	0.0129	0	0.0388
	0.6	4.525	0.0934	0.0129	0	0.0388
	0.9	8.085	0.0756	0.0072	0	0.0397
	T_{crl}	(4.524)	0.0934	0.0129	0	0.0388
ΔT= -200^{0}C ΔC=0.03	0.3	6.516	0.0813	0.0242	0	0.0329
	0.6	7.324	0.0771	0.0203	0	0.0344
	0.9	8.121	0.0756	0.0183	0	0.0366
	T_{crl}	(4.557)	0.0956	0.0129	0	0.0339

TABLE 8 (D) EFFECTS OF ENVIRONMENTAL CONDITIONS, AMPLITUDE RATIOS (W_{MAX}/H) AND INPUT RANDOM VARIABLES BI{I=1…10, 7-8, 9, 10 = 0.10} ON THE EXPECTED MEAN (T_{CRNL}) AND DIMENSIONLESS COEFFICIENT OF VARIATION (λ_{CRNL}) OF HYGROTHERMALLY INDUCED POST BUCKLING LOAD NX (KN) OF A PERFECT ANGLE PLY $(\pm45)_{2T}$ SQUARE LAMINATED COMPOSITE PLATE, PLATE THICKNESS RATIO (A/H=50), FIBER VOLUME FRACTION (VF=0.6), INITIAL TEMPERATURE (T_0=25^{0}C), INITIAL MOISTURE PERCENTAGE (C_0 =0%), TEMPERATURE AND MOISTURE DEPENDENT MATERIAL PROPERTIES (TD) AND SIMPLE SUPPORT(S2).

Environmental conditions	W_{max}/h	TD				
		Mean T_{crnl}	COV, λ_{crnl}			
			bi			
			(i=1,..10)	i=(7,8)	(i=9)	(i=10)
ΔT=0^{0}C ΔC=0.0	0.3	5.7175	0.0802	0.0031	0	0.0357
	0.6	6.8169	0.0773	0.0026	0	0.0375
	0.9	7.5892	0.0764	0.0023	0	0.0400
	T_{crl}	(4.2161)	0.0930	0.0042	0	0.0389
ΔT=100^{0}C ΔC=0.01	0.3	5.3769	0.0826	0.0153	0.0028	0.0372
	0.6	6.1484	0.0792	0.0128	0.0023	0.0388
	0.9	7.1453	0.0781	0.0153	0.0021	0.0411
	T_{crl}	(3.9695)	0.0954	0.0207	0.0038	0.0391
ΔT= 200^{0}C ΔC=0.03	0.3	5.0354	0.0868	0.0269	0.0083	0.0372
	0.6	6.0212	0.0825	0.0225	0.0070	0.0388
	0.9	4.7133	0.0809	0.0202	0.0062	0.0411
	T_{crl}	(3.7137)	0.1014	0.0364	0.0113	0.0391
ΔT= 300^{0}C ΔC=0.05	0.3	5.5178	0.0897	0.0376	0.0139	0.0382
	0.6	6.5806	0.0850	0.0314	0.0116	0.0397
	0.9	7.3164	0.0832	0.0281	0.0104	0.0420
	T_{crl}	(4.0906)	0.1052	0.0511	0.0188	0.0400
ΔT= -100^{0}C ΔC=0.01	0.3	4.5252	0.0934	0.0090	0.0027	0.0389
	0.6	4.5254	0.0934	0.0076	0.0023	0.0403
	0.9	8.0857	0.0756	0.0068	0.0020	0.0403
	T_{crl}	(4.5248)	0.0934	0.0122	0.0036	0.0394
ΔT= -200^{0}C ΔC=0.03	0.3	6.5160	0.0813	0.0214	0.0083	0.0334
	0.6	7.3244	0.0771	0.0181	0.0070	0.0349
	0.9	8.1216	0.0756	0.0163	0.0063	0.0371
	T_{crl}	(4.5574)	0.0956	0.0289	0.0111	0.0341

Conclusions

The stochastic DISFOPT procedure has been used to obtain the expected mean and COV of the hygrothermal buckling and postbuckling load of the laminated composite plates resting on elastic foundations and without foundations, subjected to uniform temperature and moisture rise with random system parameters. The following conclusion can be drawn from this limited study:

1. The first order perturbation technique gives acceptable results for the range of coefficient of variation (SD/mean) taken in the study. It is observed that coefficient of variance for E_{11} and E_{22} is of significance as compared with all other random input variables in case plate resting on Winkler and Pasternak foundations

2. The characteristics of hygrothermal buckling and post buckling load of laminated composite plate are significantly influenced by various support conditions, plate thickness ratios, aspect ratios, fiber volume fractions, elastic foundations, changes of temperature and moisture. The mean hygrothermal buckling load and coefficient of variation of plate is significant when the plate is subjected to temperature dependent hygrothermo-material properties.

3. The clamp supported plate buckle at slightly higher temperature and moisture as compared with other supports when resting on Pasternak elastic foundation. Buckling and post buckling are less dominant for moderately thick plate as compared with thin plate made of temperature and moisture dependent material properties. It is also noticed that with Pasternak foundation support, the expected mean values are higher and coefficient of variation is lower as compared with Winkler foundation.
4. The expected mean and COV is drastically influenced for thin plates and amplitude ratio.
5. The sensitivity of hygrothermal buckling and post buckling load, coefficient of variation due to variation in material properties which is dependent on thickness ratio and boundary conditions of the laminate. The study is meaningful for the aerospace applications where such environmental conditions may occur and the importance of elastic foundations is quite clear.

REFERENCES

[1] J.M. Whitney and J.E. Ashton, "Effect of environment on the elastic response of layered composite plates", *AIAA*, vol. 9, pp1708–13, 1971.

[2] D.L. Flaggs and J.R. Vinson, "Hygrothermal effects on the buckling of laminated composite plates", *Fiber Sci.Technology*, vol. 1, pp353–65, 1978.

[3] S.Y. Lee, Chou C.J., J.L. Jang, and J.S. Lin, "Hygrothermal effects on linear and non-linear analysis of symmetric angle-ply laminated plates", *Compos Struct*, vol. 21, pp41-48, 1992.

[4] K.S. SaiRam and P.K. Sinha, "Hygrothermal effects on the buckling of laminated composite plates", *Compos Struct*, vol. 21, pp 233- 247, 1992.

[5] H.S. Shen, "Hygrothermal effects on the post buckling of shear deformable laminated plates", *Int. J Mech. Sci*, vol. 43, pp1259-1281, 2001.

[6] B.P. Patel, M. Ganapati and Makhecha, "Hygrothermal effects on the structural behaviour of thick composite laminates using higher-order theory", *Compos Struct,* vol. 56, pp 25-34, 2002.

[7] S. Nakagiri, H. Tatabatake and S. Tani, "Uncertain eigen value analysis of composite laminated plates by SFEM", *Compos Struct*, pp149–12, 1990.

[8] S.P. Englested and J.N. Reddy, "Probabilistic methods for the analysis of matrix composite", *Compos Sci Techn*, vol. 50, pp 91–107. 1994.

[9] B.N. Singh, D. Yadav and N.G.R. Iyenger, "Stability analysis of laminated composite cylindrical panels with uncertain material properties", *Compos Structm*, vol. 54, pp 17-26, 2001.

[10] A. Lal, B.N. Singh and R. Kumar, "Effect of random system properties on initial buckling of composite plates resting on elastic foundation", *Int. J Struct. Stab. Dyn*, vol. 1, pp103-130, 2008.

[11] B.N. Singh, A. Lal, and R. Kumar, "Post buckling of laminated composite plate on elastic foundation with random system properties", *Communi. Nonlr. Sci Numer. Simul,* vol. 14, pp284-300, 2009.

[12] S. Chen, Z. Lin and Z. Zhang, "Random Variation Analysis for larger scale structures with random parameters", *Compos. Struct.* Vol. 43, pp 247-254, 1992.

[13] B.N. Singh, V.K. Verma, "Hygrothermal effects on the buckling of laminated composite plates with random geometric and material properties", *J Reinf. Plast and Compos*, vol. 28(4), pp 409-427, 2009.

[14] Ramesh. Pandey, K.K. Shukla and Anuj Jain, "Thermoelastic stability analysis of laminated composite plates", An analytical approach, *Communications in Nonlinear Science and Numerical Simulation*, vol.14(4), pp1679-1699, 2009.

[15] B.N. Singh, N.G.R. Iyengar and D. Yadav, "Effects of random material properties on buckling of composite plates", *ASCE J Eng. Mech*, vol. 127(9), pp 873-879, 2001.

[16] B.N. Singh, D. Yadav and N.G.R. Iyengar, "Initial buckling of composite cylindrical panels with random material properties", *Compos. Struct*, vol. 53(1), pp 55-64, 2001.

[17] A.K. Onkar, C.S. Upadhyay and D, Yadav, "Generalized buckling analysis of laminated plates with random material properties using stochastic finite elements", *Int. J Mech. Sci*, vol. 48, pp780–798, 2006.

[18] A.K. Onkar , C.S. Upadhyay and D. Yadav, "Stochastic finite element buckling analysis of laminated plates with circular cutout under uniaxial compression", *J Appl. Mech*, vol. 74(4), pp 798 -810, 2007.

[19] A. Lal, B.N. Singh, Rajesh Kumar, "Effects of random system properties on the thermal buckling analysis of laminated composite plates", *Comput. & Struct.*, vol. 87 (17-18) , pp1119-1128, 2009.

[20] V.K. Verma, B.N. Singh, "Thermal buckling of laminated composite plates with random geometric and material properties", *Int J Struct. Stab. Dyn.*, vol. 9(2) , pp187-211, 2009.

[21] J.N. Reddy, "A Simple higher order theory for laminated composite plates", *ASME J Appl Mech*, vol. 51, pp745–752, 1984.

[22] J.N. Reddy, "Mechanics of laminated composite plates, theory and analysis", *CRC press,* Boca Raton Florida, 1997.

[23] R.M. Jones, "Mechanics of composite materials", *McGraw-Hill*, New York, 1975.

[24] B.D. Agarwal, L.J. Broutman, "Analysis and performance of fiber composites", Second edition, *John Wiley & sons*, New York, 1990.

[25] B.N. Singh, N.G.R. Iyengar and D. Yadav, "A C^0 Finite element investigation for buckling analysis of composite plates with random material properties", *Struct Engrg and Mech*, vol. 113(1), pp 53-74, 2002.

[26] C.A. Shankara and N.G.R. Iyenger, "A C^0 element for the free vibration analysis of laminated composite plates" *J Sound. Vib*, vol. 191 (5), pp 721–738. 1996.

[27] J.N. Reddy, "Energy and Variational methods in applied mechanics", *Wiley*, New York, 1981.

[28] M. Kleiber and T.D. Hien, "The Stochastic finite element method" *Wiley*, New York, 1992.

[29] L.L. Graham and E.F. Siragy, "Stochastic finite element analysis for elastic buckling of stiffened panels", *J Eng. Mech*, vol. 127, pp 91–7, 2001.

[30] Z .Yamin, S. Chen and Q. Lue, "Stochastic perturbation finite elements", *Comp and Struct*, vol. 59 (3), pp 425- 429, 1996 .

[31] W.K.. Liu, T. Belytschko and Mani, "A Random field finite elements", *Int J Num. Meth Engrg*, vol. 23, pp1831-1845, 1986.

[32] L.L. Graham and G. Deodatis "Response and eigenvalue analysis of stochastic finite element systems with multiple correlated material and geometric properties", *Probab. Eng. Mech,* pp1611–29, 2001.

[33] C.Y. Chia, "Nonlinear analysis of plates", *McGraw-Hill*, New York, 1980.

[34] J.N. Franklin,"Matrix theory", *Englewood cliffs*. JN Prentice Hall, 1968.

[35] Ramesh Pandey et al., "Hygrothermoelastic Postbuckling Response of Laminated Composite Plates, *Journal of Aerospace Engineering*, vol. 23(1), January 1, 2010.

[36] Rajesh Kumar et al, "Hygrothermal buckling response of laminated composite plates with random material properties, Micro-mechanical model," *Journal of Applied Mechanics and Materials,* vol. 110-116 pp 113-119. 2012.

[37] Rajesh Kumar et al, "Hygrothermal buckling analysis of laminated composite plates with random system properties and resting on Elastic foundations", *Journal of Composite Materials, SAGE Publications*, 0(0)1-20, DOI: 1177/0021998311431993. 2012.

[38] Rajesh Kumar, H S Patil, "Hygrothermally Induced Postbuckling Response of Non-linear Elastically Supported Laminated Composite Plates with Uncertain System Properties: Stochastic Finite Elemental Macro mechanical Model" *Journal of Frontiers in Aerospace Engg,* vol. 2(1) PP.13-28. 2013.

[39] Rajesh Kumar et al, " Hygrothermoelastic Buckling Response of Laminated Composite Plates with Random System Properties, Macro and Micro Mechanical Model, *Journal of Aerospace Engineering*, vol. .25 (5), September 2015, DOI: 10.1061/ AS.1943-5525.0000241, 2013.

Notations

Aij, Bij, etc :	Laminate stiffnesses
BB :	Strain-displacement matrix
a, b :	Plate length and breadth
bi :	Basic random system properties
*E*11, *E*22 :	Longitudinal and Transverse elastic moduli
*G*12, *G*13, *G*23 :	Shear moduli
h :	Thickness of the plate
Kl :	Linear bending stiffness matrix
Kg :	Thermal geometric stiffness matrix
M, m :	Mass and inertia matrices
NE, NL :	Number of elements, number of layers in the laminated plate
Nx, Ny, Nxy	In-plane thermal buckling loads
NN :	Number of nodes per element
ϕ_i	Shape function of ith node
Qij :	Reduced elastic material constants
$\{\Lambda\}^{(e)}, \{\Lambda\}^{(e)}$	: Vector of unknown displacements, displacement vector of eth element
U,	Strain energy due to bending
u , v , w :	Displacements of a point on the mid plane of plate
u, v, w :	Displacement of a point (x, y, z)
{σ }, { ε} :	Stress vector, Strain vector
y, x :	Rotations of normal to mid plane about the x and y axis respectively
x, y, k :	Two slopes and angle of fiber orientation wrt x-axis for kth layer
x, y, z :	Cartesian coordínales
Var( ) :	Variance
RVs :	Random variables
T :	Difference in temperatures
α_1, α_2:	Thermal expansion coefficients along x and y direction
β_1, β_2:	Coefficients of hygroscopic expansion along x and y direction.

Appendix (A)

$$\left(A_{ij}, B_{ij}, D_{ij}, E_{ij}, F_{ij}, H_{ij}\right) = \int_{-h/2}^{h/2} Q_{ij}\left(1, z, z^2, z^3, z^4, z^6\right)dz \text{ ;(i,j=1,2,6)}, \quad \left(A_{ij}, D_{ij}, F_{ij}\right) = \int_{-h/2}^{h/2} Q_{ij}\left(1, z^2, z^4\right)dz \text{ ;} \qquad \text{(i,j=4,5)}$$

$$\left[K_b\right] = \sum_{i=1}^{n} \int_{A^{(e)}} \left[B_b\right]^T \left[D_b\right]\left[B_b\right] dA \text{ ; } \left[K_s\right] = \sum_{i=1}^{n} \int_{A^{(e)}} \left[B_s\right]^T \left[D_s\right]\left[B_s\right] dA \text{ , } \left[K_g\right] = \sum_{i=1}^{n} \int_{A^{(e)}} \left[B_g\right]^T \left[N_0\right]\left[B_g\right] dA \ \{q\} = \sum_{e=1}^{NE} \{\Lambda\}$$

$$\left[F^T\right] = \sum_{i=1}^{n} \int_{A^{(e)}} \left[\left[B_{1i}\right]^T \left[N^T\right] + \left[B_{b1i}\right]^T \left[M^T\right] + \left[B_{b2i}\right]^T \left[P^T\right]\right] dA$$

where

$$[D_b]=\begin{bmatrix} \varphi_i,_x & 0 & 0 & 0 & 0 & 0 & 0 \\ \varphi_i,_y & 0 & 0 & 0 & 0 & 0 & 0 \\ 0 & \varphi_i,_x & 0 & 0 & 0 & 0 & 0 \\ 0 & \varphi_i,_y & 0 & 0 & 0 & 0 & 0 \\ 0 & 0 & \varphi_i,_x & 0 & 0 & 0 & 0 \\ 0 & 0 & \varphi_i,_y & 0 & 0 & 0 & 0 \\ 0 & 0 & 0 & C_1\varphi_i,_x & 0 & 0 & 0 \\ 0 & 0 & 0 & 0 & C_1\varphi_i,_y & 0 & 0 \\ 0 & 0 & 0 & C_1\varphi_i,_y & C_1\varphi_i,_x & 0 & 0 \\ 0 & 0 & 0 & -C_2\varphi_i,_x & 0 & -C_2\varphi_i,_x & 0 \\ 0 & 0 & 0 & 0 & -C_2\varphi_i,_y & 0 & -C_2\varphi_i,_y \\ 0 & 0 & 0 & -C_2\varphi_i,_y & -C_2\varphi_i,_x & -C_2\varphi_i,_y & -C_2\varphi_i,_x \end{bmatrix}\{q\} \quad [D_s]=\begin{bmatrix} 0 & 0 & \varphi_i,_x & 1 & 0 & 0 & 0 \\ 0 & 0 & \varphi_i,_x & 0 & 1 & 0 & 0 \\ 0 & 0 & 0 & -3 & 0 & -3 & 0 \\ 0 & 0 & 0 & 0 & -3 & 0 & -3 \end{bmatrix}\{q\}$$

$$[B_{ti}]=\begin{bmatrix} \varphi_i,_x & 0 & 0 & 0 & 0 & 0 & 0 \\ 0 & \varphi_i,_y & 0 & 0 & 0 & 0 & 0 \\ 0 & 0 & 0 & 0 & 0 & 0 & 0 \\ \varphi_i,_y & \varphi_i,_x & 0 & 0 & 0 & 0 & 0 \end{bmatrix} \quad [B_{bi}]=\begin{bmatrix} 0 & 0 & 0 & 0 & 0 & C_1\varphi_i,_x & 0 \\ 0 & 0 & 0 & 0 & 0 & 0 & C_1\varphi_i,_y \\ 0 & 0 & 0 & 0 & 0 & C_1\varphi_i,_y & C_1\varphi_i,_x \end{bmatrix} \quad [B_{si}]=\begin{bmatrix} 0 & 0 & \varphi_i,_x & 0 & 0 & C_1\varphi_i & 0 \\ 0 & 0 & \varphi_i,_y & 0 & 0 & 0 & C_1\varphi_i \end{bmatrix}$$

$$[B_{gi}]=\begin{bmatrix} 0 & 0 & \varphi_i,_x & 0 & 0 & 0 & 0 \\ 0 & 0 & \varphi_i,_y & 0 & 0 & 0 & 0 \end{bmatrix} \quad [N_0]=\begin{bmatrix} N_x & N_{xy} \\ N_{xy} & N_y \end{bmatrix} \quad [B_{1i}]=[B_{ti}];\ [B_{bii}]=[B_{bt}];\ [B_{b2i}]=[B_{si}];$$

$$\bar{Q}_{11}=Q_{11}\cos^4\alpha+2(Q_{12}+2Q_{66})\cos^2\alpha\sin^2\alpha+Q_{22}\sin^4\alpha$$
$$\bar{Q}_{12}=\bar{Q}_{21}=(Q_{11}+Q_{22}-4Q_{66})\cos^2\alpha\sin^2\alpha+Q_{12}(\cos^4\alpha+\sin^4\alpha)$$
$$\bar{Q}_{16}=(Q_{11}-Q_{12}-2Q_{66})\sin\alpha\cos^3\alpha+(Q_{12}-Q_{22}+2Q_{66})\sin^3\alpha\cos\alpha$$
$$\bar{Q}_{22}=Q_{11}\sin^4\alpha+2(Q_{12}+2Q_{66})\cos^2\alpha\sin^2\alpha+Q_{22}\cos^4\alpha$$
$$\bar{Q}_{26}=(Q_{11}-Q_{12}-2Q_{66})\sin^3\alpha\cos\alpha+(Q_{12}-Q_{22}+2Q_{66})\sin\alpha\cos^3\alpha$$
$$\bar{Q}_{66}=(Q_{11}+Q_{22}-2Q_{12}-2Q_{66})\cos^2\alpha\sin^2\alpha+Q_{66}(\cos^4\alpha+\sin^4\alpha)$$
$$\bar{Q}_{44}=Q_{44}\cos^2\alpha+Q_{55}\sin^2\alpha$$
$$\bar{Q}_{45}=(Q_{55}-Q_{44})\,sin\alpha\cos\alpha-Q_{54}$$
$$\bar{Q}_{55}=Q_{55}\cos^2\alpha+Q_{44}\sin^2\alpha$$

$$Q_{11}=\frac{E_{11}}{(1-\nu_{12}\nu_{21})}\ ,\ Q_{12}=\frac{\nu_{12}E_{22}}{(1-\nu_{12}\nu_{21})}=\frac{\nu_{21}E_{11}}{(1-\nu_{12}\nu_{21})}=Q_{21}\,,Q_{22}=\frac{E_{22}}{(1-\nu_{12}\nu_{21})}\ ,\ Q_{66}=G_{12}\ ,\ Q_{44}=G_{13}\,,Q_{55}=G_{12}\ ,\ \nu_{21}=\frac{\nu_{12}E_{22}}{E_{11}}$$

Systems Engineering for the Design and Fabrication of a Screw-Propelled Automated Martian Regolith Collector Robot

Washington University in St. Louis

Michael Bouchard[1], Nathaniel Stein[2], Hans McConnell[3], Bradley Settle[4], Sam Lazecheko[5], Michael Kelley[6], Michael Zanetti[7], Ramesh Agarwal[8+]

Washington University in St. Louis, Missouri 63130, USA

[1]mcbouchard@wustl.edu; [2]n.stein@wustl.edu;[3]hmcconnell@wustl.edu; [4]bsettle@wustl.edu; [5]slazechko@wustl.edu; [6]kelleym@wustl.edu;[7]mikezanetti@yahoo.com;[8]rka@wustl.edu

Abstract

The Screw-Propelled Automated Martian Regolith CollectorRobot Version 2.0 system was designed by a team of students from Washington University in St. Louis through the implementation of an iterative and increasingly detailed design process directed by a systems engineering management plan. The team made decisions based on Key Performance Attributes and a set of functions allocated from NASA specifications. The team derived the robot's physical architecture from these functions and principal fabrication was completed by the team. The completed system was entered in the sixth annual Robotic Mining Competition at Kennedy Space Center in May 2015 where the team was ranked10thout of 46 teams.

Keywords

Systems Engineering; Systems Architecture; Robotic Mining, Screw-Propelled Automated Regolith Collector

System Architecture

Design Philosophy

1) Introduction

In the spring of 2015 the Washington University in St. Louis Robotic Mining Club (WuRMC) adapted a full systems engineering program for the implementation of their Screw-Propelled Automated Regolith Collector (SPARC) Robot. Systems engineering is an interdisciplinary process that allows for the hierarchical reduction in ambiguities of an infinite solution space in order to realize the best possible solution to a complex problem(Blanchard, 2011). It is a heuristic driven application of an overarching program which controls the transition of capability to an operational and suitable system. The WuRMC applied this systems engineering approach across the entire project life cycle from ideation to design to fabrication, integration, and testing.

FIG. 1 WURMC'S SCREW-PROPELLED AUTOMATED REGOLITH COLLECTOR

2325-6796/16/02 112-14, © 2016 DEStech Publications, Inc.
doi: 10.12783/fae.2016.0502.03

In this paper the system is defined as the SPARC V-2.0, its components, attributes, interfaces, and their interaction with the environment (Fig. 1)(Blanchard, 2011). These four elements comprise the foundation of systems engineering. The system's environment is defined as the operational setting of the Sixth Annual NASA Robotic Mining Competition, which was held in May 2015 at the Kennedy Space Center(KSC, 2014).

Through an iterative design process the team was able to specify requirements, allocate functions, derive a physical architecture, and perform several trade studies for the selection of the best fit subsystems. WuRMC adapted a system architecture with specific application and organization of the system engineering process and tools following the specifications in the NASA's Systems Engineering Processes and Requirements Handbook version 2012 (NASA, 2012).

The system architecture of SPARC V-2.0 is represented by the V-diagram in Fig. 2. Along the leading diagonal is the System Design Process which includes the Stakeholder Expectation Definition, the Technical Requirements Definition, the Logical Decomposition, and Design Solution steps. These steps represent an iterative and increasingly detailed design process starting with the customer (NASA) needs and ending with a mature mining robot design. The following diagonal represents the Product Realization Process and includes the Product Implementation, Product Integration, Product Verification and Validation, and Product Transition steps. These steps represent an increasingly more complex integration of components until the complete system is capable of executing the intended capabilities. The center section in Fig. 2 describes the Technical Management Process which calls out the various planning and management lines that were monitored.

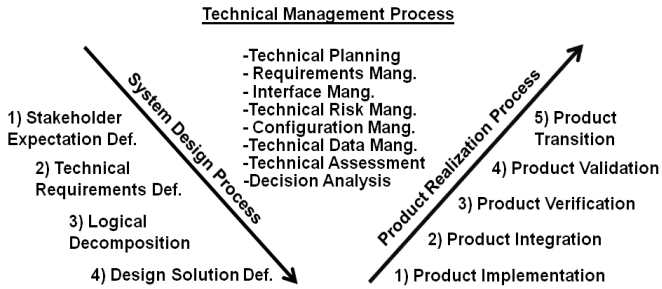

Fig. 2 WuRMC's SYSTEMS ENGINEERING PROCESS

2) Stake Holder's Expectation Definition

The first step of any systems engineering process is to clearly articulate the desires of the customer. This step is crucial to the success of the system because ultimately it is the satisfaction of the customer that dictates the success of the project. The customer in this interaction is the NASA Mining Robotics Competition Entity(KSC, 2014). This process begins with a need statement.

The expressed need is for a remote controlled or autonomous robot that is capable of transporting itself across a simulated Martian chaotic terrain of loose regolith, craters and boulders collecting regolith at depth and transporting and ultimately depositing the regolith into collection bins(KSC, 2014). The purpose of this competition was to engage university students in addressing and solving some of the challenges that would be encountered by the future planetary pioneers.

The next step for both the systems engineer and the customer is to expand upon the needs statement with a list of requirements. These requirements, when fulfilled, should meet the intended needs of the customer, and should be detailed and specific enough so that they can be included later in the System Design Process. The ability of the system to meet design requirements was tested in the Product Verification stage. For this competition the customer's requirements were detailed in the competition's 2015 Rules and Rubrics document(KSC, 2014), and state of the art planetary mining technologies were researched (Boucher, 1999; Boucher, 2004; Dissly, 2004; Feng, 2009; McKay, 1992; Stoker, 2004; Taylor, 2004).

The WuRMC team divided the competition requirements into three categories: static requirements, active requirements, and logistical requirements. The static requirements represent the innate on-robot structural attributes such as mass and volume restrictions. The motor requirements explain the operational needs and

actionable capabilities of the robot, and include data volume, power usage, startup and shutdown procedures, and completion operations. The logistical requirements refer to requirements that do not directly apply to the robot functions, but are required by the competition such as task timing and safety protocols.

3) Technical Requirements Definition

Once the customer and system engineer have agreed on the design requirements, the system engineer turns these requirements into a more detailed set of specifications that the participating team engineers can include in the design. This is done in a top down fashion with form following function. The primary function that the team's robot seeks to accomplish is to robotically mine planetary regolith. In order to accomplish this, three principal actions are required, which can be described as "the three d's": Dig, Drive, and Dump. This colloquial summary can be allocated into a series of technical functions. These functions are traverse (drive); excavate (dig), deposit (dump), and the latent functions (Fig. 3). Latent functions are actions the robot must be capable of carrying out in order to accomplish all other functions, but they do not tie directly to a single function. Each of these functions flows down into more detailed sub-functions under each heading. These functions represent the capabilities of the system, that is what the system will be able to accomplish once it is functional.

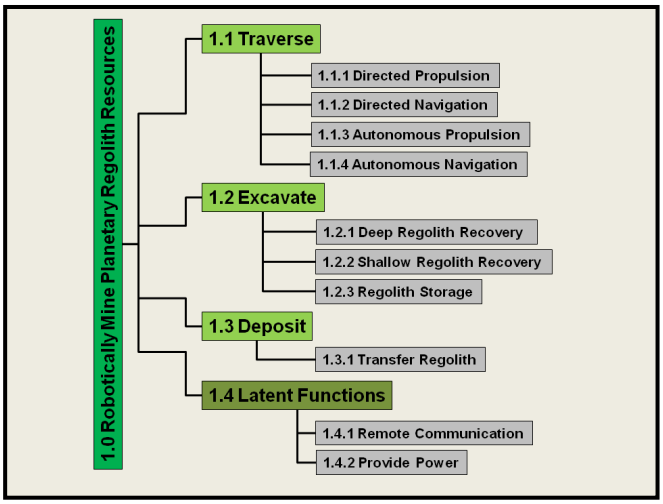

FIG. 3 THREE TIERED FUNCTIONAL ALLOCATION

4) Decision Analysis

The decision making process is of paramount importance to any engineering project. The team decided as a group on their Key Performance Attributes (KPA). These attributes describe the system performance, what the team values in the system, and drive how trade-off decisions for the design phase were made. The KPAs were prioritized to allow efficient decision making, and are displayed in a Kiviat Chart (Fig. 4). Kiviat Charts are a quick way to assess how well a system meets its desired attributes. The goal is to maximize the area within the Kiviat. If the system as a whole scores is less than 12, or any one KPA score is less than 2, the system will be deemed unacceptable. The preferred score would be 18, with not more than one KPA below 3. The team's final system assessment Kiviat can be found in section 2.4.5 in the Performance Summary. The team selected the following attributes as the system's KPAs:

1. *Functionality*: A measure of how well the system actually operates in response to commands and the environment.
2. *Excavation*: Maximization of the amount of regolith mined and returned to the dump site.
3. *Producibility*: A measure of the proposed design's ability to be fabricated given the team member's skills and timeline.
4. *Innovation*: Approaches to the design problems that are considered new and creative.
5. *Automation*: A measure of how well the robot operates without any human operation.

Within the scope of this system, decisions were driven by the prioritized KPAs. These decisions were made in iterative phases of increasing detail so that other subsystems could stay up to date with the whole design as the

system matured. Many of these decisions were made through the application of trade-off studies and are detailed in section 2.3 describing the Design Selection.

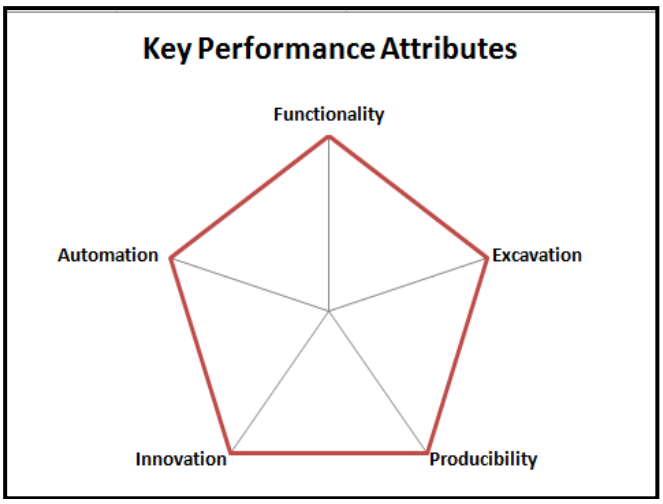

FIG. 4 IDEAL KIVIAT ASSESSMENT OF KPA'S

Project Life Cycle

The team's project life cycle followed the systems engineering v-diagram dividing the design process into conceptual, preliminary, and critical phases. Each of these phases became increasingly more detailed and had unique exit requirements. The conceptual design phase consisted of open brain storming periods where all ideas were considered. This process included the entire team and from the variety of ideas, a general concept was agreed on. Based on the target KPAs and function capability, the team decided to design a reciprocal-excavation, screw-propelled mining robot(Boucher, 2004). These two primary systems were chosen to give the best chance of functionality maximizing the regolith return, and still resulting in an innovative design.

1) Schedule

The team stayed on schedule through the preliminary design phase. However the critical design phase, which involved several detailed trade studies ended up taking much longer than was anticipated. The team ended up prototyping and began preliminary fabrication while still completing the critical design reviews. This was not ideal, since usually the completion of the critical design review preceded the beginning of fabrication. The team also ran into unanticipated issues such as procurement of the rotating screws (drive pontoons)from Australian tailings mining company 'Residue Solutions'. However, the basic frame design was mature enough that subsystems fabrication could begin in late January of 2015. The delay on pontoon specifications and complexities in the final set of critical design trade studies caused a delay in the team's Critical Design Review. However, additional time reserve was built into the schedule for this kind of unforeseen situation; thus the internal due dates were set well before the external due dates allowing the team to meet the competition deadlines.

The major internal deadline of 13 April 2015 got the team motivated and back on track with completion of the robot. However, this left the team about a month behind the final phases of the originally planned schedule. Therefore, system integration, testing, training, travel logistics, and verification were completed simultaneously by dividing tasks among different team members, and the team was able to compete at the end of May 2015 to meet the NASA competition deadline.

2) ***Major Reviews***

Each of the three design phases had an exit requirement of a design review. These were conducted at varying levels of detail as was required by the level of design. As described previously, the conceptual design review included the entire team. Members submitted their conceptual level designs, sketches and ideas and the team discussed the merits, draw-backs and potential of each idea. Once each major subsystem was whittled down to one or two concepts, the conceptual level review was completed. Decisions were documented and the groups

were assigned to investigate the remaining major design decisions. Major trade-offs were completed which are discussed in section 2.4.1 on Trade-Off Assessments.

The Preliminary Design Review (PDR) was a structured and formaldesign review and the WuRMC team had an actual organization(Residual Solutions) to interact with. In the conceptual design review, the WuRMC team decided to go with the unique and innovative screw propulsion system they had pioneered a year before in 2014 competition. The team's principal company sponsor, Residue Solutions, utilizes screw propulsion for major mining, mineral processing, and land reclamation equipment. For the PDR the WuRMC team sent design documentation and basic robot specifications to be reviewed by the Residue Solutions engineering team. The Residue Solutions team sent back comments and questions regarding the screw flight angles and spacing. The WuRMC team responded to the comments and questions, and the pontoon external design was finalized with the help of Residue Solutions. This review also required a near final estimate of weight, size and speed to be selected. The objective of the PDR was to get external feedback on the team's in-process design, the finalization of one major subsystem, the traverse system, and the vetting of these systems specifications in order for the pontoon hardware to begin production. The selected design specifications are given in section 2.3 on Design Selection.

The Critical Design Review (CDR) was more rigorous and included a detailed report on the system design and constituted the team's proposed final design. This documentation was sent to Residue Solutions, who acted as a stand in for the competition entity, and the team's faculty professor. Ideally this CDR would have been completed before principal fabrication began, but due to challenges described above the design were not finalized until late March of 2015. Once the comments on CDR documentation from the Residue Solutions were received and addressed, the team officially closed the Critical Design Phase. The objectives of the CDR were to have at least two experienced engineers from two different entities examine the team's final design and provide comments to the team. The review of these comments and the implementation of any final alterations or adjustments constituted the exit requirements of the CDR.

Team Management

1) *Work Flow*

The WuRMC team designed their Work Breakdown Structure (WBS) to reflect the project execution and team's needs (Fig. 5). The elected team leadership was placed into upper management positions while team members with experience in technical fields were put into positions where their direct experience would be most useful. New team members were assigned to specific projects or sub-teams. In 2014, the team arrived at competition behind schedule and with robot one inch too wide. In 2015, the team operated with several levels of management reserve built into both the design and team operation. Three team members were assigned the specific duties of managing power, data, and mass and volume budgets, and were responsible for ensuring that at no point the design would exceed any of the limiting specifications. The management team allotted reserve time in the schedule in order to allow the inevitable schedule creep, and made sure to raise enough funds to ensure a margin of safety for last-minute procurements.

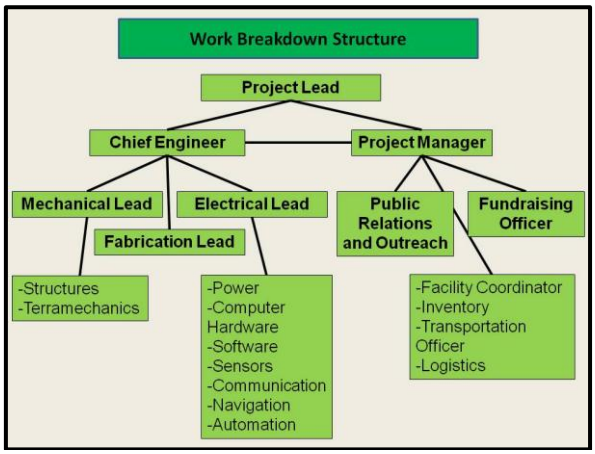

FIG. 5 WuRMC'S WORK BREAKDOWN STRUCTURE (WBS)

2) ***Cost Budget***

The team had a very successful fundraising campaign and raised a total of $7,400 from various sources including Washington Universityin St. Louis, corporate sponsorships, and research grants. The team also secured significant donations in parts and equipment, the most notable of which was the donation of a 2-D Laser Scanning LiDAR system from SICK incorporated with a $7,000 off-the-shelf value. The team's principal sponsor also donated the drive pontoons, valued at $1,500 in materials. These contributions drove down the technical costs of the team significantly, and allowed excess money to be allocated for the entire team's transportation needs to the competition site. The team created an estimated budget based on year 2014's procurements, and carefully monitored the year 2015's spending.

System Design & Fabrication

Concept of Operations

1) ***Operation Control Diagram***

The flow of operations is summarized in the OV-1 operational control document (Fig. 6). There are two phases of operation: remote control (yellow) and autonomous (orange). For the remote control human-in-the-loop operation there is a necessary telemetry feedback loop. Humans send commands via the wireless blue tooth connection to the onboard rover transmitter/receiver, a panda wireless-N USB adapter. Data travels from the receiver and is relayed to the onboard computation center, a Raspberry Pi. The Raspberry Pi relays control commands to the Arduino Uno microcontroller which communicatesby PWM and series signals to the slave Sabertooth 2x6 and Talon SR motor controllers. The Sabertooth and Talon motor controllers control the drive and dig motors respectively. The team receives telemetry from the Raspberry Pi in the form of camera feed and power data.

During autonomous operational control, the wireless communication, camera feed, and human command station are completely removed from the system. The LiDAR system collects a 3-dimensional point cloud in which the robot locates itself. Then the Raspberry Pi uses this information to make decisions about navigation and execute the predetermined excavation routine. Once the robot collects a full dump receptacle of regolith, it autonomously traverses and deposits the regolith in the competition collection site. This process continues until the competition run time has expired. During this whole operation the robot streams its camera feed to the command station to allow the humans to monitor the robots progress. If at any time the robot performs off-nominally, the team has the ability to get into the system and return to human-in-loop control operations.

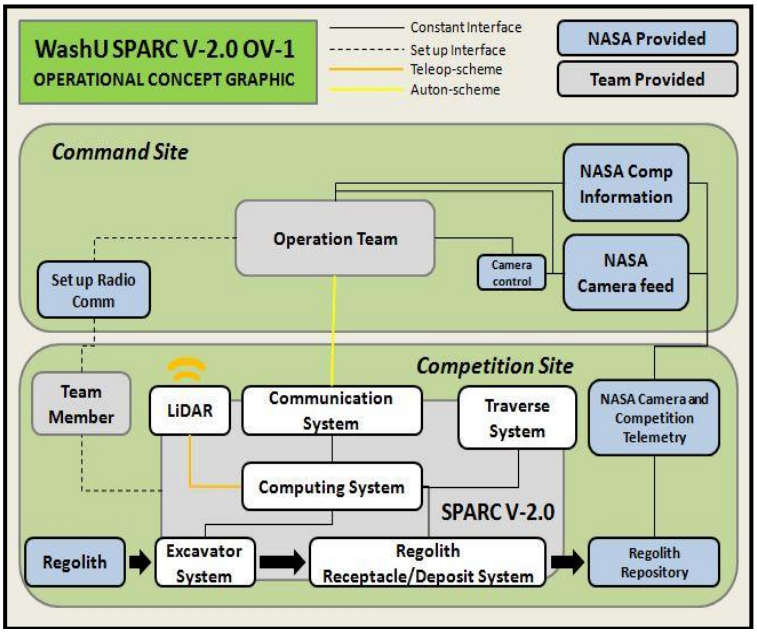

FIG. 6 SPARC 2.0 OPERATIONAL CONTROL DOCUMENT

Logical Decomposition

1) Systems Hierarchy

The SPARCV-2.0 system was designed through an iterative, top down approach. The team worked through a series of increasingly detailed design phases and made decisions based on the KPAs. The team allocated a set of functions which the system was capable of completing and from these functions derived the robots physical architecture. The principal fabrication work was completed by two sub-teams: a Mechanical sub-team and an Electrical sub-team. The Mechanical sub-team machined all the aluminum frame parts, connectors and housings, while the Electrical sub-team programmed and wired all the electronics.

2) Physical Architecture

The SPARC V-2.0 robot's physical architecture is derived from the system functions (Fig. 7). The physical components are grouped into four sub-systems: the Traverse, Excavation, Deposition, and Latent subsystems. These sub-systems comprise of all physical components of the robot. The Traverse sub-system comprises of the drive pontoons, the drive motors, the batteries (located within each pontoon), and the traverse motor controllers. It also comprises the general on-board computing, wireless communication,and mapping sensor. The Excavation sub-system includes the excavation receptacle and excavation motor system, while the Deposition sub-system consists of the regolith receptacle and deposition mechanism(Boucher, 2004). The remaining components fall into the Latent sub-system. These include the general frame, power distribution, and safety and support electronics. Structural components are discussed in detail in section 2.2.3.1.

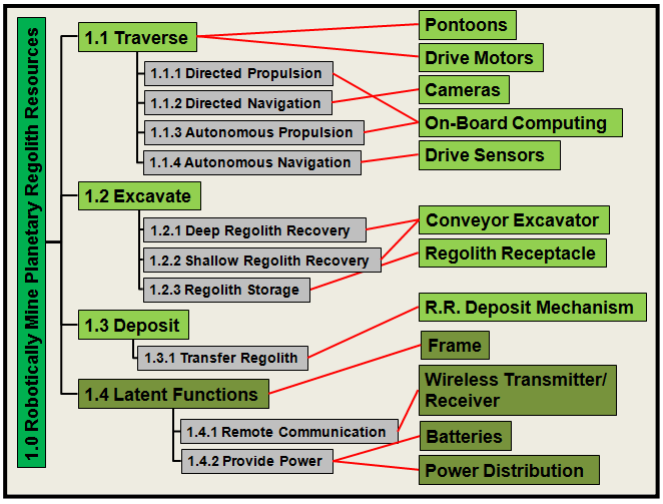

FIG. 7 PHYSICAL ARCHITECTURE TIED TO FUNCTIONS

3) Interfaces

The connection points between all the components are important sources of potential failure and must be monitored closely. The internal connections are represented using interface control documents. The system's interaction with the environment is another important level of interaction and is already represented with the OV-1 operation control document.

3.1) Structural Components

The SPARC V-2.0 robot's structural interfaces show how the different sub-systems physically interact. The drive motors, controllers and power source are within the drive pontoons (Fig. 8). The remaining electrical and computing components, power distribution, and communication components are housed in the electronics box. This box and the pontoons are fixed to the robot frame. Also fixed to the frame are the exaction and deposition systems. These two components are structurally fixed to reduce the number of required actuators and reduce the complexity. The same actuators that lower the reciprocating excavation system raise the attached deposition system for regolith delivery. The SPARC V-2.0 is constructed out of t6-6061 aluminum, and measures 1.45 m long, 0.74 m tall, and 0.70 m wide.

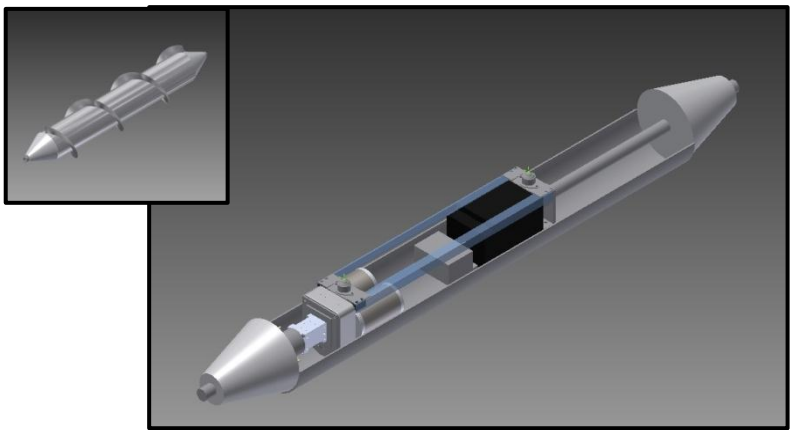

FIG. 8 INTERNAL PONTOON LAYOUT

3.2) Electrical and Data Components

The electrical and data interfaces are very important to plan for both the design and its implementation. These are detailed in the following wiring diagram, which is also a graphical representation of the electrical and computing interfaces (Fig. 9).

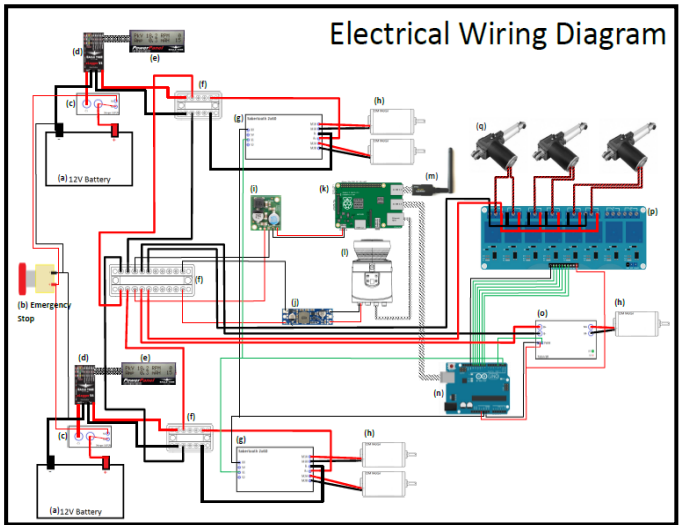

FIG. 9 ELECTRICAL AND DATA WIRING AND INTERFACES

Figure 9 shows the following components:

a) Two 12V Batteries provide electrical power for the robot.
b) Emergency Stop Button allows for emergency battery disconnect.
c) Stinger SGP38 Relay disconnects the batteries when E-Stop is triggered.
d) Eagle Tree eLogger V4 provides power consumption measurement. Each logger measures the power output from one battery.
e) Eagle Tree PowerPanel displays the power consumption of the robot.
f) Blue Sea Systems DualBus Bus Bars provide power distribution throughout the robot.
g) Sabertooth 2x60 Motor Controllers are used to control the drive motors speed.
h) CIM Motors are used to rotate the drive pontoons, and for digging system.
i) Pololu 5V, 5A Step-Down Voltage Regulator lowers the voltage from 12V to 5V in order to power the Raspberry Pi.
j) Pololu 24V Step-Up Voltage Regulator raises the voltage from 12V to 24V in order to power the Sick LMS111 laser.
k) Raspberry Pi acts as primary computing module on the robot.

l) Sick LMS111 laser provides positioning data for autonomous operation.

m) Panda Wireless-N USB Adapter provides networking capability to allow the robot to communicate wirelessly.

n) Arduino Uno relays commands from the Raspberry Pi via USB to other electrical components using digital, PWM, and serial signals.

o) Talon SR Motor Controller provides motor control for the digging motor.

p) The SainSmart 8 Channel Relay Module provides on/off control of the actuators in the digging system.

q) PA 02-24-200 linear actuators are used for the digging system.

Design Selection

Once the physical architecture was derived, the next stage of the iterative design cycle - the detailed subsystem design and part selectionbegan. First this was completed at a preliminary level to decide between major design options and then at a critical level to bring the design to completion. These were principally completed in a series of trade-off studies. These trade-off studies were given to small groups of specialized team members who completed investigations that ranged from research to prototyping to modeling. The ultimate decisions of the trade-off studies were driven by the team's Key Performance Attributes.

1) Trade-off Assessments

Here only two of the trade-off studies completed by the team are highlighted. These trade-off studies were done as a part of the design process to make informed decisions. Other trade-off studies that were completed but are not described in this paper included: excavation trade-off (front loader vs. backhoe vs. reciprocating digger), deposit system trade-off, computing hardware trade-off (Raspberry Pi vs. Tablet), sensor mounting trade-off (telescoping vs. pivoting), and a materials trade-off (aluminum vs. composites vs. carbon fiber).

1.1) Power Supply Selection Trade-off Study

In order to select an appropriate power supply system, the team completed a trade-off study. After research the team down-selected and sourced three different battery options: a Sealed Lead Acid, a Lithium Iron Phosphate, and a Nickel Metal Hydride battery. Each of the batteries was evaluated in seven categories derived from the KPA values. The categories were prioritized and given relative weights (Fig. 10). This resulted in the selection of the Lithium Iron Phosphate as the battery of choice.

(All Values Per Pontoon)	Sealed Lead Acid	Lithium Iron Phosphate	Nickel Metal Hydride	Relative Value
Maximum Pulse Current	180 A	70 A	~30 A	3
Maximum Constant Current	~40 A	25 A	~15 A	2
Weight	9.25 lb	3.55 lb	3.6375 lb	5
Volume	88.5 in^3	90.3 in^3	11.8 in^3	1
Capacity	13 Ah	12 Ah	12 Ah	1
Damage-Tolerance	High	High	Low	2
Price	$47.99	$139.00	$195.00	1
Unweighted Score	9	8	5	
Weighted Score	17	21	13	

FIG. 10 POWER SUPPLY SELECTION TRADE-OFF STUDY MATRIX

1.2) Traverse Design Trade-off Study

The team ultimately selected rotating screws as the propulsion method for terrain traversing. This was selected after evaluating several traditional drive mechanisms. The screw propulsion outperformed all the other mechanisms in every KPA. In 2014, this drive system proved very capable in the BP-1 regolith, and easily handled maneuvers and obstacles proving its functionality. The screw-propulsion is the most innovative propulsion system in the field.

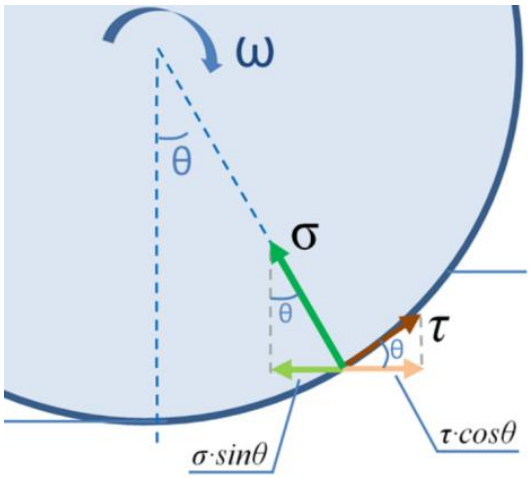

FIG. 11 CUTAWAY VIEW OF PONTOON, LATERAL MOTION IS DOMINATED BY SHEAR AND NORMAL STRESS (STEIN, 2014)

Screw-propelled vehicles use one or more cylinders fitted with helical flanges to navigate terrains typically characterized by high sinkage(Stein, 2014). Two-cylinder screw-propelled vehicles such as SPARC V-1.0 and V-2.0 are capable of forwarding and backwarding (longitudinal) motion during which the pontoons are rotated inward and outward respectively, and in side-to-side (lateral) motion in which the pontoons are simultaneously rotated in the drive direction(Stein, 2014). During lateral drives, the screws can be treated as long, non-deformable wheels with motion dominated by shear-stresses between the cylinder surface and the soil(Stein, 2014). Ignoring flight-soil interactions, lateral motion is controlled by motion resistance(R) and traction (T) which are related to normal and shear stresses as $T = \tau\cos\theta$ and $R = \sigma\sin\theta$ where τ and σ are shear and normal stress respectively, and θ is the angle between the side of the screw and the terrain at the exit point (Fig. 11)(Stein, 2014). In deformable surfaces such as lunar regolith, τ and σ are a function of soil properties including cohesion, internal friction angle, and shear modulus (Wong, 2001). Traction and motion resistance are functions of wheel sinkage. Due to the large area of the screw-terrain interface which reduces surface pressure, screw-propelled vehicles are characterized by relatively low sinkage that minimizes motion resistance and maximizes traction(Stein, 2014).

During longitudinal drives, the vehicle is propelled by interactions between the flanges and surrounding medium with efficiency proportional to the helix angle (Fig. 12)(Stein, 2014). Variations in helix angle affect multiple parameters including ground deformation, drawbar pull and slip, although no single angle optimizes every parameter (Cole, 1961).

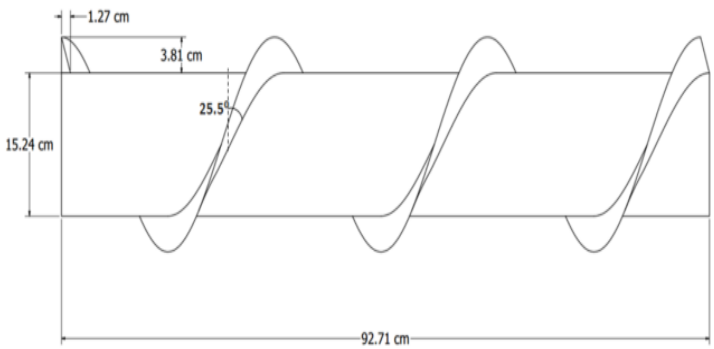

FIG. 12 SIDE VIEW OF SPARC PONTOON (STEIN, 2014)

The SPARC V-2.0 Mobility Design consisted of two 91.45 cm long, 15.25 cm wide aluminum tubes with oppositely threaded 3.8 cm high continuous aluminum helix grousers each driven by 88:1 geared 12 V 6.35 cm CIM brushed DC motors(Stein, 2014). Motors and batteries were mounted on an axle within the pontoons, which were shielded from dust by PVC endcaps that served the additional purpose of bulldozing material during longitudinal drives. A helix angle of ~25^0 was selected to balance motor efficiency with slip and drawbar pull(Stein, 2014). The team presented this screw propulsion design at the 14th ASCE International Conference on Engineering and at the 2015 Lunar Planetary Science Conference (Stein, 2014).

1.3) Torque Selection Trade-off Study

The next level of detail was addressed with a complimentary trade-off study to select the optimal torque. The team member completing this trade-off created a model to evaluate various inputs to output relationships which allowed the team to quantitatively select the appropriate level of torque required (Fig. 13). The model computed current, speed, power, and efficiency plotted as a function of torque for a generic CIM motor. The model was developed using motor performance research (FIRSTintern, 2015). As the model stepped from no torque to stall torque, the RPM changed linearly.

	Last Year	This Year		Motor Torque	Motor RPM	Amperage	Gear for Torq	RPS at Gear	RPS Difference
Total Torque	142.55	142.55		0	5310	2.7	#DIV/0!	#DIV/0!	#DIV/0!
Torque per Motor	71.27	35.64		0.01	5288.09406	3.23754125	3563.72648	0.02473111	1.47526889
Amperage	50	49.47		0.02	5266.18812	3.77508251	1781.86324	0.04925732	1.45074268
Gearing	81	40.96		0.03	5244.28218	4.31262376	1187.90883	0.07357863	1.42642137
Predicted RevPS	0.696	1.044		0.04	5222.37624	4.85016502	890.931619	0.09769504	1.40230496
Actual RevPS		1.385		0.05	5200.4703	5.38770627	712.745295	0.12160656	1.37839344
				0.06	5178.56436	5.92524752	593.954413	0.14531318	1.35468682
				0.07	5156.65842	6.46278878	509.103782	0.16881491	1.33118509
				0.08	5134.75248	7.00033003	445.46581	0.19211173	1.30788827
Speed Ratio	1.5			0.09	5112.84653	7.53787129	395.969609	0.21520366	1.28479634
Amp Cutoff	50			0.1	5090.94059	8.07541254	356.372648	0.23809069	1.26190931
Row of Best Gear	89			0.11	5069.03465	8.6129538	323.975134	0.26077282	1.23922718
				0.12	5047.12871	9.15049505	296.977206	0.28325006	1.21674994

FIG. 13 SELECTION FROM EXCEL MODEL FOR DRIVE TORQUE

The gearing ratios from year 2014 competitionwere used as an input to determine the torque output from the motors. If the current is known, the unguarded torque of each motor can be derived. Multiplying the torque by the gearing ratio gives the total torque, which is used to derive the revolutions per second. The model allowed the team to understand how changing various factors affected the ultimate drive torque of the robot, and allowed a quantitative decision to be reached.

Management of Fabrication and Testing

The systems engineering process starts at the top and guides the design and implementation phases of the project all the way to product delivery. However in both the design and implementation phase(see v-diagram in Fig. 2), there was an active level of internal monitoring and evaluation that constituted the Technical Management Process. Internal monitoring is the glue which holds the v together in Fig. 2, and was divided up into sub-disciplines and was delegated to different team members to monitor as various phases occurred.

The initial plans were laid out to incorporate management reserves. For example, there was a conscious effort to ensure that the year 2015's robot would not exceed the volume restrictions which required major last-minute adjustments in year 2014's competition. There was also management reserve built into the schedule, which allowed for the inevitable schedule creep. One of the most important aspects of keeping a team on track was inter-team communication. This was facilitated through weekly group administrative meetings beyond the weekly work periods, at which sub-systems were evaluated and updates were given. Major decisions and plans were documented and were sent out as electronic tag-ups allowing absent members to stay informed, and ensuring that changes were adequately documented.

1) Technical Budgets

The first technical budget required consideration of the mass and volume restrictions. The competition rules required the mass limit to be 80 kg, with penalty points for each kg of the robot's total unloaded mass. The volume limit was 1.5 m length x 0.75 m width x 0.75 m height. A team member was assigned to monitor both of these metrics through the entire design phase and was responsible for letting the team know if the potential design decisions were in jeopardy due to exceeding ofthe dimensional and/or weight restrictions. The ultimate decision to build the robot out of aluminum came out of a materials trade-off study where it was determined that aluminum offered the best strength to weight ratio, and was within the team's fabrication capability. Volume was also monitored by the configuration manager, who organized the physical layout of the internal electronic components within the electronics box. This was done in a fashion to minimize complexity in wiring to minimize the total volume and thus the weight.

The data budget was the responsibility of the chief programmer. He advised the computing decisions and hardware selection accordingly. The competition rules stated that the average maximum bandwidth use must be less than5 Mbps average. However it was in the interest of the team to keep the bandwidth as low as possible since every 50 Kbps results in a point deduction. The team used the NASA provided camera, which started the team off at a base data usage of 120 Megabits. In year 2014, the team used an average of 8 bps, but SPARC V-2.0's maximum usage was 32 bps. There was no telemetry feed back to the operating team members; this was a design decision to keep the transmitted bandwidth as low as possible. There was also a data cost due to the use of WiFi and TCP/IP. The code ran on the onboard Raspberry pi, which counted toward the total number of packets sent. In testing, the team was able to predict the robots data consumption for a typical run.

The team's electrical lead was responsible for monitoring the projected power production and consumption. The power supply was two 12.8 V, 12 Ah, 153.6 Wh rechargeable Lithium Iron Phosphate batteries. Based on a ten minute run, the SPARC V-2.0 consumed 80 watt hours of energy, which was an estimated 25-30% draw out of the total power source. The batteries contained enough power to perform both competition runs on a single charge.

2) Reliability

One of the most important duties of the technical managers was to ensure that the product was reliable. This meant that the product could safely execute its intended capabilities within the operational environment. Safety was the first priority of the group. Nothing within the team's scope was worth endangering anyone and themselves. This was handled on two fronts. First the robot itself was designed with safety in mind. The team implemented the required off-the-shelf voltage meter in order to allow the competition entities to monitor the power situation, and intervene or remove personnel from a potentially dangerous situation. The team also considered safety during the design process, and the robot was equipped with a well labeled easily accessible emergency stop button.

The second part of project safety included the actual team operations. The team went through safety training for access to the campus machine shop, encouraged people to work in pairs, and followed common sense safety protocols. The other aspect of reliability is that the system can actually complete the assigned functions completely and satisfactorily and consistently. The team evaluated the system's performance in both of these categories through implementing system technical assessments for verification and validation

3) Verification

The process of product verification is a measure of how well the system meets the needs and requirements of the customer. This can be best evaluated by examining the initial requirements which were used to inform the design process, and to determine if the product actually met these requirements. As previously stated, the WuRMC derived the requirements from the competition rules and rubrics, and divided them into three categories, static requirements, active requirements, and logistical requirements. Each of these three different categories required a different approach to verification.

The static requirements mostly pertain to the robot's structural and physical attributes such as mass and volume. These were straight forward to verify and their compliance was guaranteed bytaking static measurements of the robot and comparing them to the requirements of the customer. The SPARC V-2.0 met all the prescribed innate static requirements.

The active requirements were more complex and required a full system operations test. The test involved putting the robot through several steps of the competition run both in selected sub-operations and in full operation. These tests included excavation tests where the team practiced recovering regolith from different depths and traverse tests where the team practiced driving the robot across mocked up terrain and obstacles, and deposition tests where the robot deposited various payloads into a model reception bin. The final set of tests was a series of timed full operation practice runs. These tests took place in a reduced scale test pit. These tests evaluated the robot's ability to meet the operational functions as defined in Fig. 3. The robot was able to accomplish all intended operational tasks required in the competition in these tests. This was made possible due

to the team's commitment to delivering an operational robot to the competition, as has been previously articulated in the paper through having set functionality relative to the primary KPA's.

The final set of verification tests was designed to address the logistical requirements. These requirements concerned competition logistics such as timing and safety protocol. The final round of motor tests was timed, allowing the team to be able to evaluate how the robot performed under competition conditions. The robot regolith collection was slower than was desired, but this allowed the team to address options to boost recovery rate. The robot passed all safety tests in the implemented safety hardware.

4) Validation

The process of product validation usually involves the customer and its assessment of the systems performance. Ideally the initial steps of deriving the needs statement, requirements, functional allocation, and further design flow down should be carried out reasonably well so that the ultimate product is what the customer desires. However this is not always the case, that is why customer's interaction is very crucial in the early phases of the process. The validation of SPARC V-2.0 occurred at NASA's Sixth Annual Robotic Mining Competition, held at the Kennedy Space Center from the 18to 22 May 2015. This competition was NASA's opportunity to evaluate SPARC V-2.0 in action. The team did their best to design to the customer's satisfaction, which was the fundamental purpose of adoptinga systems engineering process. The team competed against 46 other university teams from across the country. In order to transport the robot to competition, the team disassembled the entire robot and had to re-assemble it onsite. Unfortunately the re-assembly contaminated the pontoons and created motor control issues resulting in some performance problems during the two runs of the robot. Despite these challenges, the team's final score placed WuRMC in 10th place.

System Summary

Performance Summary

Prior to competition at Kennedy Spae Center, the performance of SPARC V-2.0 was assessed using the data collected during the tests run at Washington University by conducting the Kiviat assessment (Fig 14). This assessment graphically shows how well the system performs in each of the five KPA's. In order to pass this assessment the robot's individual KPA value should be greater than two on one to five scale, with a total score greater than 12. The preferred score for SPARC V-2.0 was 18, with not more than one KPA below a 3. The Kiviat assessment ranked Functionality as 4/5, excavation as 3/5, Producibility as 5/5, Innovation as 5/5, and Automation as 3/5. The robot functioned well, but not perfectly. The robot turned out to be very dependable and quite innovative withthe employment of screw propelled drive system. Its total KPA score was 20. This score met an acceptable system performance metric. Unfortunately, the robot's overall performance in the 2015 competition at Kennedy Space Center was less than nominal due to problems resulting from onsite re-assembly, power management, and water contamination in the competition site.

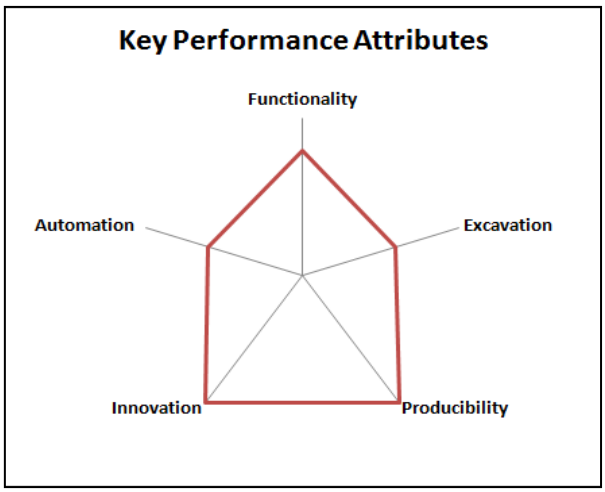

FIG 14: FINAL KIVIAT ASSESSMENT

Systems Engineering Summary

In the 2015 NASA Robotic Mining competition, WuRMC team adopted a full systems engineering approach, incorporating an iterative design cycle, KPA and function driven design choices, and a much more extensive verification, validation, and testing regime. As a second year team in 2015, WuRMC was able to build upon the baseline robot from the 2014 competition and incorporate the concept of management reserve into the project. The higher level of planning and attention to details helped the team to address problems and implement the best solution comprehensively. The team demonstrated itself to be capable to address the challenge of planetary regolith mining. There were necessary evolutions of plans, schedules and even designs over time as the team learned or discovered new things, but these were implemented within the procedures, styles, and resources of the systems engineering process. Through the systems engineering process, the team was able to meet the competition's requirements, designing an innovative robotic excavation platform that could remotely recover planetary materials. In this manner, WuMRC hopes to contribute to NASA and the nation's vision of a bright future in space exploration.

ACKNOWLEDGEMENTS

The last author of this paper is Dr. Ramesh Agarwal who served as the team's faculty advisor. Fabrication and storage space, and machine shop tools were provided by Washington University in St. Louis.

REFERENCES

[1] Blanchard B.S., and Fabrycky W.J., "Systems Engineering and Analysis Fifth Edition" Prentice Hall Internatoinal Series in Industrial and Systems Engineering (2011)

[2] Boucher D., Richard J., "Report on the Construction and Testinf of a Bucket Wheel Excavator,"Space Resources Roundtable 6, Colorado School of Mines , (2004) LPI Contribution No. 1224, pg 13

[3] Boucher D., "Planetary Mining: Planning the Dig anf d Digging the Plan," Lunar Planetary Science Conference 30,(1999) #988

[4] Cole N., *Proc. Inst. Mech. Eng.* (1961) 175(919).

[5] DissleyR.W., et al., "Autonomous In-Situ Resources Prospector," Space Resources Roundtable 6, Colorado School of Mines , (2004) LPI Contribution No. 1224, pg 17

[6] Feng Y.L., et al., "Obstacle performance of a planetary wheel mining vechile in the deep sea bed" Journal of Science and Technology Bejing (2009), pg. 923-928

[7] FIRSTintern , "Motor and Gearbox Design." accessed from web 4 March 2015, accessed October 2014 http://www.instructables.com/id/Understanding-Motor-and-Gearbox-Design/step3/Motor-Curves/

[8] Kennedy Space Center (KSC), NASA's Sixth Annual Robotic Mining Competition Rules & Rubrics 2015, (2014) accessed September 2014. https://www.nasa.gov/sites/default/files/robotics_mining_competition_rules_2015.pdf

[9] McKay M.F., McKay D.S., Duke M.B., editors, "Space Resources" NASA Scientific and Technical Information Program 509 (1992)

[10] NASA Systems Engineering Processes and Requirements, NPR 7123.1A, NODIS, (2007-2012).

[11] Stein N.,et. al., "A Screw Propulsion Design for Mobility in High-Sinkage Media," Lunar Planetary Science Conference 45,(2014) #2352

[12] Stoker C., "Drilling to Extract Liquid Water on Mars: Feasible and Worth the Investment," Space Resources Roundtable 6, Colorado School of Mines , (2004) LPI Contribution No. 1224, pg 44

[13] Taylor L.A., et al., "The Nature of Lunar Soil: Considerations for Simulants" Space Resources Roundtable 6, Colorado School of Mines , (2004) LPI Contribution No. 1224, pg 46

[14] Wong J., *Theory of Ground Vehicles, 3rd ed.* (2001) 9902-4.

Hygrothermoelastic Nonlinear Flexural Response of Graphite Epoxy Laminated Composite Plates with Uncertain System Properties

SfemMicromechanical Model Approach Investigation

Rajesh Kumar*[1], Million Merid Afessa[1]

School of Mechanical Engineering, Jimma Institute of Technology,Jimma University, Jimma, Ethiopia

*[1]rajeshtripathi63@gmail.com; [2]millionmerid208@gmail.com

Abstract

This paper presents Hygrothermoelastic nonlinear flexural response of graphite epoxy composite plates with uncertain system properties. Lamina material properties, geometric properties, coefficients of thermal expansion, coefficients of hygroscopic expansion and lateral load are modeled as basic random variables using micromechanical model. A higher order shear deformation theory in the von-Karman sense is used to model the system behavior of the laminated plate. A direct iterative based C0 nonlinear finite element method in conjunction with the first order perturbation technique developed earlier is extended for hygrothermal problem to obtain the second order response statistics, i.e., mean and coefficient of variations of nonlinear transverse central deflection of the plate. Typical numerical results are obtained for various combinations of geometric parameters, uniform lateral pressures, staking sequences, volume fractions, aspect ratios, plate thickness ratios, boundary conditions under environmental conditions. The results obtained have been compared with those available in the literature and an independent Monte Carlo simulation.

Keywords

Micromechanical Model; Nonlinear Bending Response; Stochastic Finite Element Method; Uncertain System properties

I.Introduction

Composite laminated structures are being increasingly used in aeronautical and aerospace construction due to gaining wide popularity as light weight components, ability to tailor structural properties through appropriate lamination scheme for achieving high strength and stiffness to weight ratio. These plates are often combination of transverse mechanical and hygrothermal loading. Due to low shear modulus compared to in-plane Young's modulus, transverse shear deformation even more pronounced in composite laminates. The capability to predict the structural response and enable a better understanding and characterization of the actual behavior of laminated composite plates when subjected to combined load is of prime interest to structural analysis. In fact, many structures are subjected to high load levels that may result in nonlinear load-deflection relationships due to large deformations of the plates. One of the important problems deserving special attention for accurate prediction of structural response in sensitive application is the study of their nonlinear response to large deflations by assuming random system properties as independent random variables.

During typical operating conditions structures are constantly being subjected to random load like engine noise, shocks waves, turbulence, gusts, track inputs, thermal loads, winds and acoustic loads. Therefore, the external loading is also random in nature.Some of these structures are often subjected to severe loading that result in large response and consequently demand the investigation. For reliability of design, accurate prediction of system behaviour of the laminated composite structures in the presence of randomness in the system properties is needed. A considerable volume of literature is available on the static response of geometrically linear and nonlinear

2325-6796/16/02 126-25, © 2016 DEStech Publications, Inc.
doi: 10.12783/fae.2016.0502.04

composite laminated plates under various thermal and mechanical loads or combination of two. (See examples [1-9]). All based on the assumptions of the complete determinacy of structural parameters. In the deterministic analysis of structures, the variations in the system parameters are neglected and mean value of system parameters are used in the analysis. Due to the dependency of large numbers of parameters in complex production and fabrication processes of laminated composite plate. The system properties can be random in natures resulting in uncertainty in the response of the plate. Therefore to well define the original problems and enable a better understanding and characterization of the actual behaviour of the laminated composite structures, it is obviously of prime important that the inherent randomness in system parameters be incorporated in the analysis. Relatively little effort hasbeen made in the past by the researchers and investigators on the prediction of the thermo-mechanical bending response of the structures made of laminated composites plates having random system properties. Based on higher order theory, Naveenth Raj et al. [10] have evaluated the linear static response statistics of graphite-epoxy composite laminates with randomness in material properties for different boundary conditions, thickness ratios, aspect ratios and fibre orientations to deterministic loading by using combination of finite element analysis and Monte Carlo simulation (MCS). Salim et al. [11] also examined the effect of randomness in material properties (like elastic modulus Poisson's ratios etc.,) on the response statistics of a composite plate subjected to static loading using classical plate theory (CLT) in conjunction with first order perturbation techniques (FOPT). Onkar and Yadav [12] have investigated the non-linear response statistics of composite laminated flat panel with random material properties subjected to transverse random loading based on CLT in conjunction with FOPT. Yang et al. [13] have investigated the stochastic bending response of moderately thick compositionally graded plates with random system properties under lateral load and uniform temperature change.They have utilized a first order perturbation technique to obtain the response statistics, while basic formulation of the problem has been developed based on Reddy's higher order shear deformation theory (HSDT). Zongeen and Suhaun [14] presented a method to estimate the standard deviation of eigenvalue and eigenvector of random multiple degree of freedom system. Zhang et al. [15] have applied the stochastic perturbation method to vector-valued and matrix-valued function for the response and reliability of uncertain structures. Liu et al. [16] formulated the probabilistic finite element method (PFEM) for linear and nonlinear continua with homogeneous random fields of a one dimensional elastic plastic wave propagation problems and a two dimensional plane-stress beam bending problem. Zhang and Ellingwood [17] examined the effect of random material field characteristics on the instability of a simply supported beam on elastic foundation and a frame using perturbation technique. Noh [18] framed stochastic finite element analysis to investigate the effect of multiple uncertain material properties on the response variability of in-plane and plate structures with multiple uncertain material parameters. Keeping in mind above aspect, in the present work, an HSDT proposed by Lal et al. [19] and Singh et al. [20] is extended to random environments. They presented C^0 linear and nonlinear finite element method (FEM) in conjunction with a FOPT to obtain the second order response statistics of bending deflection of laminated composite plate supported with and without elastic foundation. They included the transverse shear effects in the system equation using HSDT. In order to incorporate the uncertainties of the physical properties of laminated composite structures, a stochastic finite element based second moment was developed by Park et al. [21]. Pandit et al. [22 and 23] presented the improved higher order plate model to study the response statistics of a soft core sandwich plates. A computationally efficient C^0 stochastic finite element method (SFEM) based on mean centered FOPT hasbeen proposed to obtain the second order statistics of deflection of sandwich plate under transverse loading. Lal et al. [24,25]studied the effect of random system properties on bending response of thermo-mechanically loaded laminated composite plates and stochastic nonlinear bending of thermo-mechanically loaded (consists of a lateral pressure and thermal loading) laminated composite plates for macro mechanical model in the presence of small random variation in the system variables taking into account the transverse shear strain using the HSDT with von-Karman nonlinear strain displacement relations. Shen et al. [26] studied the hygrothermal effects on the nonlinear bending of shear deformable laminated plates using deterministic finite element method and micromechanical model. Upadhyay et al. [27] investigated the nonlinear flexural response of laminated composite plates under hygro-thermo-mechanical loading using deterministic finite element method and micromechanical model. R Kumar et al. [37,38,39] investigated the linear and nonlinear flexural response of laminated composite plates with random material properties and plates restin

on a Nonlinear Elastic Foundation with Uncertain System Properties under Lateral Pressure and Hygrothermal Loading

.To the best of the authors' knowledge, there is no literature covering the second order response statistics of geometrically nonlinear laminated composite plates, subjected to combined lateral pressure and hygrothermal loading involving randomness in system properties for micromechanical model using computationally efficient C0 nonlinear finite element method in conjunction with mean centred first order perturbation technique (FOPT). This is the problems studied in the present paper.

In the present study, the stochastic nonlinear bending of hygrothermo-mechanically loaded (consists of a lateral pressure and hygrothermal loading) laminated composite plates in the presence of small random variation in the system variables taking into account the transverse shear strain using the HSDT with von-Karman nonlinear strain displacement relations is studied. A direct iterative based C^0 nonlinear FEM in conjunction with the mean centered FOPT as developed by the authors is extended and employed to determine the second-order-statistics (mean and standard deviation) of nonlinear transverse central deflection of laminated composite plates subjected to uniform constant temperature and moisture(U.T). The numerical illustrations concern the stochastic nonlinear bending response of laminated composite plate subjected to uniform temperature and moisture distribution over plate surface and through the plate thickness are obtained for various combinations of geometric parameters, uniform lateral pressures, staking sequences, volume fraction, aspect ratio, plate thickness ratio, boundary conditions under environmental conditions. It is observed that small amount of random system properties variations of the composite plate in the presence of temperature and moisture(hygrothermal) significantly affect the nonlinear transverse central deflection. The proposed probabilistic procedure would be valid for system properties with small random coefficient of variations compared to their mean value which is usually satisfied by most engineering applications.

II. Formulations

Consider geometry of laminated composite rectangular plate of length a, width b, and thickness h, which consists of N-plies located in three dimensional Cartesian coordinate system (X, Y, Z) where X- and -Y plane passes through the middle of the plate thickness with its origin placed at the corner of the plate as shown in Fig. 1. Let $(\bar{u}, \bar{v}, \bar{w})$ be the displacements parallel to the (X, Y, Z) axes, respectively. The thickness coordinate Z of the top and bottom surfaces of any k_{th} layer are denoted by $Z_{(k-1)}$ and $Z_{(k)}$ respectively. The fiber of the K_{th} layer is oriented with fiber angle θ_k to the X- axis. The plate is assumed to be subjected to uniformly distribute transverse static load is defined as $q(x,y) = q_o$.

2.1 Displacement field model

In the present study, the assumed displacement field is based on the Reddy's higher order shear deformation theory [28], which requires C^1 continuous element approximation. In order to avoid the usual difficulties associated with these elements the displacement model has been slightly modified to make the suitability of C^0 continuous element [29]. In modified form, the derivatives of out-of-plane displacement are themselves considered as separate degree of freedom (DOFs).

Thus five DOFs with C^1 continuity are transformed into seven DOFs with C^0 due to conformity with the HSDT. In this process the artificial constraints are imposed which should be enforced variationally through a penalty approach. However the literature [29] demonstrates that without enforcing these constraints the accurate results using C^0 can be obtained. The modified displacement field along the X, Y, and Z directions for an arbitrary composite laminated plate is now written as

$$\begin{aligned} \bar{u} &= u + f_1(z)\psi_x + f_2(z)\phi_x; \\ \bar{v} &= v + f_1(z)\psi_y + f_2(z)\phi_y; \\ \bar{w} &= w; \end{aligned} \tag{1}$$

where $\bar{u}$, $\bar{v}$ and $\bar{w}$ denote the displacements of a point along the (X, Y, Z) coordinates axes: u, v and w are corresponding displacements of a point on the mid plane, $\phi_x = w,_x$ and $\phi_y = w,_x$ and ψ_x, ψ_y are the rotations of normal to the mid plane about the y-axis and x-axis respectively. The functions $f_1(z)$ and $f_2(z)$ can be written as

$f_1(z) = C_1 z - C_2 z^3$; $f_2(z) = -C_4 z^3$ with $C_1 = 1, C_2 = C_4 = 4h^2/3$.

The displacement vector for the modified C^0 continuous model is denoted as

$$\{\Lambda\} = \begin{bmatrix} u & v & w & \phi_y & \phi_x & \psi_y & \psi_x \end{bmatrix}^T, \tag{2}$$

where, comma (,) denotes partial differential.

2.2 Strain Displacement Relations

For the structures considered here, the relevant strain vector consisting of strains in terms of mid-plane deformation, rotation of normal and higher order terms associated with the displacement for kth layer are as

$$\{\varepsilon\} = \{\varepsilon_l\} + \{\varepsilon_{nl}\} - \{\bar{\varepsilon}_{HT}\} \tag{3}$$

where $\{\varepsilon_l\}$, $\{\varepsilon_{nl}\}$ and $\{\bar{\varepsilon}_{HT}\}$ are the linear and nonlinear strain vectors, hygrothermal strain vector, respectively.

Using Eq. (3) the linear strain vector can be obtained using linear strain displacement relations [29, 30], which can be written as

$$\{\varepsilon_l\} = \begin{Bmatrix} \varepsilon_P^L \\ 0 \end{Bmatrix} + \begin{Bmatrix} z\varepsilon_b^L \\ \varepsilon_s \end{Bmatrix} + \begin{Bmatrix} 0 \\ z^2\varepsilon_s^* \end{Bmatrix} + \begin{Bmatrix} z^3\varepsilon^* \\ 0 \end{Bmatrix} \tag{4}$$

where,

$$\{\varepsilon_P^L\} = \begin{Bmatrix} u_{0,x} \\ v_{0,y} \\ u_{0,y} + v_{0,x} \end{Bmatrix}, \quad \{\varepsilon_b^L\} = C_1 \begin{Bmatrix} \psi_{x,x} \\ \psi_{y,y} \\ \psi_{x,y} + \psi_{y,x} \end{Bmatrix}$$

$$\{\varepsilon^*\} = -C_2 \begin{Bmatrix} \psi_{x,x} \\ \psi_{y,y} \\ \psi_{x,y} + \psi_{y,x} \end{Bmatrix} - C_4 \begin{Bmatrix} \theta_{x,x} \\ \theta_{y,y} \\ \theta_{x,y} + \theta_{y,x} \end{Bmatrix}, \tag{5}$$

$$\{\varepsilon_s\} = C_1 \begin{Bmatrix} \psi_y \\ \psi_x \end{Bmatrix} + \begin{Bmatrix} w_{,y} \\ w_{,x} \end{Bmatrix}, \{\varepsilon_s^*\} = -C_2 \begin{Bmatrix} \psi_y \\ \psi_x \end{Bmatrix} - C_4 \begin{Bmatrix} w_{,y} \\ w_{,x} \end{Bmatrix},$$

Assuming that the strains are much smaller than the rotations (in the von-Karman sense), one can obtain nonlinear strain vector $\{\varepsilon_{nl}\}$ of the Eq. (4) as [30]

$$\{\varepsilon_{nl}\} = \frac{1}{2}[A_{nl}]\{\phi\} \tag{6}$$

Where

$$\{A_{nl}\} = \frac{1}{2}\begin{bmatrix} w_{,x} & 0 \\ 0 & w_{,y} \\ w_{,x} & w_{,y} \\ 0 & 0 \\ 0 & 0 \end{bmatrix} \text{ and } \{\phi\} = \begin{Bmatrix} w_{,x} \\ w_{,y} \end{Bmatrix}, \tag{7}$$

The hygrothermal strain vector $\{\bar{\varepsilon}_{HT}\}$ is represented as [36]

$$\{\bar{\varepsilon}_{HT}\} = \begin{Bmatrix} \bar{\varepsilon}_x \\ \bar{\varepsilon}_y \\ \bar{\varepsilon}_{xy} \\ \bar{\varepsilon}_{yz} \\ \bar{\varepsilon}_{zx} \end{Bmatrix} = \Delta T \begin{Bmatrix} \alpha_1 \\ \alpha_2 \\ \alpha_{12} \\ 0 \\ 0 \end{Bmatrix} + \Delta C \begin{Bmatrix} \beta_1 \\ \beta_2 \\ \beta_{12} \\ 0 \\ 0 \end{Bmatrix} \tag{8}$$

α_1, α_2 and α_{12} are coefficients of thermal expansionand, β_1, β_2 and β_{12} are coefficients of hygroscopic expansion along the x, y, z direction respectively which can be obtained from the thermal coefficients in the longitudinal (α_l) and transverse (α_t) directions of the fibers using transformation matrix and ΔT is the change in temperature and hygroscopic coefficients in the longitudinal (β_l) and transverse (β_t) directions of the fibers using transformation matrix and ΔC is the change in moisture in percentage in the plate subjected with uniform moisture ($\Delta C = C_0$ in percentage) and temperature ($\Delta T = T_0$)rise (U.T) .

2.3 Stress–strain relation

The constitutive law of thermo-elasticity for the materials under considerations relates the stresses with strains in a plane stress state for the *k*th lamina oriented as an arbitrary angle with respect to reference axis for the orthotropic layers is given by [30] $\{\sigma\}_k = [\bar{Q}]_k \{\varepsilon\}_k$

$$\text{Or} \begin{Bmatrix} \sigma_x \\ \sigma_y \\ \sigma_{xy} \\ \sigma_{yz} \\ \sigma_{xz} \end{Bmatrix}_k = \begin{bmatrix} \bar{Q}_{11} & \bar{Q}_{12} & \bar{Q}_{16} & 0 & 0 \\ \bar{Q}_{12} & \bar{Q}_{22} & \bar{Q}_{26} & 0 & 0 \\ \bar{Q}_{16} & \bar{Q}_{26} & \bar{Q}_{66} & 0 & 0 \\ 0 & 0 & 0 & \bar{Q}_{44} & \bar{Q}_{45} \\ 0 & 0 & 0 & \bar{Q}_{45} & \bar{Q}_{55} \end{bmatrix}_k \{\{\varepsilon_l\} + \{\varepsilon_{nl}\} - \{\bar{\varepsilon}_{HT}\}\} \tag{9}$$

where, $\{\bar{Q}_{ij}\}_k$, $\{\sigma\}_k$ and $\{\varepsilon\}_k$ are transformed stiffness matrix, stress and strain vectors of the *k*th lamina, respectively.

2.4 Strain energy of the plate

The strain energy (Π) of the laminated composite plate is given by

$$\Pi = \frac{1}{2}\int_V \{\varepsilon\}^T [\sigma] \mathrm{dV}. \tag{10}$$

Using Eqs. (3)-(8), the strain energy as given above can be written as

$$\Pi = \Pi_l + \Pi_{nl} \tag{11}$$

Where, Π_l and Π_{nl} are the linear and the nonlinear strain energy respectively which are expressed as

$$\Pi_l = \frac{1}{2}\int_A \{\bar{\varepsilon}_l\}^T [\bar{Q}] \{\varepsilon_l\} dA \tag{12a}$$

$$\Pi_{nl} = \frac{1}{2}\int_A \{\varepsilon_{nl}\}^T [\bar{Q}] \{\varepsilon_l\} dA + \frac{1}{2}\int_A [\varepsilon_l]^T [\bar{Q}] \{\varepsilon_{nl}\} dA + \frac{1}{2}\int_A \{\varepsilon_{nl}\}^T [\bar{Q}] \{\varepsilon_{nl}\} dA \tag{12b}$$

1)Linear strain energy of the plate

Using linear strain displacement relations [20], the linear elastic strain energy as given in Eq. (12a) can be expressed as

$$\Pi_l = \frac{1}{2}\int_A \{\bar{\varepsilon}_l\}^T \left[\bar{Q}\right]\{\varepsilon_l\}\, dA \tag{13}$$

Where, $\{\bar{\varepsilon}_l\}$ is the linear strain vector at the reference plane, i.e.,z=0 and [D] is the laminate stiffness matrix.

2)Nonlinear strain energy of the plate

Using nonlinear strain displacement relations in the von Karman sense [30,35], the nonlinear energy as given in Eq. (12b) can be expressed as

$$\begin{aligned}\Pi_{nl} &= \frac{1}{2}\int_A [\bar{\varepsilon}_l]^T [D_3]\{A\}\{\phi\}\, dA \\ &+ \frac{1}{2}\int_A \{A\}^T \{\phi\}^T [D_4]\{\bar{\varepsilon}_l\}\, dA + \frac{1}{2}\int_A \{A\}^T \{\phi\}^T [D_5]\{A\}\{\phi\}\, dA\end{aligned} \tag{14}$$

Where, $[D_3]$, $[D_4]$ and $[D_5]$ are the laminate stiffness matrices as given in appendix and [A] and [ϕ] are defined in appendix.

2.5 Potential energy due to hygrothermal stresses

The potential energy (Π_2) storage by hygrothermal (combined temperature and moisture) load is written as

$$\begin{aligned}\Pi_2 &= \frac{1}{2}\int_A \left[N_x\left(w,_x\right)^2 + N_y\left(w,_y\right)^2 + 2N_{xy}\left(w,_x\right)\left(w,_y\right)\right] dA \\ &= \frac{1}{2}\int_A \begin{Bmatrix} w,_x \\ w,_y \end{Bmatrix}^T \begin{bmatrix} N_x & N_{xy} \\ N_{xy} & N_y \end{bmatrix} \begin{Bmatrix} w,_x \\ w,_y \end{Bmatrix} dA\end{aligned} \tag{15}$$

where, N_x, N_y andN_{xy} are pre-buckling hygrothermal stresses.

2.6 External work done

The potential energy due to distributed transverse static load $q\left(x, y\right)$ can be expressed as

$$\begin{aligned}\Pi_3 &= W_{ext} \\ &= -W_q = \int_A q\left(x, y\right)\, w\, dA\end{aligned} \tag{16}$$

where, $q(x, y)$ is the intensity of distributed transverse static load which is defined as $q\left(x, y\right) = \frac{QE_{22}h^3}{b^4}$ here Q is represented as uniform lateral load.

2.7. Finite element model

In the present study a C^0 nine-noded isoparametric finite element with 7 DOFs per node is employed. The domain is discretized into a set of finite elements. Over each of the element, the displacement vector and the element geometry are expressed as

$$\{\Lambda\} = \sum_{i=1}^{NN} \varphi_i \{\Lambda\}_i\,; \qquad x = \sum_{i=1}^{NN} \varphi_i x_i\,; \text{and } y = \sum_{i=1}^{NN} \varphi_i y_i \tag{17}$$

where, φ_i is the interpolation (shape function) function for the ith node, $\{\Lambda\}_i$ is the vector of unknown displacements for the ith node, NN is the number of nodes per element and xi and yiare Cartesian coordinate of the ith node.

1)Strain energy of the laminated plate

The linear and nonlinear functional are computed for each element and then summed over all the elements in the domain to get the total functional. Following this, and using Eq. (17), Eq. (10) can be written as

$$\Pi = \sum_{e=1}^{NE} (\Pi_l^{(e)} + \Pi_{nl}^{(e)}) \tag{18}$$

where,

$$\begin{aligned} \Pi_{nl}^{(e)} &= \frac{1}{2}\int_A \left\{\Lambda^{(e)}\right\}[K_{1nl}]^{(e)}\left\{\Lambda^{(e)}\right\} + \frac{1}{2}\int_A \left\{\Lambda^{(e)}\right\}[K_{2nl}]^{(e)}\left\{\Lambda^{(e)}\right\} \\ &+ \frac{1}{2}\int_A \left\{\Lambda^{(e)}\right\}[K_{3nl}]^{(e)}\left\{\Lambda^{(e)}\right\} \\ \Pi_l^{(e)} &= \left\{\Lambda^{T(e)}\right\}[K_l]^{(e)}\left\{\Lambda\right\}^{(e)} \end{aligned} \tag{19}$$

Here, [Knl](e), [K2nl](e) and [K3nl](e) are the elemental nonlinear stiffness matrices. [Kl](e) is the linear stiffness matrix and {Λ}(e) is the elemental nodal displacement vector.

Following the assembly procedure, Eq. (18) can be further written as

$$\Pi_1 = \frac{1}{2}\{q\}^T\left[K_l + K_{nl}\{q\}\right]\{q\} - \{q\}^T\left[F^{HT}\right] \tag{20}$$

With $\left[K_l\right] = \left[K_b\right] + \left[K_s\right]$ $\left[K_{nl}\right] = \left[K_b\right] + \left[K_s\right]$

where global bending stiffness matrix [Kb], shear stiffness matrix[Ks], global nonlinear stiffness matrix [Knl], global displacement vector {q}and hygrothermal load vector [FHT] are defined in the appendix.

2) Hygrothermal buckling analysis

Using finite element model (Eq. (20)), Eq. (18) can also be written as

$$\Pi_2 = \sum_{e=1}^{NE} \Pi_2^{(e)} = \frac{1}{2}\lambda\{q\}^T\left[K_g\right]\{q\} \tag{21}$$

Were, λ and $\left[K_g\right]$are defined as the hygrothermal buckling load parameters and the global geometric stiffness matrix, respectively.

3)Work done due to external transverse load

Using finite element model (Eq. (20), Equation (19) may be written as

$$\Pi_3 = \sum_{e=1}^{NE} \Pi_3^{(e)} \tag{22}$$

where

$$\begin{aligned} \Pi_3^{(e)} &= -\int_{A^{(e)}} \{\Lambda\}^{(e)T}\{P_M\}^{(e)}\, dA \\ &= -\{q\}^{(e)T}\{P_M\}^{(e)} \end{aligned} \tag{23}$$

with $\{P_M\}^{\{e\}} = \begin{pmatrix} 0 & 0 & q & 0 & 0 & 0 & 0 \end{pmatrix}^{T\{e\}}$

Adopting Gauss quadrature integration numerical rule, the element stiffness and geometric stiffness matrices, load vectors, respectively can be obtained by transforming expression in x, y coordinate system to natural coordinate system ξ, η.

III.Governing equation

The governing equation for the nonlinear static analysis can be derived using Variational principle, which is generalization of the principle of virtual displacement [30]. For the bending analysis, the minimization of first variation of total potential energy Π (Π1+Π2 + Π3) with respect to displacement vector is given by

$$\delta(\Pi_1+\Pi_2+\Pi_3) = 0 \tag{24}$$

by substituting Eqs. and simplification gives us.

$$[K_s]\{W\} = \{F\}, \tag{25}$$

with $[K_s] = [K_l + K_{nl}\{q\}]$ and $\{F\} = \{P_M\} + \{P_{HT}\}$

Where, [Kl], [Knl], {PM}and{PHT} are global linear, nonlinear stiffness matrix, global mechanical and hygrothermal force vector respectively defined in appendix.The stiffness matrix [Ks], displacement vector {W} and force vector [F] is random in nature, being dependent on the system properties. Therefore the eigenvalues and eigenvectors also become random. In deterministic environment, the solution of Eq. (25) can be obtained using iterative, incremental methods etc. However in random environment, it is not possible to obtain the solution using above mentioned numerical methods. Further analysis is required to obtain the complete solution of solution of Eq. (25).

For this purpose novel probabilistic procedure as developed by the authors [20] is extended for this problem in the present work. The direct iterative method combined with nonlinear finite element method, i.e., direct iterative based nonlinear finite element method in conjunction with mean centered FOPT (DISFEM) with a reasonable accuracy to obtain the second order statistics of nonlinear static response.

3.1 Solution approach — a DISFEM for nonlinear static bending problem

The random governing equation as given in Eq. (30) is solved by employing a DISFEM, assuming that the random changes in the transverse displacements do not affect much the nonlinear stiffness matrices with the following steps:

(i) The stiffness matrix [Ks] is obtained in the first step neglecting all nonlinear terms, yielding the linear stiffness matrix. Using the linear stiffness matrix and the displacement vector, the random governing equation is broken into the zeroth order and the first order equations using the perturbation technique. Then the displacement vector {W} is obtained from any standard deterministic method using the zeroth order equation. The first order perturbation technique as presented in the next Section 4.2 is then employed to obtain the standard deviation of the displacement response using the first order equation.

(ii) The displacement vector is normalized. For a specified maximum deflection C at the centre of the plate, the displacement vector is scaled up by C times, so that the resultant vector will have a displacement C at the maximum deflection point.

(iii) Using the scaled-up normalized displacement vector, the nonlinear terms in stiffness matrix [Ks] can be obtained. The problem may now be treated as a linear random static problem with the updated nonlinear stiffness matrix. The random linear static problem can again be broken up as stated in step (i) into the zeroth and the first order equations. The zeroth order can be used to obtain the nonlinear displacement vector {Wnl} and the random first order equations can be used to obtain standard deviation of the nonlinear displacement vector using the first order perturbation technique as presented in Section 4.2.

(iv) Steps (ii) and (iii) are repeated to obtain the converged nonlinear response vector {Wnl} to a prescribed accuracy (say ≈10−3).(v)Steps (i)–(iv) are repeated for various values of C.

3.2 Solution approach: perturbation technique

The governing equation (25) can be written in the most general form as:

$$\left[K_s^{\ R}\right]\left\{W^R\right\}=\left\{F^R\right\} \tag{26}$$

Where, $\left[K_s^{\ R}\right]$, $\left[W^R\right]$ and $\left\{F^R\right\}$ are represented as the random stiffness matrix, the random response vector and the random force vector respectively and superscript '*R*' denotes random.

Any random variable can be expressed as the sum of its mean and the zero mean random variable which is expressed as ,

random variable $\left(RV^R\right)$=mean $\left(RV^d\right)$+ zero-mean random variable $\left(RV^r\right)$

The operating random variables in the present case are defined as [31, 32]

$$b^R=b^d+b^r\ ;\ K_s^{\ R}=K_s^{\ d}+K_s^{\ r}\ ;\ W^R=W^d+W^r\ ;\ F^R=F^d+F^r \tag{27}$$

We can express the above relations in the form:

$$b^R=b^d+\in b^r\ ;\ K_s^{\ R}=K_s^{\ d}+\in K_s^{\ r}\ ;\ W^R=W^d+\in W^r\ ;\ F^R=F^d+\in F^r \tag{28}$$

Where, $\in$ is a scaling parameter, and is small in magnitude. The superscripts 'd' and 'r' denote the mean and zero mean random part.

We consider a class of problems where the zero-mean random variation is very small as compared to its mean part. Using the Taylor series expansion and neglecting the second and higher-order terms since the first order approximation is sufficient to yield results with desired accuracy having low variability as is the case in most of the sensitive application [31, 33 and 34]. Substituting Eq. (28) in Eq. (26) we get:

$$\left[K_s^{\ d}+\in K_s^{\ r}\right]\left\{W^d+\in W^r\right\}=\left\{F^d+\in F^r\right\} \tag{29}$$

Equating the terms of same order, we obtain the zeroth order perturbation equation and first order perturbation equation as fallows [34].

The zeroth order perturbation equation $\left(\in^0\right)$:

$$\left[K_s^{\ d}\right]\left\{W^d\right\}=\left\{F^d\right\} \tag{30}$$

The first order perturbation equation $\left(\in^1\right)$:

$$\left[K_s^{\ d}\right]\left\{W^r\right\}+\left[K_s^{\ r}\right]\left\{W^d\right\}=\left\{F^r\right\} \tag{31}$$

Obviously, the zeroth order Eq. (35) is the deterministic and gives the mean response. The first order Eq. (31) on other hand represents its random counterpart and solution of this equation provides the statistics of the nonlinear bending response, which can be solved using the probabilistic methods like perturbation technique, Monte Carlo simulation, Newman's expansion technique [31, 33 and 34].

Using Taylor's series expansion the system matrix,the displacement vector and forced vector can be expressed as [34];

$$\left[K_s^{\,r}\right]=\sum_l \frac{\partial K_s^{\,d}}{\partial b_l^{\,R}} b_l^{\,r}\ ,\ \left[W^r\right]=\sum_l \frac{\partial W^d}{\partial b_l^{\,R}} b_l^{\,r}\ ,\left[F^r\right]=\sum_l \frac{\partial F^d}{\partial b_l^{\,R}} b_l^{\,r} \tag{32}$$

Substituting Eq. (32) in Eq. (31) and equating the coefficients of b_l^r . For each l, we get:

$$\left[K_s^{\,d}\right]\left\{\frac{\partial W^d}{\partial b_l^{\,R}}\right\}+\left[\frac{\partial K_s^{\,d}}{\partial b_l^{\,R}}\right]\left\{W^d\right\}=\left\{\frac{\partial F^d}{\partial b_l^{\,R}}\right\},\ \ l\ =1,2\ldots \tag{33}$$

Using Eq. (33) we can solve the only unknown $\left\{\frac{\partial W^d}{\partial b_l^{\,R}}\right\}$, for each *l*.

Using Eq. (33), the total deflection response and its variance can be written as [32]

$$W=W^d+\left\{\frac{\partial W^d}{\partial b_l^r}\right\}b_l^r \text{ and } \operatorname{var}(W)=E\left[\sum_l \frac{\partial W^d}{\partial b_l^{\,R}} b_l^{\,r}\right]^2 \tag{34}$$

Where E [ ] and var (.) are the expectation and variance respectively. The variance can further be written as [32]

$$\operatorname{var}(W)=\sum_l^N\sum_l^N diag\left[\frac{\partial W^d}{\partial b_l^{\,R}}\left(\frac{\partial W^d}{\partial b_l^{\,R}}\right)^T\right]E\left(b_l^{\,r},b_l^{\,r}\right) \tag{35}$$

where, N is the number of variables and $E\left(b_l^{\,r},b_l^{\,r}\right)$ is determined from the autocorrelation function of the underlying stochastic field of b, which can be written as

$$E\left(b_l^{\,r},b_l^{\,r}\right)=[\sigma_b][\rho][\sigma_b] \tag{36}$$

$$\text{where, } [\sigma_b]=\begin{bmatrix}\sigma_{b1} & \ldots & \ldots & 0\\ 0 & \sigma_{b2} & \ldots & 0\\ \ldots & \ldots & \ldots & \ldots\\ 0 & \ldots & \ldots & \sigma_{bm}\end{bmatrix} \text{ and } [\rho]=\begin{bmatrix}1 & \rho_{12} & \ldots & \rho_{1m}\\ \rho_{21} & 1 & \ldots & \rho_{2m}\\ \ldots & \ldots & .. & \ldots\\ \rho_{m1} & \rho_{m2} & \ldots & 1\end{bmatrix} \tag{37}$$

Where, $[\sigma_b]$, $[\rho]$ and m are the standard deviation (SD) of random variables, the correlation coefficient matrix and number of random variables, respectively. Substituting Eq. (42) in Eq. (41), we obtain as:

$$\operatorname{var}(W)=\left(\frac{\partial W^d}{\partial b_l^{\,R}}\right)[\sigma_b][\rho][\sigma_b]\left(\frac{\partial W^d}{\partial b_l^{\,R}}\right)^T \tag{38}$$

Eq. (38) expressesthe covariance of the deflection in terms of the SD of random variables b_i (i=1, 2,…, R) and correlation coefficients. It is evident from Eq.(38) that the response coefficient of variation obtained by using the first perturbation techniques exhibits linear variation with all random variables in material properties, expansion of the thermal coefficients, lamina plate thickness and lateral loading.

IV.Results and discussion

The second-order statistics of nonlinear transverse central deflection is examined for laminated composite plates under lateral pressure and hygrothermal loading subjected to uniform temperature and moisture distribution over plate surface and through the plate thickness are obtained for various geometric parameters, uniform lateral pressures, staking sequences, volume fraction, aspect ratio, plate thickness ratio, boundary supports under

environmental conditions. A nine noded Lagrange isoparamatric element, with 63 DOFs per element for the present HSDT model has been used for discretizing the laminate. Based on convergence study conducted a (8 × 8) mesh has been used throughout the study.

The mean and coefficient of variation or variance (SD/mean) of the central nonlinear transverse deflection are obtained considering the random material input variables, hygroscopic expansion coefficients, thermal expansion coefficients, geometric parameters and lateral pressure taking combined as well as separately as basic random variables (RVs) as stated earlier. However, the results are only presented taking SD/mean of the system property equal to 0.10 [16] as the nature of the SD variation is linear and passing through the origin. Hence, the presented results would be sufficient to extrapolate the results for other COV value keeping in mind the limitation of FOPT. The basic random system variables such as E1, E2, G12, G13, G23, υ12, α1, α2, β2, h and Q are sequenced and defined as

$$b_1 = E_{11},\quad b_2 = E_{22},\quad b_3 = G_{12},\quad b_4 = G_{13},\quad b_5 = G_{23},\ b_6 = \upsilon_{12},$$
$$b_7 = \alpha_1,\quad b_8 = \alpha_2,\quad b_9 = \beta_2, b_{10} = h, b_{11} = Q$$

The following dimensionless nonlinear transverse mean central deflection and uniform lateral pressure has been used in this study.

$$W_{0nl} = W_{nl} / h, \qquad q(x, y) = \frac{QE_{22}h^3}{b^4}$$

where W_{nl} is dimensionalized mean transverse central deflection.

In the present study, various combination of boundary edge support conditions namely, simply supported (S1 and S2), clamped and combination of clamped and simply supported have been used and shown in Fig. 3. These are written as

All edges simply supported (SSSS):S1

$$u = v = w = \theta_y = \psi_y = 0, at\ x = 0, a;\quad u = v = w = \theta_x = \psi_x = 0\ at\ y = 0, b;$$

All edges simply supported (SSSS): S2

$$v = w = \theta_y = \psi_y = 0, at\ x = 0, a;\quad u = w = \theta_x = \psi_x = 0\ at\ y = 0, b;$$

All edges clamped (CCCC):

$$u = v = w = \psi_x = \psi_y = \theta_x = \theta_y = 0, at\ x = 0, a \quad and\ y = 0, b;$$

Two opposite edges clamped and other two simply supported (CSCS):

$$u = v = w = \psi_x = \psi_y = \theta_x = \theta_y = 0, at\ x = 0 \quad and\ y = 0;$$

$$v = w = \theta_y = \psi_y = 0, at\ x = a\ \ u = w = \theta_x = \psi_x = 0, at\ y = b;$$

The plate geometry used is characterized by aspect ratios (a/b) = 1and 2, side to thickness ratios (a/h) = 10, 20, 30 and 40. T=To+ΔT; where T= total temperature, To = Initial Temperature, ΔT = rise in temperature. C=Co+ΔC where C= total moisture concentration, Co= Initial moisture concentration, ΔC= rise in moisture concentration. The following material properties are used for computation Shen [26]:

To=25; Co=0; ΔT=00; ΔC=0.0;; Vf=0.5; Ef=230.0×1e9;

Gf=9.0×1e9; cfm=0; ϱc=1.5; vf=0.203; αf=-0.54×1e-6;

ϱf=1750; cfm=0; vm=0.34; αm=45×1e-6; ϱm=1200;

βm=2.68×1e-3; βf=0; Em=(3.51-0.003×T-0.142×C) ×1e9;

$G_m=E_m(\frac{2}{1+v_m})$, $E_{10}=(V_fE_f+V_mE_m)$

$$\alpha_{11}=\frac{VfEf\alpha f+VmEm\alpha m}{VfEf+VmEm}$$
$$\alpha_{22}=(1+\upsilon f)Vf\alpha f+(1+\upsilon m)Vm\alpha m-\upsilon_{12}\alpha_{11}$$
$$\beta_{11}=\frac{VfEfcfm\beta f+VmEm\beta m}{E_{11}(Vf\rho fcfm+Vm\rho m)}\rho$$
$$\beta_{22}=\frac{Vf(1+\upsilon f)cfm\beta f+Vm(1+\upsilon m)\beta m}{(Vf\rho fcfm+Vm\rho m)}\rho-\upsilon_{12}\beta_{11}$$
$$\rho=Vf\rho f+Vm\rho m$$
$$Vm+Vf=1$$
$$E_{11}=VfEf+VmEm$$
$$\frac{1}{E_{22}}=\frac{Vf}{Ef}+\frac{Vm}{Em}-VfVm\frac{Vf^2\frac{Em}{Ef}+\upsilon m^2\frac{Ef}{Em}-2\upsilon f\upsilon m}{VfEf+VmEm}$$
$$\frac{1}{G_{12}}=\frac{Vf}{Ef}+\frac{Vm}{Gm}$$
$$\upsilon_{12}=Vf\upsilon f+Vm\upsilon m$$

E111=-0.5×1e-3;E21=-0.2×1e-3;G121=-0.2×1e-3;G131=-0.2×1e-3;G231=-0.2×1e-3;α11=0.5×1e-3;

α21=0.5×1e-3;β11=0.5×1e-3;β21=0.5×1e-3; E1(TC)=E10(1+E111(T+C); E2(TC)=E20(1+E21(T+C);

G12(TC)=G120(1+G121(T+C); G13(TC)=G130(1+G131(T+C); G23(TC)=G230(1+G231(T+C); α1(T)=α110(1+α11T);

α2(T)=α210(1+α21T); β1(C)=β1(1+β11C); β2(C)=β2(1+β21C);

Temperature and moisture independent (TID) material properties constants used for present study are

E111=0; E21=0; G121=0; G131=0; G231=0; α11=0; α21=0; β11=0; β21=0;

4. 1 Validation study for mean transverse central deflection

The mean transverse central deflection of the of symmetric angle-ply $[\pm45^0]_{2T}$ simply supported (S2) laminated composite square plates subjected uniform lateral pressure combined with and without rise in uniform temperatureand moisture, volume fraction (Vf) = 0.6, plate thickness ratio a/h=10 is shown in Table 1 and compared with [26]. From the table it is clear that the present DISFEM results using HSDT are in good agreement with the available results using higher shear deformation theory of [26].

4.2 Validation study for random nonlinear transverse central deflection

Hence no results are available in reported literatures for structural response of laminated composite plates with system randomness in hygrothermal environments therefore; the outlined DISFEM approach can be validated with standard results using Independent Monte Carlo simulation. The influence of scattering in the material properties has been examined by allowing the coefficients of variation (SD/mean) changing from 0 to 20% [16]. The schematics procedure of DISFEM is given in Fig. 2. Validation study for random hygrothermal non-linear bending of material properties (E_{22}), plate thickness ratio (a/h)=30, angle ply $[\pm45^0]_{2T}$ square laminated plate, rise in temperature (ΔT)=200^0C, rise in moisture in percentage (ΔC=2%), simple support SSSS S2, fiber volume fraction (Vf) =0.6, load deflection(Q)=100 andfor random hygrothermal non-linear bending of geometric properties (h), plate thickness ratio (a/h)=40, angle ply $[\pm45^0]_{2T}$ square laminated plate, rise in temperature (ΔT)=200^0C, rise in moisture in percentage (ΔC=2%), simple support SSSS S2, fiber volume fraction (Vf) =0.6, load deflection(Q)=100 is presented. It is seen that present FOPT results are satisfactory with the MCS results as shown in Fig 4(a)&(b).For the MCS approach, the sample values are generated using MATLAB to fit it desired mean and Standard Deviation assuming

Gaussian probabilistic distribution function (PDF). However, the DISFEM does not put any limitation as regards to PDF of the material properties which is an advantageous over the MCS. The convergence of MCS results is studied by taking different number of samples which are given input to the present deterministic Eq. (16) and the response is calculated numerically to obtain the statistics of the sample of response.

From the convergence study, it is experience that 12000 samples are sufficient to give desired statistics for the present problem. It is observed the present results are very close to MCS results. This indicates the good accuracy of the present formulation for the range of COV considered.

4. 3 Sensitiveness of the second order deflection response to input parameters

Table 2 shows the effects of load deflection (Q) and variation of individual random system property bi, [{(i =1 to 11), = 0.10] on the dimensionless mean(W0nl) and coefficient of variation (Wnl) of hygrothermal transverse central deflection of angle ply [±450]2Tsquare laminated composite plates subjected to uniform constant temperature and moisture (U.T), in-plane bi-axial compression, a/h=20, with simple support S2 boundary conditions. The dimensionless nonlinear mean hygrothermal transverse central deflections (W0l) are given in brackets. Load deflection (Q) = 100, fiber volume fraction (Vf) =0.6. It is observed that without considering moisture and temperature for plates the COV of hygrothermal central deflection for V12is significant. On increasing moisture and temperature concentration the mean hygrothermal transverse central deflection decreases.

The effects of thickness ratios (a/h), load deflection (Q) andrandom input variables bi, [{(i =1 to 9), (7..9),(10) and (11)} = 0.10]on the dimensionless non-linearmean (W0nl) and coefficient of variation (Wnl) of hygrothermal transverse central deflection of angle ply [±450]2T square laminated composite plate subjected in-plane bi-axial compressionwith simple support S2 boundary conditions. It is seen that on increase of plate thickness ratio the expected mean central deflection decreases, however for higher load deflection it is in increasing order. On increasing moisture and temperature the mean transverse central deflection further decreases. The COV of hygrothermal transverse central deflection in both cases significantly varies as shown in Table 3.

Table 4 shows the effects of aspect ratios (a/b) , load deflection (Q) and random input variables b_i, [{(i =1 to 9), (7..9),(10) and (11)} = 0.10] on the dimensionless non-linear mean (W_{0nl}) and coefficient of variation (W_{nl}) hygrothermal transversecentral deflection of angle ply $[\pm 45^0]_{2T}$ laminated composite plates subjected to in-plane bi-axial compression with simple support S2 boundary conditions in hygrothermal environments . Plate thickness ratio (a/h)=40 , fiber volume fraction(Vf) =0.6.It is seen that the effects of aspect ratio is significant for the rectangular plates with increasing load deflection, there arefurther variations for mean and COV of transverse central deflection when the rectangular plates are subjected to rise in moisture and temperatures.

Table 5 shows the effects of support conditions, load deflection (Q) and random input variables bi, [{(i =1 to 9), (7..9),(10) and (11)} = 0.10] on the dimensionless non-linear mean(W0nl) and coefficient of variation (Wnl) of hygrothermal transverse central deflection, plate thickness ratio (a/h) =50, of angle ply [±450]2T laminatedsquare composite plates subjected to in-plane bi-axial compression and fiber volume fraction (Vf) =0.6. It is noticed that simple supported (S2) and CSCS supported plates are significantly influenced by variation of load deflection, rise in moisture and temperature. The effects for combined random input variables are significant.

The effects of Lay-up, load deflection (Q) with random input variables bi, [{(i =1 to 9), (7..9),(10) and (11)} = 0.10] on the dimensionless non-linear mean(W0nl) and coefficient of variation (Wnl) of hygrothermal transverse central deflection, plate thickness ratio (a/h) =50, of laminated square composite plate, simple support S2 boundary conditions subjected to in-plane bi-axial compression and fiber volume fraction (Vf) =0.6. It is noticed that plates with cross ply and antisymmetric are highly influenced for mean and COV of hygrothermal transverse central deflection on increasing load deflection. However the values are further increased when plates are subjected to rise in moisture and temperatures is shown in Table 6.

Table 7 shows the effects offiber volume fraction (Vf) , load deflection (Q) andrandom input variables bi, [{(i =1 to 9), (7..9),(10) and (11)} = 0.10] on the dimensionless non-linear mean (W0nl) and coefficient of variation (Wnl) of

hygrothermal transverse central deflection of angle ply[±450]2T laminated composite plates subjected to in-plane bi-axial compression with simple support S2 boundary conditions .Plate thickness ratio (a/h)=40.

It is observed that effects of volume fraction with increase in load deflection mean and COV hygrothermal transverse central deflection of all combined random input variables is significant when there is rise in moisture and temperatures.

The effects of temperature and moisture rise (ΔT, ΔC) , load deflection (Q)andrandom input variables bi, [{(i =1 to 9), (7..9),(10) and (11)} = 0.10]on the dimensionless non-linearmean (W0nl) and coefficient of variation (Wnl) of hygrothermal transverse central deflection , plate thickness ratio(a/h) =20, of angle ply [±450]2T laminatedsquare composite plate subjected to in-plane bi-axial compression and fiber volume fraction(Vf)=0.6.

It is noticed that increase in moisture and temperature with load deflection is significant for both mean transverse central deflection and random input variables.

Conclusions

A DISFEM probabilistic procedure is presented to study the second order statistics, i.e., mean and COV of transverse central deflection of laminated composite plate with randomness in material properties, coefficients of thermal expansion, coefficients of hygroscopic expansion, geometric parameters and lateral loading. The effects of the mean value of lateral load combination of multiple random variables varying simultaneously or individually, plate geometric parameters, boundary supporting and various modes of temperature and moisture change are addressed in analysis.

The following conclusions are noted from this study.

1.The COV of the transverse central deflection shows different sensitivity to different system properties. The sensitivity changes with the lay-up sequence, the plate to side ratio, the plate aspect ratio, fiber volume fractions, the boundary conditions, temperature and moisture increments , material properties and geometric parameters.

2.Among the different system properties studied, the elastic moduli, lamina plate thickness lateral loading have dominant effect on the COV of the transverse central deflection as compared to other system properties subjected to uniform and uniform temperature and moisture distribution. The strict control of these random parameters is therefore, required if high reliability of the laminated composite is desired.

3.The coefficient of variation of the plate increases as distribution in temperature & moisture and lateral pressure increases, This bring out importance of considering hygrothermal loading along with lateral pressure as one of the essential parameters from design point of view . In general, the rectangular plate is more sensitive as compared to the square plate.

4.The plate with all edges clamped support conditions is more desirable as compared to other support conditions from sensitivity point of view. The effect of randomness in thermal expansion coefficients, moisture expansion coefficients, fiber volume fractions, lamina plate thickness and lateral load on the coefficient of variation of nonlinear transverse central deflection subjected to lateral pressure and hygrothermal loading is quite significant.

Figure captions

1.Geometry of laminated composite plate

2.(a) Schematic of stochastic analysis procedure.

(b)Flow chart of solution procedure of stochastic nonlinear bending problemSchematic of various boundary conditions

4.(a) Validation of present DISFEM results with independent MCS results for only one material property E22 varying subjected lateral loading having SSSS (S2) support condition with uniform temperature and moisture distribution.

(b) Validation of present DISFEM results with independent MCS results for only one geometric property hvarying subjected lateral loading having SSSS (S2) support condition with uniform temperature and moisture distribution.

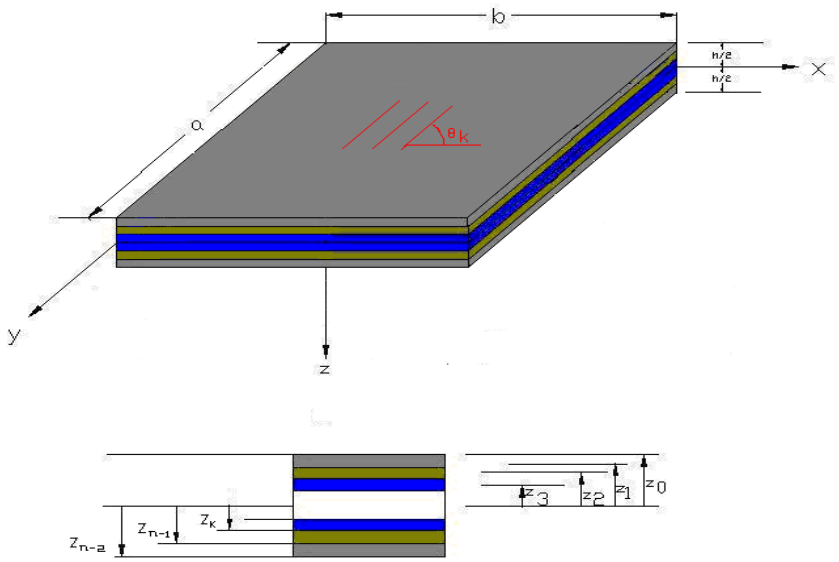

FIG.1 GEOMETRY OF LAMINATED COMPOSITE PAATE

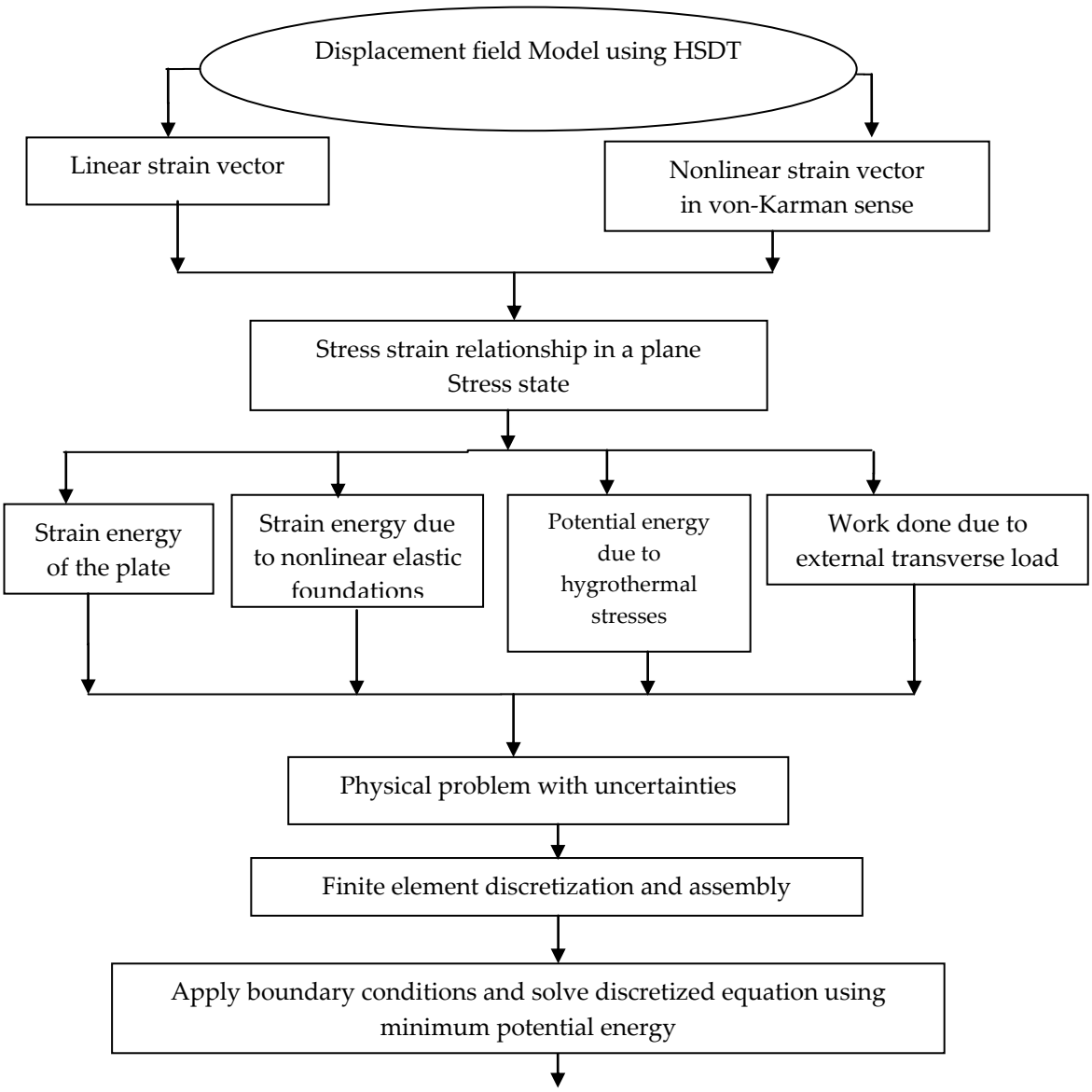

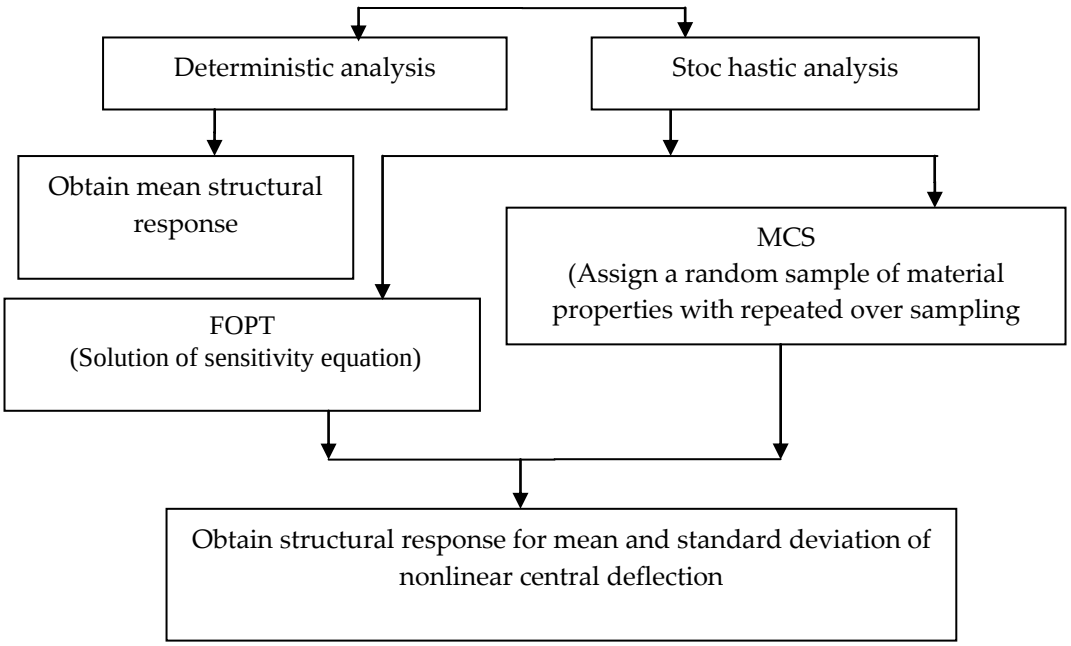

FIG.2(a) SCHEMATIC OF STOCHASTIC ANALYSIS PROCEDURE

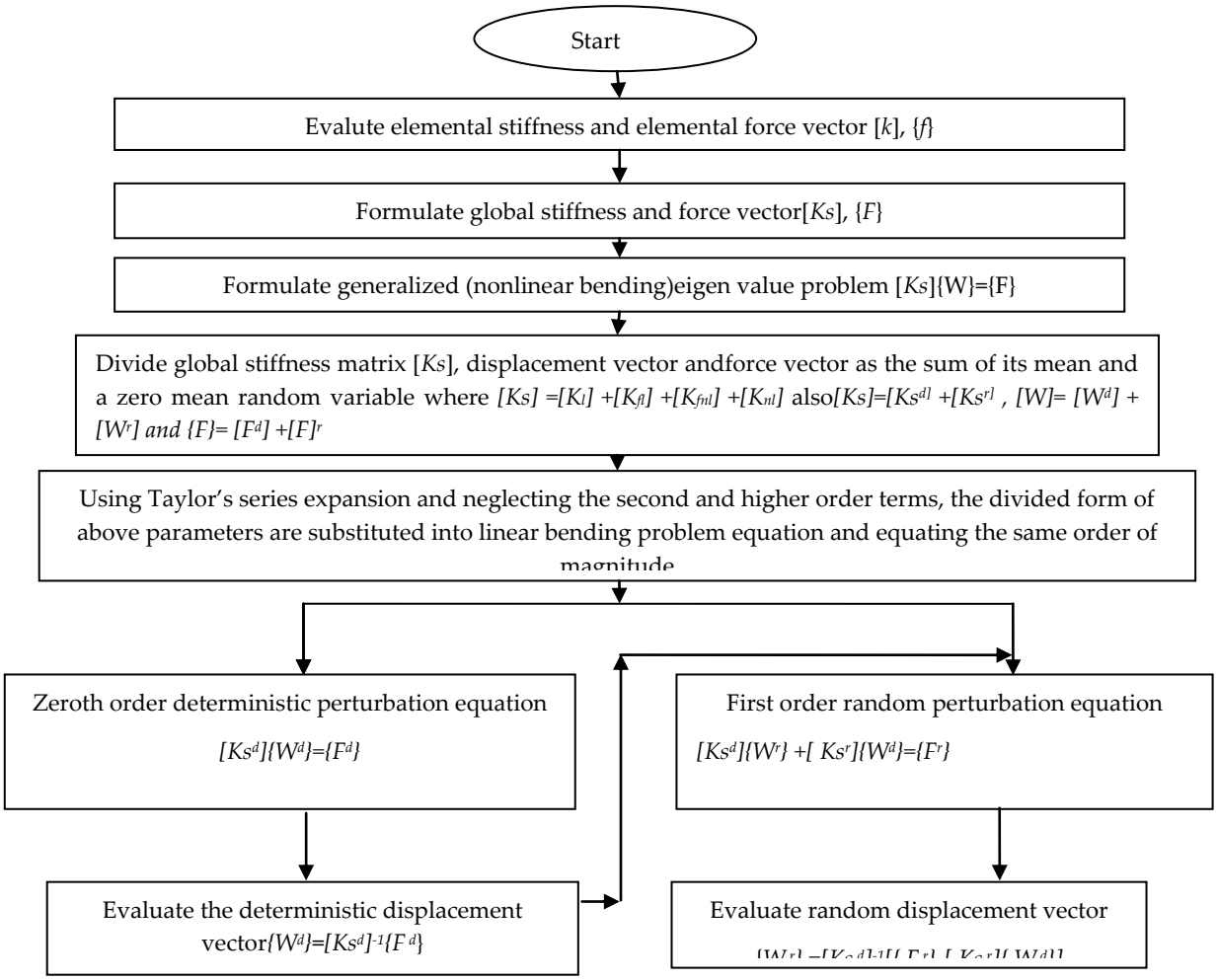

FIG.2(b) FLOW CHART OF SOLOUTION PROCEDURE OF STOCHASTIC NONLINEAR BENDING PROBALEM

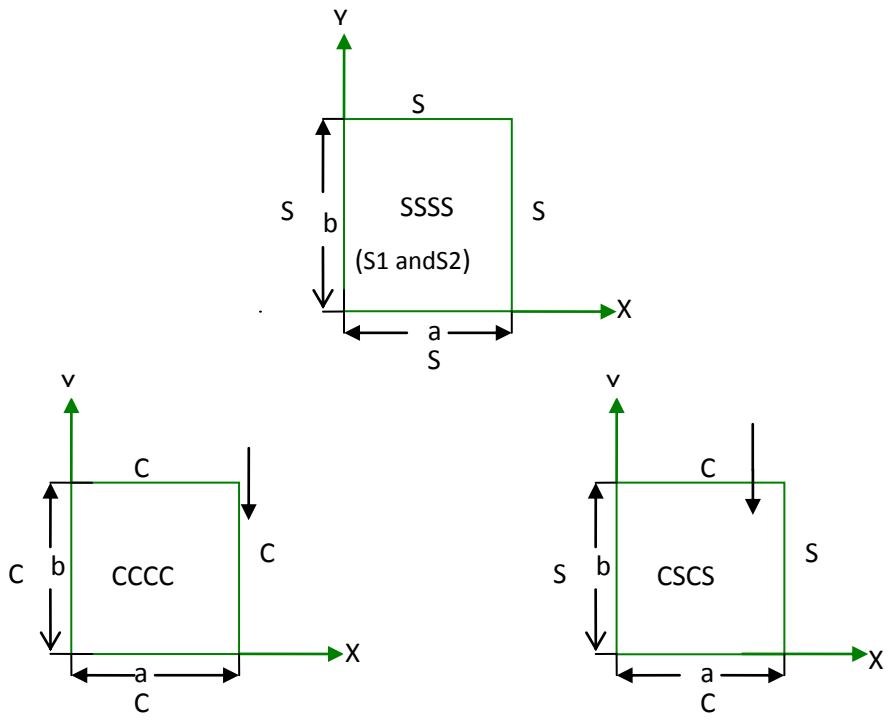

FIG.3 SCHEMATIC OF VAAIOUS BOUNDARY CONDITIONS

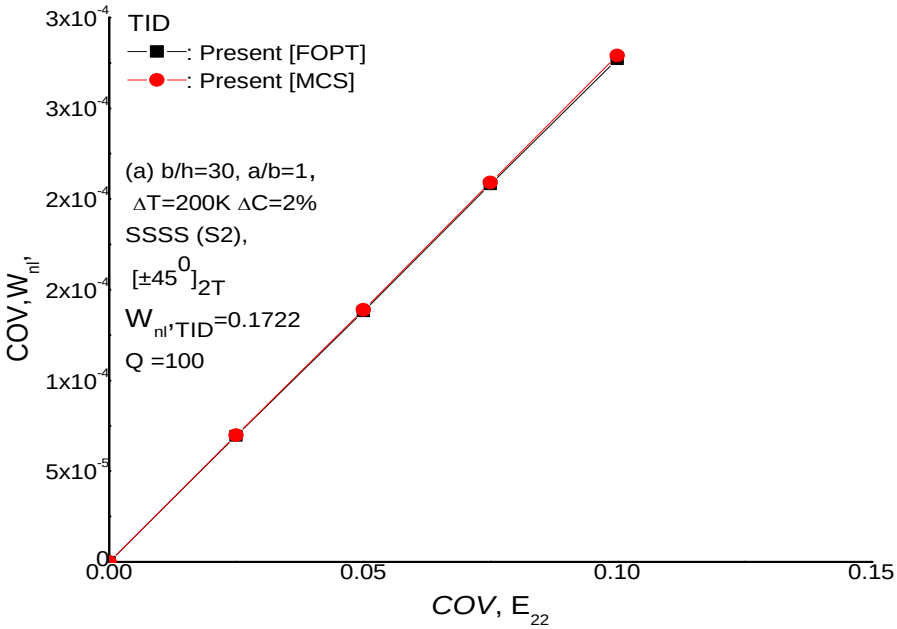

FIG.4(a) VALIDATION OF PRESENT DISFEM RESULTS WITH INDEPENDENT MCS RESULTS FOR ONLY ONE MATERIAL PROPERTY E_{22} VARYING SUBJECTED LATERAL LOADIN HAVING SSSS(S2) SUPPORT CONDITION WITH UNIFORM TEMPERATURE AND MOISTURE DISTRIBUTION

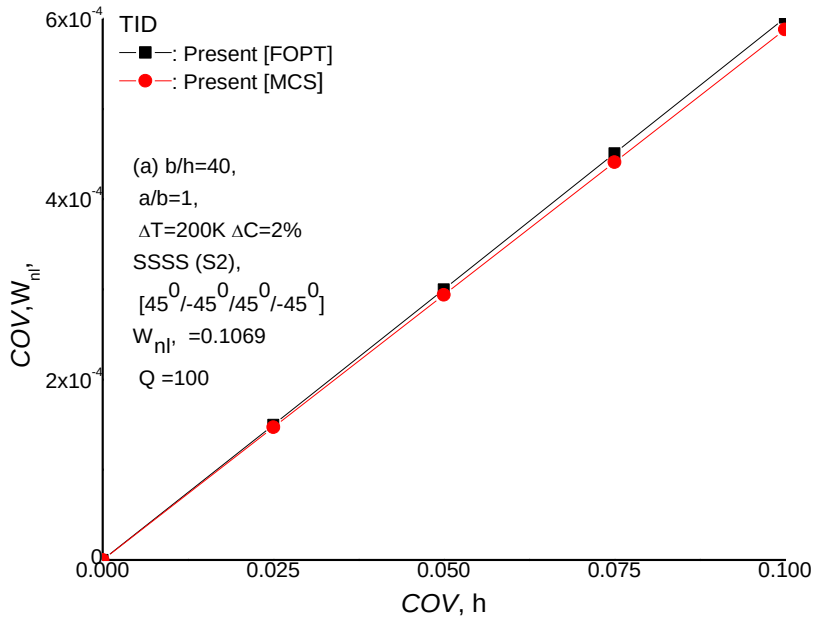

FIG.4(b) VALIDATION OF PRESENT DISFEM RESULTS WITH INDEPENDENT MCS RESULTS FOR ONLY ONE GEOMETRIC PROPETRY HAVING SUBJECTED TO LATERAL LOADING HAVING SSSS(S2) SUPPORT CONDITION WITH UNIFORM TEMPERATURE AND MOISTURE DISTRIBUTION

TABLE 1. HYGROTHERMAL EFFECTS ON THE NONLINEAR BENDING BEHAVIOR OF ANGLE PLY $(\pm 45^0)_{2T}$ LAMINATED SQUARE PLATE WITH LOAD DEFLECTIONS (Q)= Q $b^4/E_{22}h^4$,FIBER VOLUME FRACTION (VF) =0.6, PLATE THICKNESS RATIO (A/H)=10, SIMPLE SUPPORT SSSS(S2) BOUNDARY CONDITIONS

Q	Non-dimensional Hygrothermal Bending Load (W_{0nl})			
	Ref. [26]		Present HSDT	
	ΔT=00, ΔC=0%	ΔT=300, ΔC=3%	ΔT=00, ΔC=0%	ΔT=300, ΔC=3%
100	0.6683	0.5957	0.6687	0.5878
150	0.8243	0.6717	0.8422	0.6829
200	0.9400	0.7161	0.9397	0.7127

TABLE 2. EFFECTS OF LOAD DEFLECTION (Q) AND VARIATION OF INDIVIDUAL RANDOM SYSTEM PROPERTY B_I, [{(I =1 TO 11), = 0.10] ON THE DIMENSIONLESS MEAN(W_{0nl}) AND COEFFICIENT OF VARIATION (W_{nl} OF HYGROTHERMAL TRANSVERSE CENTRAL DEFLECTION OF ANGLE PLY $[\pm 45^0]_{2T}$SQUARE LAMINATED COMPOSITE PLATES SUBJECTED TO UNIFORM CONSTANT TEMPERATURE AND MOISTURE (U.T),IN-PLANE BI-AXIAL COMPRESSION, A/H=20, WITH SIMPLE SUPPORT S2 BOUNDARY CONDITIONS. THE DIMENSIONLESS NONLINEAR MEAN HYGROTHERMAL TRANSVERSE CENTRAL DEFLECTIONS (W_{OL}) ARE GIVEN IN BRACKETS. LOAD DEFLECTION (Q) = 100, FIBER VOLUME FRACTION (VF) =0.6.

b_i	(Q)	COV, W_{nl}			
		ΔT= 0⁰C, ΔC= 0.00	ΔT =100⁰C, ΔC= 0.01	ΔT =200⁰C, ΔC= 0.02	ΔT =300⁰C, ΔC= 0.03
E_{11} (i=1)	100	(0.5031) 2.55e-04	(0.4797) 2.10e-04	(0.4416) 1.77e-04	(0.3689)1.56e-04
	150	(0.7027)2.66e-04	(0.6361)2.31e-04	(0.5708)2.06e-04	(0.5024)1.85e-04
	200	(0.8760)2.73e-04	(0.7729)2.45e-04	(0.6823)2.25e-04	(0.5957) 2.12e-04
E_{22}(i=2)	100	0.0022	3.52e-05	1.90e-04	2.32e-04
	150	9.59e-04	1.61e-04	2.24e-04	2.40e-04
	200	4.90e-04	2.06e-04	2.40e-04	2.48e-04
G_{12}(i=3)	100	0.0031	7.78e-04	1.87e-04	7.65e-05
	150	0.0032	7.53e-04	1.89e-04	7.74e-05
	200	0.0045	8.73e-04	2.16e-04	9.13e-05

G_{13} (i=4)	100	2.39e-05	3.20e-05	4.15e-05	5.36e-05
	150	1.45e-05	1.80e-05	2.24e-05	2.80e-05
	200	7.35e-06	8.01e-06	9.13e-06	1.08e-05
G_{23}(i=5)	100	1.19e-05	1.60e-05	2.07e-05	2.68e-05
	150	7.29e-06	9.00e-06	1.12e-05	1.40e-05
	200	3.67e-06	4.00e-06	4.56e-06	5.40e-06
V_{12}(i=6)	100	0.0280	0.0022	4.21e-04	1.77e-04
	150	0.0273	0.0021	4.13e-04	1.72e-04
	200	0.0260	0.0019	3.69e-04	1.54e-04
α_{11} (i=7)	100	4.49e-09	5.93e-09	7.24e-09	8.31e-09
	150	4.11e-09	5.47e-09	6.70e-09	7.98e-09
	200	3.77e-09	5.03e-09	6.20e-09	7.33e-09
α_{22} (i=8)	100	4.90e-08	4.15e-08	3.57e-08	3.01e-08
	150	4.49e-08	3.83e-08	3.29e-08	2.88e-08
	200	4.13e-08	3.53e-08	3.05e-08	2.64e-08
β_2(i=9)	100	9.39e-06	7.94e-06	6.82e-06	5.73e-06
	150	8.61e-06	7.34e-06	6.29e-06	5.49e-06
	200	7.91e-06	6.76e-06	5.82e-06	5.03e-06
h (i=10)	100	0.0011	8.68e-04	7.40e-04	7.24e-04
	150	0.0011	9.81e-04	8.83e-04	8.37e-04
	200	0.0011	0.0011	0.0010	9.73e-04
Q(i=11)	100	2.56e-04	2.33e-04	2.27e-04	2.47e-04
	150	2.55e-04	2.43e-04	2.38e-04	2.45e-04
	200	2.54e-04	2.48e-04	2.46e-04	2.49e-04

TABLE 3 . THE EFFECTS OF THICKNESS RATIOS (A/H, LOAD DEFLECTION (Q) AND RANDOM INPUT VARIABLES B_I, [{(I=1 to 9), (7..9),(10) AND (11)} = 0.10 ON THE DIMENSIONLESS NON-LINEARMEAN (W_{ONL}) AND COEFFICIENT OF VARIATION (W_{NL}) of HYGROTHERMAL TRANSVERSE CENTRAL DEFLECTION of ANGLE PLY$[\pm 45^0]_{2T}$SQUARE LAMINATED COMPOSITE PLATE SUBJECTED TO IN-PLANE BI-AXIAL COMPRESSIONwith SIMPLE SUPPORT S2 BOUNDARY CONDITIONS AND VOLUME FRACTION (VF)=0.6.

a/h	Q	(TID)									
		(ΔT= 0^0C, ΔC= 0.0)					(ΔT =100^0C, ΔC =0.01)				
		mean W_{0nl}	COV, W_{nl}				mean W_{0nl}	COV, W_{nl}			
			bi					bi			
			(i=1..9)	(i=7.. 9)	(i=10)	(i=11)		(i=1..9)	(i=7.. 9)	(i=10)	(i=11)
10	100	0.6952	0.0588	6.57e-06	0.0021	5.00e-04	0.6685	0.0040	5.96e-06	0.0020	4.74e-04
	150	0.8830	0.0555	5.48e-06	0.0022	5.01e-04	0.8262	0.0040	4.97e-06	0.0021	4.87e-04
	200	0.9989	0.0526	4.55e-06	0.0022	5.01e-04	0.9171	0.0039	4.12e-06	0.0021	4.94e-04
30	100	0.4330	0.0201	1.24e-05	7.66e-04	1.81e-04	0.3585	0.0023	9.50e-06	6.48e-04	1.85e-04
	150	0.6335	0.0187	1.18e-05	7.67e-04	1.76e-04	0.5267	0.0019	9.12e-06	6.84e-04	1.73e-04
	200	0.8158	0.0175	1.12e-05	7.65e-04	1.74e-04	0.6671	0.0016	8.64e-06	7.20e-04	1.70e-04
50	100	0.3287	0.0147	1.72e-05	5.59e-04	1.30e-04	0.0904	0.0039	1.32e-05	7.69e-04	2.51e-04
	150	0.5053	0.0116	1.68e-05	5.22e-04	1.19e-04	0.2696	0.0017	1.00e-05	5.52e-04	1.41e-04
	200	0.6698	0.0101	1.61e-05	5.00e-04	1.13e-04	0.3712	0.0013	9.05e-06	5.47e-04	1.30e-04
60	100	0.2745	0.0141	1.77e-05	5.16e-04	1.18e-04	0.0120	0.0176	6.11e-05	0.0031	0.0012
	150	0.4349	0.0100	1.78e-05	4.70e-04	1.07e-04	0.1814	0.0017	1.12e-05	5.10e-04	1.34e-04
	200	0.5887	0.0081	1.74e-05	4.40e-04	1.00e-04	0.2380	0.0013	9.20e-06	5.47e-04	1.32e-04

TABLE. 4 EFFECTS OF ASPECT RATIOS (A/B) , LOAD DEFLECTION (Q) AND RANDOM INPUT VARIABLES B_I, [{(I =1 to 9), (7..9),(10) AND (11)} = 0.10] ON THE DIMENSIONLESS NON-LINEARMEAN (W_{ONL} AND COEFFICIENT OF VARIATION (W_{NL}) HYGROTHERMAL TRANSVERSECENTRAL DEFLECTION OF ANGLE PLY $[\pm 45^0]_{2T}$LAMINATED COMPOSITE PLATES SUBJECTED TO IN-PLANE BI-AXIAL COMPRESSION WITH SIMPLE SUPPORT S2 BOUNDARY CONDITIONS IN HYGROTHERMAL ENVIRONMENTS . PLATE THICKNESS RATIO (A/H)=40 , FIBER VOLUME FRACTION(VF) =0.6.

a/b	Q	(TID)									
		(ΔT= 0^0C, ΔC= 0.0)					(ΔT =100^0C, ΔC =0.01)				
		mean W_{0nl}	COV, W_{nl} bi				mean W_{0nl}	COV, W_{nl} bi			
			(i=1..9)	(i=7..9)	(i=10)	(i=11)		(i=1..9)	(i=7.. 9)	(i=10)	(i=11)
1.0	100	0.3811	0.0164	1.53e-05	6.27e-04	1.47e-04	0.2016	0.0029	9.71e-06	6.56e-04	1.93e-04
	150	0.5684	0.0143	1.46e-05	6.08e-04	1.39e-04	0.3850	0.0018	9.61e-06	6.01e-04	1.53e-04
	200	0.7489	0.0129	1.40e-05	5.96e-04	1.35e-04	0.5354	0.0013	9.44e-06	5.91e-04	1.40e-04
1.5	100	0.9545	0.0274	1.03e-05	8.47e-04	1.96e-04	0.7429	0.0022	7.68e-06	7.39e-04	1.89e-04
	150	1.3731	0.0257	9.79e-06	8.46e-04	1.93e-04	1.0652	0.0019	7.29e-06	7.77e-04	1.87e-04
	200	1.7374	0.0239	9.19e-06	8.44e-04	1.92e-04	1.3486	0.0017	6.89e-06	7.98e-04	1.86e-04
2.0	100	1.5059	0.0439	6.58e-06	0.0011	2.55e-04	1.2329	0.0029	5.01e-06	9.90e-04	2.40e-04
	150	2.1367	0.0417	6.21e-06	0.0011	2.54e-04	1.7231	0.0027	4.79e-06	0.0010	2.44e-04
	200	2.6505	0.0387	5.77e-06	0.0011	2.53e-04	2.1354	0.0025	4.50e-06	0.0011	2.46e-04

TABLE. 5EFFECTS OF SUPPORT CONDITIONS, LOAD DEFLECTION (Q) ANDRANDOM INPUT VARIABLES BI, [{(I =1 TO 9), (7..9),(10) AND (11)} = 0.10]ON THE DIMENSIONLESS NON-LINEARMEAN(W0NL)AND COEFFICIENT OF VARIATION (WNL) OF HYGROTHERMAL TRANSVERSE CENTRAL DEFLECTION, PLATE THICKNESS RATIO (A/H) =50, OF ANGLE PLY [±450]2TLAMINATEDSQUARE COMPOSITE PLATES SUBJECTED TO IN-PLANE BI-AXIAL COMPRESSION AND FIBER VOLUME FRACTION (VF) =0.6.

BCs	Q	(TID)									
		(ΔT= 0^0C, ΔC= 0.0)					(ΔT =100^0C, ΔC =0.01)				
		mean W_{0nl}	COV, W_{nl} bi				mean W_{0nl}	COV, W_{nl} bi			
			(i=1..9)	(i=7.. 9)	(i=10)	(i=11)		(i=1..9)	(i=7.. 9)	(i=10)	(i=11)
SSSS (S1)	100	0.2984	0.0123	1.52e-05	4.99e-04	1.24e-04	0.1709	0.0024	9.95e-06	3.43e-04	1.24e-04
	150	0.4572	0.0098	1.47e-05	4.73e-04	1.13e-04	0.2646	0.0016	9.03e-06	4.50e-04	1.19e-04
	200	0.6019	0.0083	1.40e-05	4.60e-04	1.08e-04	0.3410	0.0012	7.96e-06	5.22e-04	1.25e-04
SSSS (S2)	100	0.3287	0.0147	1.72e-05	5.59e-04	1.30e-04	0.0904	0.0039	1.32e-05	7.69e-04	2.51e-04
	150	0.5053	0.0116	1.68e-05	5.22e-04	1.19e-04	0.2696	0.0017	1.00e-05	5.52e-04	1.41e-04
	200	0.6698	0.0101	1.61e-05	5.00e-04	1.13e-04	0.3712	0.0013	9.05e-06	5.47e-04	1.30e-04
CCCC	100	0.2194	0.0112	1.16e-05	3.96e-04	1.00e-04	0.1687	3.86e-04	7.16e-06	1.04e-04	8.05e-05
	150	0.3061	0.0099	1.08e-05	4.18e-04	1.00e-04	0.2719	7.62e-04	7.15e-06	2.15e-04	7.43e-05
	200	0.3657	0.0090	9.87e-06	4.30e-04	1.00e-04	0.3318	7.19e-04	6.90e-06	2.89e-04	7.68e-05
CSCS	100	0.3522	0.0117	1.36e-05	3.64e-04	8.58e-05	0.5133	8.57e-04	7.23e-06	8.77e-05	3.73e-05
	150	0.4639	0.0108	1.32e-05	4.05e-04	9.19e-05	0.5340	8.09e-04	7.25e-06	1.87e-04	5.19e-05
	200	0.5519	0.0102	1.25e-05	4.27e-04	9.51e-05	0.5388	7.35e-04	7.22e-06	2.73e-04	6.53e-05

TABLE. 6 EFFECTS OF LAY-UP, LOAD DEFLECTION (Q)WITH RANDOM INPUT VARIABLES BI, [{(I =1 TO 9), (7..9),(10) AND (11)} = 0.10]ON THE DIMENSIONLESS NON-LINEARMEAN(W0NL)AND COEFFICIENT OF VARIATION (WNL) OF HYGROTHERMAL TRANSVERSE CENTRAL DEFLECTION , PLATE THICKNESS RATIO (A/H) =50, OF LAMINATEDSQUARE COMPOSITE PLATE , SIMPLE SUPPORT S2 BOUNDARY CONDITIONS SUBJECTED TO IN-PLANE BI-AXIAL COMPRESSION AND FIBER VOLUME FRACTION (VF) =0.6.

Lay-up	Q	(TID)									
		(ΔT= 0^0C, ΔC= 0.0)					(ΔT =100^0C, ΔC =0.01)				
		mean W_{0nl}	COV, W_{nl} bi				mean W_{0nl}	COV, W_{nl} bi			
			(i=1..9)	(i=7.. 9)	(i=10)	(i=11)		(i=1..9)	(i=7.. 9)	(i=10)	(i=11)
$[\pm 45^0]_{2T}$	100	0.3287	0.0147	1.72e-05	5.59e-04	1.30e-04	0.0904	0.0039	1.32e-05	7.69e-04	2.51e-04
	150	0.5053	0.0116	1.68e-05	5.22e-04	1.19e-04	0.2696	0.0017	1.00e-05	5.52e-04	1.41e-04
	200	0.6698	0.0101	1.61e-05	5.00e-04	1.13e-04	0.3712	0.0013	9.05e-06	5.47e-04	1.30e-04
$[\pm 45^0]_S$	100	0.3850	0.0114	1.94e-05	5.04e-04	1.11e-04	0.4569	6.77e-04	1.09e-05	2.48e-04	5.46e-05
	150	0.5857	0.0112	1.88e-05	4.87e-04	1.07e-04	0.5668	6.24e-04	1.09e-05	2.88e-04	6.49e-05
	200	0.7719	0.0108	1.81e-05	4.77e-04	1.05e-04	0.6690	5.82e-04	1.06e-05	3.15e-04	7.17e-05
$[0^0/90^0]_{2T}$	100	0.5076	0.0105	2.36e-05	4.69e-04	1.08e-04	0.5246	5.02e-04	1.27e-05	2.46e-04	5.61e-05
	150	0.6813	0.0092	2.06e-05	4.59e-04	1.05e-04	0.6110	4.55e-04	1.16e-05	2.85e-04	6.60e-05
	200	0.9164	0.0092	2.05e-05	4.53e-04	1.04e-04	0.7397	4.50e-04	1.15e-05	3.10e-04	7.22e-05
$[0^0/90^0]_S$	100	0.4649	0.0090	2.23e-05	4.73e-04	1.10e-04	0.5154	4.80e-04	1.22e-05	2.37e-04	5.45e-05
	150	0.6313	0.0079	1.95e-05	4.60e-04	1.07e-04	0.5968	4.27e-04	1.12e-05	2.78e-04	6.47e-05
	200	0.8519	0.0079	1.94e-05	4.52e-04	1.05e-04	0.7212	4.14e-04	1.12e-05	3.03e-04	7.12e-05

TABLE 7 EFFECTS OFFIBER VOLUME FRACTION (VF) , LOAD DEFLECTION (Q) ANDRANDOM INPUT VARIABLES BI, [{(I =1 TO 9), (7..9),(10) AND (11)} = 0.10]ON THE DIMENSIONLESS NON-LINEARMEAN (W0NL) AND COEFFICIENT OF VARIATION (WNL) OF HYGROTHERMAL TRANSVERSE CENTRAL DEFLECTION OF ANGLE PLY[±450]2TLAMINATED COMPOSITE PLATES SUBJECTED TO IN-PLANE BI-AXIAL COMPRESSION WITH SIMPLE SUPPORT S2 BOUNDARY CONDITIONS . PLATE THICKNESS RATIO (A/H)=40.

Vf	Q	(TID)									
		(ΔT= 0^0C, ΔC= 0.0)					(ΔT =100^0C, ΔC =0.01)				
		mean W_{0nl}	COV, W_{nl} bi				mean W_{0nl}	COV, W_{nl} bi			
			(i=1..9)	(i=7.. 9)	(i=10)	(i=11)		(i=1..9)	(i=7. 9)	(i=10)	(i=11)
0.50	100	0.3525	4.16e-04	1.40e-05	6.43e-04	1.52e-04	0.1879	3.84e-04	8.82e-06	6.51e-04	1.92e-04
	150	0.5263	3.70e-04	1.34e-05	6.20e-04	1.42e-04	0.3343	2.75e-04	8.49e-06	6.40e-04	1.62e-04
	200	0.6920	3.36e-04	1.27e-05	6.04e-04	1.37e-04	0.4629	2.24e-04	8.29e-06	6.36e-04	1.50e-04
0.55	100	0.3637	0.0015	1.45e-05	6.35e-04	1.50e-04	0.1911	6.73e-04	9.22e-06	6.60e-04	1.95e-04
	150	0.5417	0.0013	1.38e-05	6.15e-04	1.41e-04	0.3540	4.39e-04	8.97e-06	6.24e-04	1.58e-04
	200	0.7141	0.0011	1.32e-05	6.00e-04	1.36e-04	0.4929	3.30e-04	8.79e-06	6.17e-04	1.46e-04
0.60	100	0.3811	0.0164	1.53e-05	6.27e-04	1.47e-04	0.2016	0.0029	9.71e-06	6.56e-04	1.93e-04
	150	0.5684	0.0143	1.46e-05	6.08e-04	1.39e-04	0.3850	0.0018	9.61e-06	6.01e-04	1.53e-04
	200	0.7489	0.0129	1.40e-05	5.96e-04	1.35e-04	0.5354	0.0013	9.44e-06	5.91e-04	1.40e-04

0.65	100	0.4061	4.15e-04	1.63e-05	6.18e-04	1.45e-04	0.2270	0.0114	1.04e-05	6.30e-04	1.83e-04
	150	0.6071	3.74e-04	1.56e-05	6.01e-04	1.38e-04	0.4312	0.0072	1.04e-05	5.68e-04	1.44e-04
	200	0.7995	3.48e-04	1.50e-05	5.90e-04	1.34e-04	0.5939	0.0054	1.02e-05	5.61e-04	1.34e-04
0.70	100	0.4415	2.04e-04	1.77e-05	6.09e-04	1.42e-04	0.2998	4.49e-04	1.19e-05	5.50e-04	1.56e-04
	150	0.6621	1.98e-04	1.71e-05	5.94e-04	1.36e-04	0.4983	3.23e-04	1.15e-05	5.27e-04	1.34e-04
	200	0.8718	1.95e-04	1.65e-05	5.85e-04	1.33e-04	0.6770	2.67e-04	1.12e-05	5.22e-04	1.24e-04

TABLE 8 EFFECTS OF TEMPERATURE AND MOISTURE RISE (ΔT, ΔC) , LOAD DEFLECTION (Q)ANDRANDOM INPUT VARIABLES BI, [{(I =1 TO 9), (7..9),(10) AND (11)} = 0.10]ON THE DIMENSIONLESS NON-LINEARMEAN (W0NL) AND COEFFICIENT OF VARIATION (WNL) OF HYGROTHERMAL TRANSVERSE CENTRAL DEFLECTION , PLATE THICKNESS RATIO (A/H) =20, OF ANGLE PLY [±450]2TLAMINATEDSQUARE COMPOSITE PLATE SUBJECTEDTO IN-PLANE BI-AXIAL COMPRESSION AND FIBER VOLUME FRACTION(VF)=0.6.

Environmental Conditions	Q	(TID)				
		mean W_{0nl}	COV, W_{nl} bi			
			(i=1..9)	(i=7.. 9)	(i=10)	(i=11)
ΔT= 0^0C ΔC= 0.0	100	0.5031	0.0283	9.39e-06	0.0011	8.68e-04
	150	0.7027	0.0275	8.61e-06	0.0011	9.81e-04
	200	0.8760	0.0264	7.91e-06	0.0011	0.0011
ΔT=100^0C ΔC= 0.01	100	0.4797	0.0023	7.94e-06	2.56e-04	2.33e-04
	150	0.6361	0.0023	7.34e-06	2.55e-04	2.43e-04
	200	0.7729	0.0022	6.76e-06	2.54e-04	2.48e-04
ΔT=200^0C ΔC= 0.02	100	0.4416	5.31e-04	6.82e-06	7.40e-04	7.24e-04
	150	0.5708	5.48e-04	6.29e-06	8.83e-04	8.37e-04
	200	0.6823	5.40e-04	5.82e-06	0.0010	9.73e-04
ΔT= 300^0C ΔC= 0.03	100	0.3689	3.45e-04	5.73e-06	2.27e-04	2.47e-04
	150	0.5024	3.59e-04	5.49e-06	2.38e-04	2.45e-04
	200	0.5957	3.73e-04	5.03e-06	2.46e-04	2.49e-04
ΔT= 400^0C ΔC= 0.04	100	0.2533	3.66e-04	4.43e-06	9.03e-04	3.12e-04
	150	0.4104	3.39e-04	4.67e-06	8.55e-04	2.70e-04
	200	0.5075	3.46e-04	4.38e-06	9.84e-04	2.64e-04
ΔT= 500^0C ΔC= 0.05	100	0.0536	0.0011	3.15e-06	9.43e-04	0.0011
	150	0.2992	3.75e-04	3.85e-06	9.91e-04	3.23e-04
	200	0.4033	3.63e-04	3.70e-06	0.0010	2.95e-04

REFERENCES

[1] Shen,HS."Nonlinear analysis of composite laminated thin plates subjected to lateral pressure and thermal loading resting on elastic foundation." Comp. Struct. 49(2000): 115-128.

[2] Huang, NN, Tauchert, TR. "Large deformation of anti-symmetric angle-ply laminated composites resulting from non-uniform temperature loading." J. Therm. Stress. 11(1998): 287-297.

[3] Shen HS.Nonlinear bending analysis of unsymmetric cross-ply laminated plates with piezoelectric actuators in thermal environment. Comput. Struct. 2004; 63: 167-177.

[4] Lin R M, Lim M K, Du H. Large deflection analysis of plates under thermal loading. Comput. Meth. Appl. Mecha. Engng. 1994; 117: 381-390.

[5] Shen HS. Non-linear bending of shear deformable laminated plates under lateral pressure and thermal loading and resting on elastic foundations. J. Strain Anal. Eng. Des. 2000; 35(2): 93-108.

[6] Khdeir A A, Reddy J N. Thermal stresses and deflections of cross-ply laminated plates using refined plate theories. J. Therm. Stress. 1991; 14: 419-38.

[7] Chanderashekhara K, Tenneti R. Non-linear static and dynamic analysis of heated laminated plates, A Finite Element approach. Compos. Sci. Tech. 1994; 51: 85-94 .

[8] Fares ME, Zenkour AM. Mixed variational formula for the thermal bending of laminated plates, J. Therm. Stress. 1999; 22(3): 347-65.

[9] Zenkour AM. Analytical solution for bending of cross ply laminated plates under thermo-mechanical loading. Compos. Struct. 2004; 65: 367-379.

[10] Naveenthraj B, Iyengar N G R, Yadav D. Response of composite plates with random material properties using FEM and MCS. Adva. Compos.Mater. 1998; 7: 219–237.

[11] [11] Salim S, Yadav D, Iyengar NGR. Analysis of composite plates with random material characteristics,Mechan. Resear. Comm, 1993; 20(5): 405–14.

[12] Onkar A K, Yadav, D. Non-linear response statistics of composite laminates with random material properties under random loading. Compos. Struct. 2003; 60(4): 375–383.

[13] Yang J, Liew KM, Kitipornchai S. Stochastic analysis of compositionally graded plates with system randomness under static loading. Int. J. Mech. Sci, 2005; 47: 1519-1541.

[14] Zongeen Z, Suhaun C. The standard deviation of the eigen solutions for random multi degree freedom systems.J. Comput. Struct. 1990; 39(6): 603–607.

[15] Zhang Y, Chen S, Liu Q, Liu T. Stochastic perturbation finite elements. Comput. Struct. 1996; 59(3): 425–429.

[16] Liu W K, Ted B, Mani A.A random field finite elements. Int. J. Numer. Meth. Engrg, 1986; 23: 1831–1845.

[17] Zhang J, Ellingwood B. Effects of uncertain material properties on structural stability. J. Struct. Engrg. 1993; 121: 705–716.

[18] Noh H C. Effect of multiple uncertain material properties on the response variability of in-plane and plate structures, Comput. Methods Appl. Mech. Engrg. 2006; 195: 2697-2718.

[19] Lal A, Singh B N, Kumar R. Static response of laminated composite plates resting on elastic foundation with uncertain system properties.J. Reinf. Plast. Compos. 2007; 26(8): 807-829.

[20] [20] Singh B N, Lal A, Kumar R. Nonlinear bending response of laminated composite plates on nonlinear elastic foundation with uncertain system properties. Engrg. Struct. 2008; 30: 1101–1112.

[21] Park JS, Kim CG, Hong CS. Stochastic finite element method for laminated composite structures. J. Reinf. Plas. Compos. 1995; 14: 675-93.

[22] Pandit MK, Singh BN, Sheikh AH. Stochastic perturbation based finite element for deflection statistics of soft core sandwich plate with random material properties. Int. J. Mech. Sci, 2009; 51: 363-371.

[23] Pandit MK, Sheikh AH, Singh BN. An improved higher order Zigzag theory for the static analysis of laminated sandwich plate with soft core, Finite Elem. Anal, 2008; 44 (9-10): 602-610.

[24] Lal A, Singh B N. Effect of random system properties on bending response of thermo-mechanically loaded laminated composite plates. Applied Mathematical Modelling. 2011; Doi:10.1016/j.apm.2011.05.014

[25] Lal A, Singh BN, Kumar R. Stochastic nonlinear bending response of laminated composite plates with system randomness under lateral pressure and thermal loading. Arch.Appl.Mech. 2011; 81: 727-743.

[26] Shen HS, M.ASCE.Hygrothermal effects on the nonlinear bending of shear deformable laminated plates.Journal of Engineering Mechanics, 2002; 128.

[27] Upadhyay AK, Pandey Ramesh, Shukla KK. Nonlinear flexural response of laminated composite plates under hygro-thermo-mechanical loading, Commun Nonlinear Sci Numer Simulat, 2010;15: 2634–2650.

[28] Reddy JN. A simple higher order theory for laminated composite plates,Trans ASME J. Applied. Mech. 1984; 51: 745-752.

[29] Shankara CA, Iyengar NGR. A C0 element for analysis of laminated composite plate. J. Sound Vibr. 1996; 191 (5): 721-738.

[30] Reddy JN. Mechanics of laminated composite plates: Theory and Analysis, CRC Press, Florida, 1996.

[31] Peng XQ, Geng L, Liyan W, Liu GR, Lam KY. A stochastic finite element method for fatigue reliability analysis of gear teeth subjected to bending. Int. J. Comput. Mech. 1998; 21: 253–61.

[32] Nigam NC, Narayanan S. Applications of random vibrations, Narosa, New Delhi, 1994.

[33] Kaminski M M. Computational mechanics of composite materials:Sensitivity, Randomness and multis. Springer Verlag , 2002.

[34] Kleiber M, Hien TD.The stochastic finite element method. John Wiley & Sons, 1992.

[35] Chia YA. Nonlinear analysis of plates,McGraw-Hill, New York, 1980.

[36] Jones RM.Mechanics of Composite Materials. 2ndedition,McGraw-Hill, Taylor & Francis group.New York, 1998.

[37] R, Kumar, Lal, A and Patil,HS. "Hygrothermal effects on the flexural response of laminated composite plates with random material properties." , Micromechanical Model. J. of Applied Engineering and Research, Research India Publication, India(2011).

[38] R, Kumar, Lal, A and Patil,HS. "Hygrothermal effects on the flexural response of laminated composite plates with random material properties." Micromechanical Model. 2nd International conference on emerging trends in Engineering and Technology (IETET-2011), Oct 20-22(2011), Kurukhetra,Haryana, India.

[39] R, Kumar, Lal, A and Patil,HS. "Nonlinear Flexural Response of Laminated Composite Plates on a Nonlinear Elastic Foundation with Uncertain System Properties under Lateral Pressure and Hygrothermal Loading." , Micromechanical Model. J. of Aerospace Engineering1,168 (2012).J.Aerosp. Eng. 27, special section: Advances in Ballistic Impact and Crashworthiness Response of Aerospace Structures, 529–547.

APPENDIX

$$\left(A_{ij}, B_{ij}, D_{ij}, E_{ij}, F_{ij}, H_{ij}\right) = \int_{-h/2}^{h/2} Q_{ij}\left(1, z, z^2, z^3, z^4, z^6\right) dz \text{ ; (i,j=1,2,6)}$$

$$\left(A_{ij}, D_{ij}, F_{ij}\right) = \int_{-h/2}^{h/2} Q_{ij}\left(1, z^2, z^4\right) dz \text{ ;(i,j=4,5)}$$

$$\left[D_3\right] = \begin{bmatrix} \left[A_1\right] & 0 \\ \left[B\right] & 0 \\ \left[E\right] & 0 \\ 0 & \left[A_2\right] \\ 0 & \left[C_2\right] \end{bmatrix}, \left[D_4\right] = \left[D_3\right]^T \text{ and } \left[D_5\right] = \begin{bmatrix} \left[A_1\right] & 0 \\ 0 & \left[A_2\right] \end{bmatrix}$$

$$\left[K_b\right] = \sum_{i=1}^{n} \int_{A^{(e)}} \left[B_b^{(e)}\right]^T \left[D_b\right] \left[B_b^{(e)}\right] dA;$$

$$\left[K_s\right] = \sum_{i=1}^{n} \int_{A^{(e)}} \left[B_s^{(e)}\right]^T \left[D_s\right] \left[B_s^{(e)}\right] dA$$

$$\left[K_{NL}\left\{q\right\}\right] = \int_A \left[B_{NL}\right]^T \left[D\right]\left[B_L\right] dA + \frac{1}{2}\int_A \left[B_L\right]^T \left[D\right]\left[B_{NL}\right] dA + \frac{1}{2}\int_A \left[B_{NL}\right]^T \left[D\right]\left[B_{NL}\right] dA$$

$$\left[K_G\right] = \int_A \left[B_{NL}\right]^T \left\{N\right\} dA = \int_A \left[G\right]^T \left[\overline{N}\right]\left[G\right] dA$$

$$\left[K_f\right] = \frac{1}{2}\int_A \left[B_f\right]^T \left[D_f\right]\left[B_f\right] dA$$

$$\{q\} = \sum_{e=1}^{NE} \{\Lambda\}^{(e)}$$

$$\left[F^{HT}\right] = \sum_{i=1}^{n} \int_{A^{(e)}} \left[\left[B_{1i}^{(e)}\right]^T \left[N^{HT}\right] + \left[B_{b1i}^{(e)}\right]^T \left[M^{HT}\right] + \left[B_{b2i}^{(e)}\right]^T \left[P^{HT}\right] \right] dA$$